2013

Finite Element Modeling of Hot-Mix Asphalt Performance in the Laboratory

Hao Ying
Louisiana State University and Agricultural and Mechanical College

FINITE ELEMENT MODELING OF HOT-MIX ASPHALT PERFORMANCE IN THE LABORATORY

A Dissertation

Submitted to the Graduate Faculty of the
Louisiana State University and
Agricultural and Mechanical College
in partial fulfillment of the
requirements for the degree of

Doctor of Philosophy

in

The Department of Civil and Environmental Engineering

by
Hao Ying
M.S.C.E, Louisiana State University, United States, 2011
May 2013

ACKNOWLEDGEMENTS

I would like to express my deepest gratitude and sincere appreciation to my exceptional advisor, Dr. Mostafa Elseifi, for his helpful guidance, constant encouragement, and commitment to complete this dissertation. His continuous support during my Ph.D. study is greatly appreciated. He continually and greatly assisted me with technical writing. His dedication and sincere interest in transportation engineering inspired me to always try my best. I am grateful for having him as a mentor. I also wish to thank my academic committee advisors, Dr. Louay N. Mohammad, Dr. Hak-Chul Shin, and Dr. Ayman Okeil for their cooperation, guidance, and patience.

I would like to acknowledge the support of the Louisiana Transportation Research Center (LTRC) for providing me access to state-of-the-art research facilities. Thanks are due to Dr. Louay N. Mohammad and the other LTRC asphalt group personnel for their help and assistance in this dissertation. Thanks to Bhanu Vijay Vallabhu and Samuel Cooper III for helping me with preparation and testing of asphalt specimens, which was of great values to this research.

Finally, I would like to express my gratitude to my parents and my wife Xiaoling Tan for their constant support, patience and sacrifice through the years; Furthermore, I would like to thank Shen Shang, Yida Zhang, Yin Feng, Saman Salari, Samuel (Sam) Cooper, and Karthik Dasari for their encouragement and helps during these years.

TABLE OF CONTENTS

ABSTRACT

The theoretical investigation of Hot-Mix Asphalt (HMA) response in the dynamic modulus and the semi-circular bending (SCB) laboratory test procedures is necessary to understand the influence of various design parameters on the performance of the mix. In addition, laboratory tests such as the dynamic complex modulus assume that this material can be dealt with as a homogeneous material while overlooking the particulate nature of this composite. The ultimate goal of this study is to develop an advanced theoretical framework, based on three-dimensional (3D) finite element (FE) methods and digital image analysis techniques to describe the behavior of HMA in two laboratory test methods: the dynamic complex modulus test and the SCB test. The developed models were validated against experimental testing results and were used to investigate the mix constitutive behaviors in these important laboratory test methods. In addition, the cracking and damage propagation in the SCB test was investigated using cohesive zone modeling techniques. The SCB test process as well as the propagation of damage was successfully simulated using 3D FE and cohesive elements. Based on the results of the FE model, it was determined that damage propagates in the vicinity of the notch and is mainly caused by a combination of vertical and horizontal stresses in the specimen. The effect of shear was negligible in progressing damage in the specimen. In addition, the results of FE model indicated that dissipated energy due to fracture is the predominant factor controlling failure in the SCB test. A fatigue crack propagation model was developed to predict the number of cycles to failure based on a cyclic SCB test and the generalized J-integral approach. A three-dimensional (3D) heterogeneous model was developed to describe the response of asphalt mixtures in the dynamic complex modulus test using an X-ray computed tomography (CT) image-based FE modeling approach. Results of the model showed that most of the deformations during the dynamic modulus test are derived from the mastic, which controls the viscoelastic behavior of the composite. In addition, the influence of mastic is more pronounced than the aggregates in the behavior of the mixture in the dynamic modulus test.

CHAPTER 1 – INTRODUCTION

1.1 Background

Cracking is the main deterioration mechanism in flexible pavements. Cracking appears at the pavement surface as longitudinal cracks and transverse cracks, as well as a combination of both that extend over the width of the pavement, creating hazardous conditions for the road users, Figure 1.1. The rehabilitation of pavement damage caused by cracking is usually costly. Therefore, it has been suggested that cracking, especially fatigue cracking, should be primarily addressed by adequate mixture and pavement designs as well as proper construction practices. The single edged notched beam (SENB) test, the semi-circular bending (SCB) test, the indirect tensile test (IDT) fracture parameter, and the DSCE test were suggested to predict the fracture behavior of HMA in the laboratory. Each of these test procedures has unique advantages and disadvantages (Li et al. 2007). On the other hand, the dynamic modulus test was introduced in NCHRP 9-19 as a simple performance test (SPT) that can be used to predict field performance ofasphalt mixes (Witczak et al. 2002).

Figure 1.1 Fatigue cracking at the pavement surface

The theoretical investigation of HMA responses in the aforementioned laboratory test procedures is necessary to understand the influence of various design parameters on the performance of the mix. Simplified analysis methods, such as the elastic theory, assume that HMA may be described as a linear elastic material, yet overlook the particulate nature of this composite. It is well-established that HMA is a heterogeneous, elasto-viscoplastic material that is characterized by a certain level of rigidity of an elastic solid body, yet, at the same time, flows

and dissipates energy by frictional losses as a viscous fluid (Elseifi et al. 2003; Masad et al. 2007). Due to the clear limitations of the elastic continuum theory, pavement engineers have recently paid considerable attention to the use of advanced modeling techniques for simulating the accurate behavior of asphalt mixtures. One approach, which is based on a micromechanical finite element (FE) method, may be used to predict more accurately the behavior and failure mechanisms in asphalt mixtures. In this approach, the particulate nature of asphalt mixtures is described as a composite, multiphase material, consisting of aggregates, mastic, and air voids (Dai et al. 2005). Each component is described separately, thereby defining load transfer mechanisms between these constituents is important.

1.2 Problem Statement

Dynamic modulus is the most common method to describe the viscoelastic behavior of asphalt mixtures at various loading frequencies and temperatures. It is also the main material property for asphalt mixtures used in the Mechanistic-Empirical Pavement Design Guide (MEPDG). The classic approach to predict flexible pavement response to traffic loading is by using the elastic continuum theory. The theory assumes that asphalt concrete may be described as a continuum elastic material, while overlooking the particulate and viscoelastic natures of this composite. The SCB test configuration has been used to the characterize crack resistance of asphalt mixtures by many researchers. However, limited studies have investigated the effects of creep deformation and the failure mechanisms during the SCB testing. In addition, only limited studies were found in the literature to assess the fatigue resistance of HMA in the laboratory using this test setup. There are several questions that must be investigated:

- Can elastic continuum methods accurately predict asphalt mixtures response to loading?
- What is the contribution of the mix components (aggregate, mastic, and air voids) on asphalt mixture performance?
- What are the main failure mechanisms in the SCB test?
- How does damage propagate in asphalt mixtures in the SCB test?
- What are the effects of creep deformation in the SCB test?

The ultimate goal of this study is to develop an advanced theoretical framework, based on Three-dimensional (3D) finite element (FE) methods and digital image analysis techniques to describe the behavior of HMA in two laboratory test methods: the dynamic complex modulus test and the

SCB test. The developed models were validated against experimental testing results and were used to investigate the mix constitutive behaviors in these important laboratory test methods. In addition, the cracking and damage propagation in the SCB test was investigated using cohesive zone modeling techniques and a fatigue crack propagation model was developed based on the cyclic SCB test and the generalized J-integral approach.

1.3 Research Approach

The research approach adopted in this study consisted of completing the following six main tasks:

Task 1: Literature Review

A comprehensive literature review was conducted to review the following topics: (1) dynamic modulus test and semi-circular bending test; (2) X-ray CT imaging analysis of HMA; (3) heterogeneous modeling of HMA; and (4) constitutive and cohesive modeling of HMA.

Task 2: Experimental Program

Two Superpave mixture types, including one conventional HMA and one warm-mix asphalt (WMA) mix, were evaluated. Reclaimed asphalt pavement (RAP) was used in the preparation of the mixes at a content ranging from 15 to 30%. The dynamic modulus test was conducted in accordance with AASHTO T342-11. The test was conducted by applying a uniaxial sinusoidal (i.e., haversine) compressive stress to an unconfined cylindrical test specimen. The test was conducted at four temperatures (4.4, 20, 37.8, and 54.4°C) and six loading frequencies of 0.1, 0.5, 1.0, 5, 10, and 25 Hz at each temperature to allow for the development of master curves to assess and to compare the viscoelastic characteristics of the different mixes. The SCB test was conducted on three HMA and two WMA mixes at three notch depths of 25.4 mm, 31.8 mm, and 38 mm; the test temperature was selected to be 25°C.

Task 3: Capture Digital Images Using X-ray Computed Tomography

The objective of this task was to characterize the three-dimensional internal structure of laboratory-compacted HMA samples, using X-ray computed tomography imaging techniques. The imaging of 2D horizontal slices was obtained using X-ray CT along the height of the test samples at a close interval before and after loading. The captured 2D images were then used in Task 4 to develop image-based FE mesh.

Task 4: Image-Based FE Meshing

Based on the captured images in Task 3, 3D scans were converted to numerical meshes, and subsequently imported to the FE software ABAQUS version 6.9 for stress and strain analysis in the dynamic modulus tests. The commercial software Simpleware was used in the conversion process. The developed FE mesh provided an accurate representation of the mix constituents in the compacted specimens and characterized microstructural features in the mix such as air voids, orientation and shape of aggregates, and mastic distribution.

Task 5: Finite Element Modeling of Dynamic Modulus and SCB Tests

A 3D FE model, which accurately simulated the SCB test procedure, was developed and validated, based on experimental test results. The model was used to achieve two main objectives: (1) to identify the main failure mechanisms during the SCB testing process; (2) to study damage evolution and propagation in the SCB test using cohesive zone elements. In addition, 3D, heterogeneous, FE model was developed to describe the response of asphalt mixtures in the dynamic complex modulus test using an X-ray computed tomography (CT). The experimental testing results for two Superpave mixtures including one conventional hot-mix asphalt (HMA) and one warm-mix asphalt (WMA) mix were used to validate and calibrate the developed models.

Task 6: Model the Crack Propagation Phase in the SCB Test

While the use of SCB has been successful to characterize the fracture resistance of HMA, only limited attempts were found in the literature to assess the fatigue resistance of HMA in the laboratory using this test setup. Fracture and fatigue resistances of asphalt mixes can be different as the former is tested under a monotonically increasing load while the latter is associated with a cyclic load, which causes progressive and localized damage in the material. A fatigue crack propagation model was developed to predict the energy release rate in this study based on the cyclic SCB test and the generalized J-integral approach. In order to validate the proposed model, existed laboratory measurements of cyclic SCB test were used in this study.

1.4 Scope of Study

Three-Dimensional heterogeneous finite element models were developed in this study based on X-ray CT images. The proposed 3D finite element model successfully predicted the dynamic

modulus of the composite mixes across a wide range of temperatures and loading frequencies. Meanwhile, the study provided an excellent opportunity to determine the effects of mix constituents on the mix behavior in the dynamic modulus test and to study the influence of aggregate stiffness on the mix response in the dynamic modulus test. In addition, a fatigue crack propagation model was developed based on the cyclic SCB test and the generalized J-integral approach. Further, the effect of shear stresses and creep deformation on the SCB test results obtained at intermediate temperature was investigated.

In this dissertation, a paper-format was used in which each chapter is considered a standalone work with minimal references to other parts of the study. This format hypothesizes that a technical paper will result or has resulted from each chapter; therefore, each chapter possesses its own conclusions and references. An effort was, therefore, made to include in each chapter the necessary background, with special care to avoid redundancy. General background related to this study is presented in Chapter 2.

CHAPTER 2 – LITERATURE REVIEW

2.1 Introduction

Hot-mix asphalt is a viscoelastic and thermoplastic material characterized by a certain level of rigidity of an elastic solid body. At the same time, HMA flows and dissipates energy by frictional losses as a viscous fluid (Elseifi et al. 2003). As with any viscoelastic material, HMA response to stress is dependent on both temperature and loading time. At high temperatures or under slow moving loads, HMA may exhibit a purely viscous flow. This behavior results in load-associated problems, such as rutting due to its low shear modulus, as well as an inability to preserve its shape. However, at low service temperatures or rapid applied loading, HMA becomes progressively harder and eventually brittle, which makes it vulnerable to non-load-associated problems, such as low-temperature cracking. Susceptibility to fatigue-associated problems is more critical at normal (intermediate) temperatures, because a significant part of the traffic loads are applied at these temperatures.

One major distress that is considered in mix design is rutting of HMA. Rutting occurs in the pavement as a result of traffic loads. Rutting generally develops during hot weather when the asphalt is soft and viscous as a result of traffic load. It can be identified by a surface depression in the wheel path. At high temperature, rutting can also lead to bleeding, which is a phenomenon in which asphalt binder rises to the pavement surface (Panoskaltsis 2005). Rutting also increases the chances of fatigue failure of flexible pavements (Panoskaltsis 2005). An excessive level of rutting at the pavement surface is considered a serious safety issue.

Another major distress that directly affects the serviceability and quality of flexible pavement structures is cracking. Cracking can be identified at the pavement surface as transverse cracks, longitudinal cracks, and a combination of both. The development of cracking through the pavement will create hazardous driving conditions for the road users. The fracture resistance of asphalt mixture is an important property, directly related to cracking.

2.2 Laboratory Characterization of HMA

Three laboratory tests were conducted in this study to characterize the viscoelastic properties, cracking resistance, and rutting resistance of HMA: the dynamic complex modulus (|E*|) test, the Semi-Circular Bending (SCB) test, and the flow number test. The dynamic complex modulus

(|E*|) is an important design parameter for predicting rutting and fatigue cracking. Outputs from the dynamic modulus test may be used to create master curve, which is used to describe the behavior of mixtures over a wide range of temperatures and rates of loading. The dynamic modulus is also a required input parameter in the Mechanistic-Empirical Design Guide (MEPDG) software for pavement design. The flow number is the number of test cycles required until tertiary flow starts in the mixture. The higher the flow number, the longer the time until the tertiary flow in the mixture starts. The flow number varies with the change in asphalt content and percentage of air voids in HMA (Vassilis 2005). The semi-circular bending (SCB) test was conducted to evaluate asphalt mixture resistance to fatigue and cracking failure. The critical value of J-integral, as the critical strain energy release rate, was used to describe the mixture's resistance to fracture. A review of each test method is presented in the following sections.

2.2.1 Dynamic Modulus of Asphalt Mixtures

In the linear viscoelastic region, the stress-strain relationship under a continuous sinusoidal loading is defined by its complex modulus (E*). A complex number relates stress to strain for linear viscoelastic materials subjected to sinusoidal loading in the frequency domain; see Figure 2.1. The complex modulus is defined as the ratio of the amplitude of the sinusoidal stress at any given time, t, and the amplitude of the sinusoidal strain at the same time and frequency, resulting in a steady state response (Dougan et al. 2003):

$$E^* = \frac{\sigma_0}{\varepsilon_0} = \frac{\sigma_0 e^{i\omega t}}{\varepsilon_0 e^{i(\omega t - \emptyset)}} = \frac{\sigma_0 \sin \omega t}{\varepsilon_0 \sin(\omega t - \emptyset)} \quad (2.1)$$

$$\emptyset = \frac{T_i}{T_p} \quad (2.2)$$

where,
σ_o = peak (maximum) stress;
ε_o = peak (maximum) strain;
ø = phase angle, degrees;
ω = angular velocity;
t = time, seconds;
i = imaginary component of the complex modulus;
T_l = time lag (sec); and
T_p = period of sinusoidal loading (sec).

Mathematically, the dynamic modulus is defined as the absolute value of the complex modulus:

$$|E^*| = \sigma_o/\varepsilon_o \quad (2.3)$$

In the dynamic modulus test, stress level is varied until the target strain reaches a level of 100 μstrain. Two dynamic modulus test parameters have been recommended by NCHRP Project 9-19 (Witczak et al. 2002): one for permanent deformation at high temperature and one for fatigue cracking at intermediate temperature. The dynamic modulus test parameter for rutting matched well with the rutting resistance of mixtures used in experimental sections (Witczak et al. 2002). Only a fair correlation was found between cracking observed in the experimental sections and the dynamic modulus test parameter measured at 4.4 and 21.1°C.

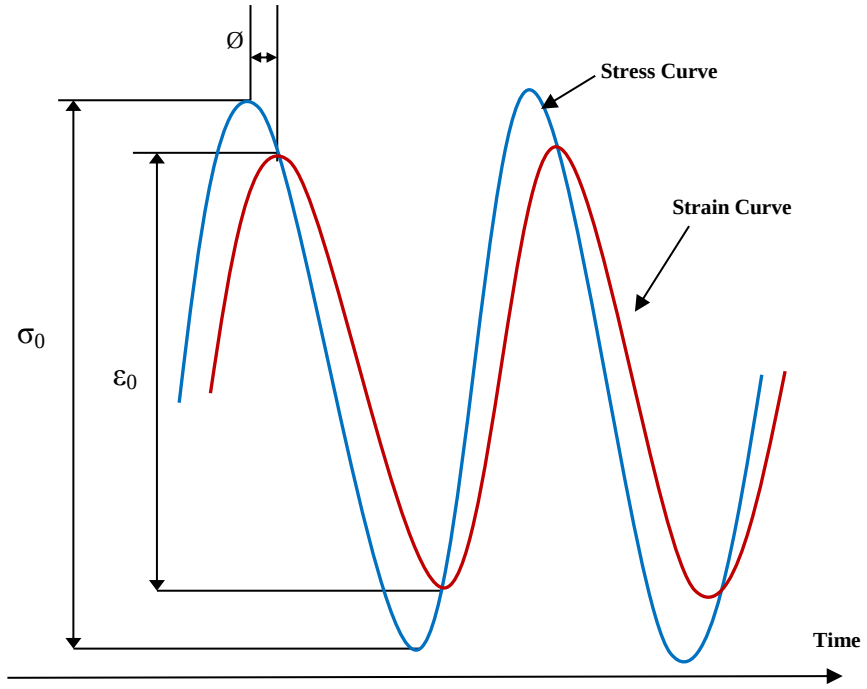

Figure 2.1 Dynamic (Complex) modulus test

According to the AASHTO mechanistic-empirical pavement design guide (MEPDG), which was developed during The National Cooperative Highway Research Program (NCHRP) Project 1-37A, the modulus HMA at all levels of temperature and rates of loading may be determined from a master curve constructed at a reference temperature, generally 21˚C. The master curve for asphalt concrete is a critical input for flexible pavement design in the MEPDG. The general master modulus curve may be mathematically described as (Witczak et al. 2002):

$$\log|E^*| = \delta + \frac{\alpha}{1+ e^{\beta+ \gamma (\log \omega_r)}} \qquad (2.4)$$

where,

E* = dynamic modulus;
ω_r = reduced frequency;
δ = minimum value of E*;
$\delta + \alpha$ = maximum value of E*; and
β , γ = parameters describing the shape of the sigmoidal function.

Dynamic modulus experimental data may be used to develop an extended master curve in accordance with the procedure suggested by Bonaquist and Christensen (2005). This procedure employs the sigmoidal function to describe the rate dependency of the complex modulus master curve (Bonaquist et al. 2005):

$$\log(E^*) = \delta + \frac{(Max - \delta)}{1 + e^{\beta + \gamma\left\{\log(t) - \frac{\Delta E_a}{19.14714}\left[\left(\frac{1}{T}\right) - \left(\frac{1}{295.25}\right)\right]\right\}}} \quad (2.5)$$

where,
E* = complex modulus;
t = loading time;
T =temperature in ° Rankine;
δ, β and γ = fitting parameters; and
Max = limiting maximum modulus.

You and co-workers (2007) simulated the dynamic modulus test of asphalt mixture using both two-dimensional (2D) and three-dimensional (3D) distinct element method (DEM), generated from X-ray CT images. The 3D internal microstructure of HMA in the X-ray CT images mixtures was used to develop 2D and 3D models. The mastic dynamic modulus and aggregate elastic modulus were used as input parameters to predict the asphalt mixture dynamic modulus in the DEM simulation. As shown in Figure 2.2, three replicates of a 3D DEM were generated from the cylindrical specimen, where the aggregates, mastics, and air voids are shown in the prisms. The measured dynamic modulus was computed from the strain response of the asphalt concrete under compressive loading cycles. Experimental measurements results were then compared with the predicted results from 2D and 3D DEM. The authors reported that 3D discrete element models can predict the asphalt mixture dynamic modulus over a range of temperatures and loading frequencies (You et al. 2007).

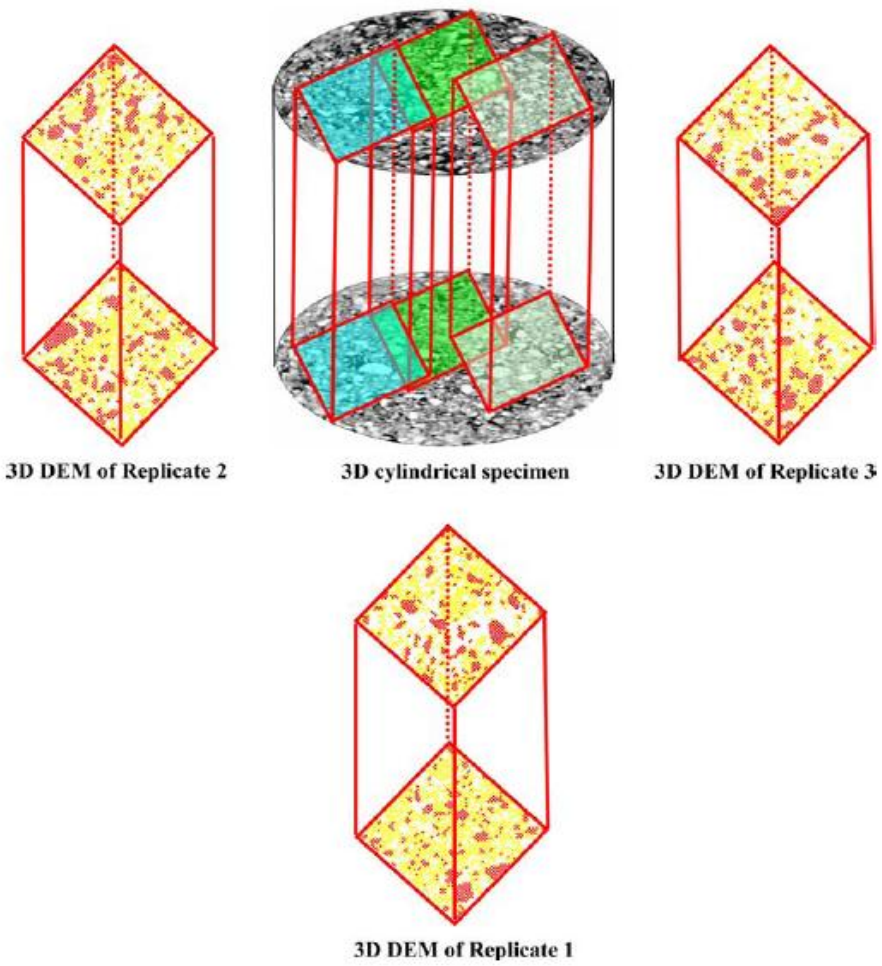

Figure 2.2 Demonstration of 3D rectangular prism DEM showing the aggregates, mastics, and air voids (You et al. 2007)

In 2008, You et al. developed a 3D microstructure-based DEM of asphalt mixtures to study the dynamic modulus from the stress-strain response during testing. The 3D models were generated from a number of 2D models, as shown in Figure 2.3. The dynamic modulus of the mastic and modulus of aggregate were used as input parameters of the DEM models. The stress-strain response of the 3D model was used to predict the asphalt mixture's stiffness modulus by using the aggregate and mastic stiffness. The relationship between the average stress tensor, $\bar{\sigma}_{ij}$, in a volume, V, of the continuous media was defined by (Cundall 1971; Itasca Consulting Group 2004a):

$$\overline{\sigma}_{ij} = \frac{1}{V}\int_{v} \sigma_{ij} dV \qquad (2.6)$$

The average stress tensor in a measurement circle was formulated as (You et al. 2008):

$$\sigma_{ij} = -\frac{1-n}{\sum_{N_p} V^{(p)}} \sum \sum \left| x_i^{(c)} - x_i^{(p)} \right| n_i^{(c,p)} F_i^{(c)} \quad (2.7)$$

where,
N_p = the centroids of the number of particles;
n = porosity within the measurement circle;
$V^{(p)}$ = volume of particle (p);
$x_i^{(c)}$ and $x_i^{(p)}$ = locations of a particle centroid and its contact, respectively;
$n_i^{(c,p)}$ = unit normal vector directed from a particle centroid to its contact location; and
$F_i^{(c)}$ = force acting at contact, (c).

Based on this analysis, You et al. (2008) reported that the 3D discrete element models were able to predict the mixture moduli across a range of temperatures (0°, −10, and −20°) and loading frequencies (0.1, 1, 5, and 10 Hz).

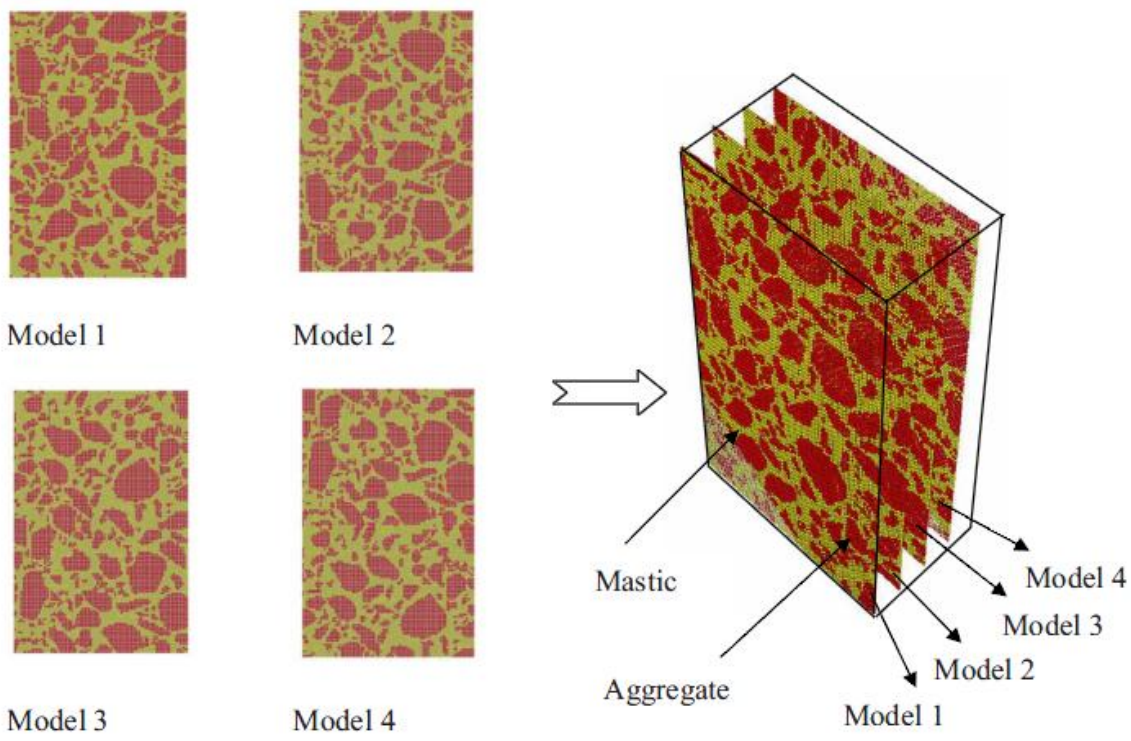

Figure 2.3 Generation of 3D model from 2D models (You et al. 2008)

Dai (2010) developed a micromechanical FE model for predicting the dynamic modulus and phase angle of asphalt mixtures using ABAQUS. The two-dimensional microstructure of asphalt

mixtures was captured using a high-resolution scanner to obtain gray-scale surface images of sectioned specimens (Figure 2.4a). FE meshes of image samples were generated within each aggregate and asphalt mastic (Figure 2.4b). Triangular elements in the mesh were bonded by sharing nodes along the aggregate boundary (Figure 2.4c). In this study, the generalized Maxwell model was used to describe viscoelastic asphalt mastic with calibrated parameters obtained from nonlinear regression analysis of the mastic test data on dynamic modulus and phase angles. The displacement-based FE simulations were conducted on the numerical samples under sinusoidal cyclic loading. Results of the simulation had good correlations with the asphalt mastic specimen measurements. The author concluded that the developed micromechanical FE model provides a computational tool for predicting the global viscoelastic properties of asphalt mixtures with captured microstructure and ingredient properties (Dai 2010).

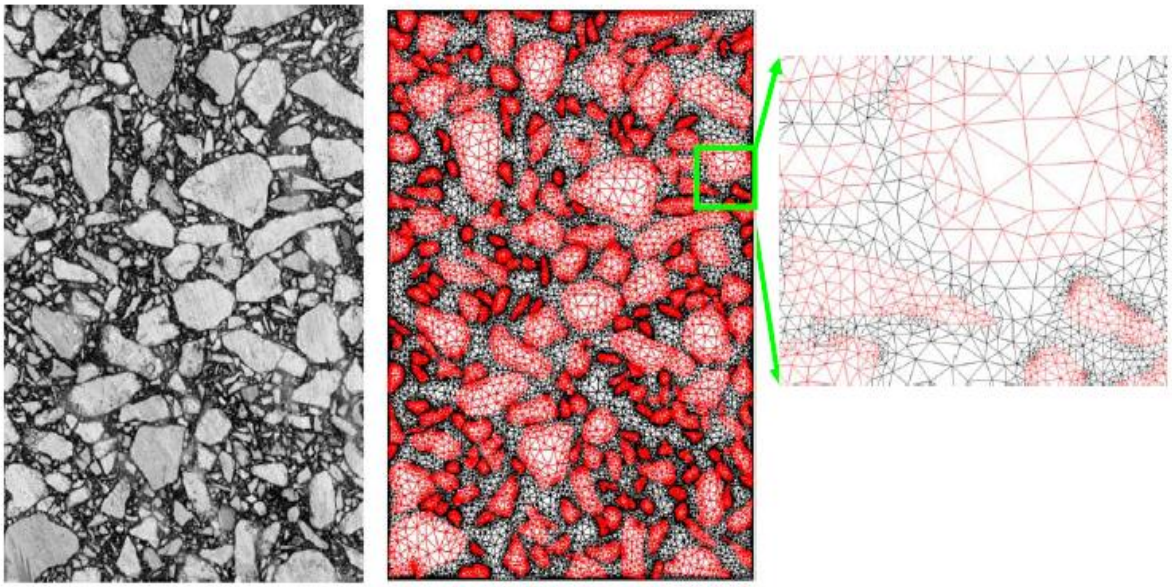

(a) (b) (c)

Figure 2.4 Two-dimensional mesh generation (Dai 2010)

Based on the successful utilization of microstructural-based DEM, Liu and You (2010) considered using a 3D viscoelastic model for microstructural-based DE simulation of asphalt mixture behaviors, based on a frequency-temperature superposition principle. The major objective of their study was to reduce the computation time required to run the 3D microstructural-based DE viscoelastic modeling process, which is extremely time-consuming.

The 3D microstructural-based DE viscoelastic model, which the authors used to predict the dynamic behaviors (dynamic modulus and phase angles) of an asphalt mixture, is shown in Figure 2.5. The white elements denote the asphalt sand mastic, and others represent coarse aggregates of different sizes. The randomly-created, irregular-shaped clusters were used to simulate aggregates, which consist of many discrete elements bonded together. The spaces between aggregates are filled with asphalt mastic and air voids. Dynamic modulus test of asphalt mixtures were conducted at four temperatures (5, 4, 13, and 21°C) and four frequencies (1, 5, 10, and 25 Hz).

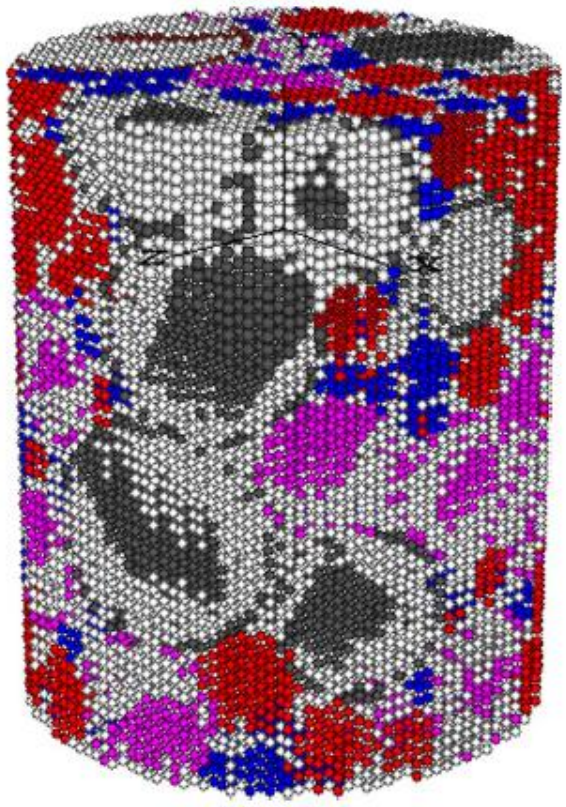

Figure 2.5 Example of the asphalt mixture microstructure model (Liu and You. 2010)

2.2.2 Semi-circular Bending Test of Asphalt Mixtures

The Semi-circular bend (SCB) test was proposed to predict the fracture behavior of HMA. The SCB test is based on fracture mechanics and the J-integral, which considers the elasto-plastic/visco-plastic relationship of HMA mixtures, rather than the stress intensity factor (K) commonly used in linear elastic fracture mechanics (Mull et al. 2006). The SCB test

configuration has been favored by many researchers, given that the specimen preparation and testing procedure for the SCB test is simple and quick; cores removed from the field can be tested (Li et al. 2007; Adamson et al. 1996). The specimen of SCB test is a half disk shape, 4-6 inch in diameter and 1.5-2 inch thick (Huang et al. 2009). In order to ensure that the crack initiates in the center of the specimen, a notch is cut in the bottom of the specimen. The specimen is loaded in compression using a three-point flexural device with a 0.05 in/min loading rate. The typical test temperatures are between 10°C (Huang et al. 2009) and 25°C (Molenaar et al. 2002).

If the distance between the supports is 0.8*D (specimen diameter), the tensile stress of the SCB test can be calculated using the following equation (Molenaar et al. 2002):

$$\sigma_t = 4.8\frac{F}{D} \tag{2.16}$$

where,

σ_t = maximum tensile stress at the bottom of the specimen;

F = load per unit width of the specimen at failure; and

D = specimen diameter.

Huang and co-workers (2009) stated that Equation 2.20 should be modified, because σ_t is only an indicator and not a true measure of the tensile characteristics of the HMA material. The adjusted equation is as follows (Huang et al. 2009):

$$\sigma = \frac{3pl}{2th^2} = \frac{6pl}{tD^2} \tag{2.17}$$

where,

σ = SCB tensile stress at the middle point of the lower surface;

P = compressive load;

L = distance between the supports;

t = specimen thickness;

h = specimen height = D/2; and

D = specimen diameter.

Huang and co-workers (2009) introduced the relationship between vertical deflection and stiffness based on the theory of elasticity:

$$S = C\left(\frac{L}{D}\right) * \left(\frac{P}{td}\right) = C\left(\frac{L}{D}\right) * \left(\frac{p}{d}\right) \tag{2.18}$$

where,

S = stiffness modulus;

L = spacing between supports;
D = specimen diameter;
C = L/D;
P = load;
t = specimen thickness;
d = deflection at the middle point of the lower surface of the specimen; and
p = P/t.

C is a function of the spacing between supports as shown in Equation (2.19):

$$C\left(\frac{L}{D}\right) = a * \left(e^{\frac{bL}{D}} - 1\right) = 1.977 * \left(e^{\frac{1.175S}{D}} - 1\right) \quad (2.19)$$

Therefore, Equation 2.(18) can be written as follows:

$$S = 1.977 * \left(e^{\frac{1.175L}{D}} - 1\right) * \left(\frac{p}{d}\right) \quad (2.20)$$

In order to make tensile stress equations more applicable to the SCB specimen geometry, Hofman et al. (2003) developed Equation (2.21) based on plane stress-state assumption. This equation only may be used to compute SCB stress with notched specimens:

$$\sigma_T = \frac{4.263P}{tD} \quad (2.21)$$

where,
σ_T = tensile strength, kPa;
P = maximum axial load, N;
t = specimen thickness, mm; and
D = specimen diameter, mm.

The SCB test is based on fracture mechanics and the J-integral, which consider the elasto-plastic/visco-plastic relationship of HMA mixtures (Mull et al. 2006). The critical value of J-integral (J_c) is determined using Equation (2.22):

$$J_c = \left(\frac{U_1}{b_1} - \frac{U_2}{b_2}\right)\frac{1}{a_2 - a_1} \quad (2.22)$$

where,
J_c= critical strain energy release rate (kJ/m^2);
b = sample thickness (m);
a = notch depth (m); and
U = strain energy to failure (N.m).

Birgisson and co-workers (2005) proved that fracture energy density is a fundamental fracture threshold in HMA using the SCB test method and the displacement discontinuity

micromechanical (DDM) boundary element method. A digital image correlation system was also used to describe the cracking behavior of composite materials at crack initiation at microstructural level. The fracture energy density of asphalt mixtures and cracking patterns were predicted using DDM. Figure 2.6 shows the simulated crack patterns for the mixture from crack initiation to major crack opening. The results of the study founded that fracture energy density for mixtures is a fundamental fracture threshold, and thus can be measured and predicted by DDM (Birgisson et al. 2005).

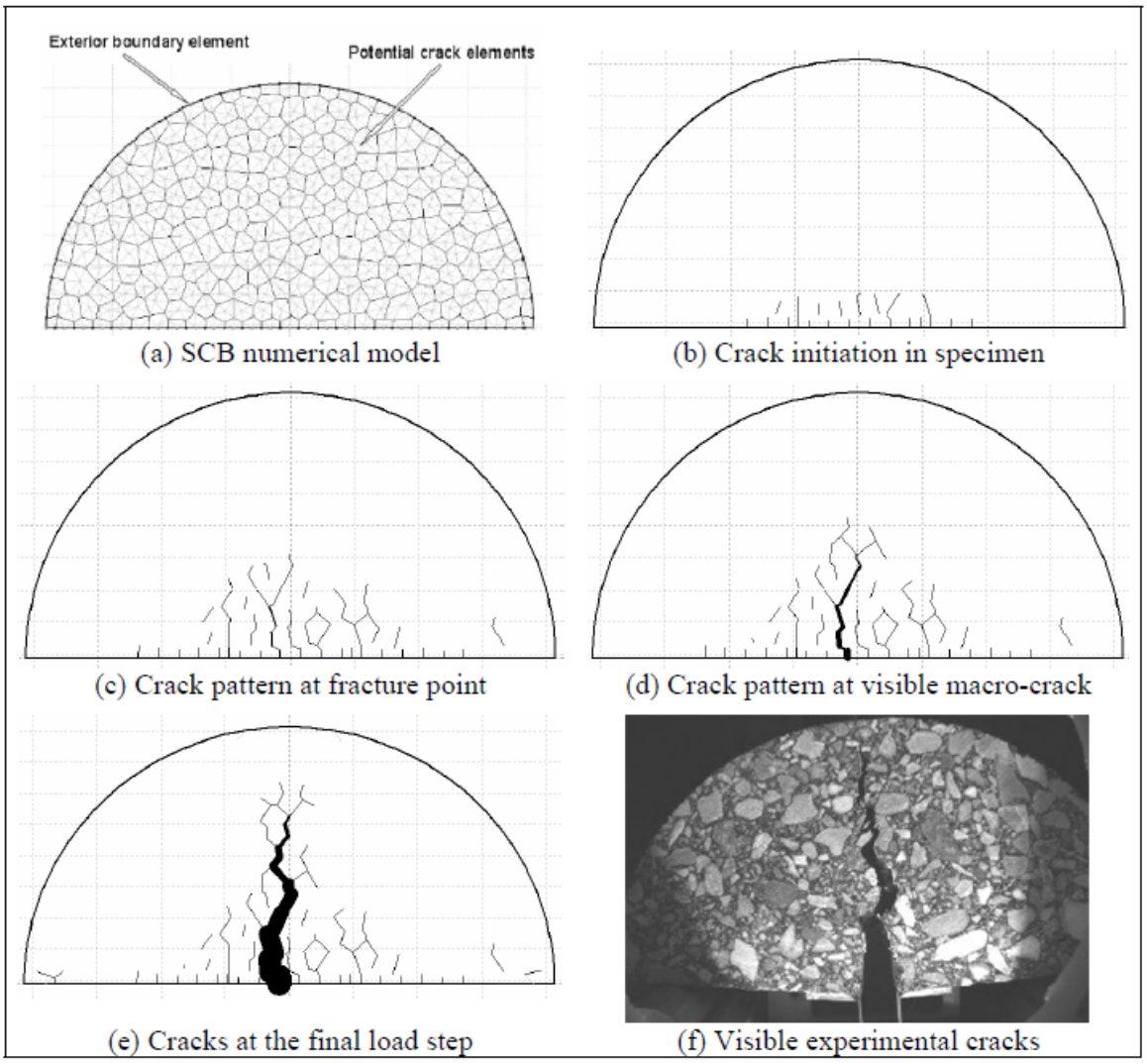

Figure 2.6. Predicted crack patterns for the mixture during the SCB test (Birgisson et al. 2005)

Li and Marasteanu (2006) evaluated the ability of the SCB test to evaluate the low temperature fracture resistance of HMA, using the cohesive zone model. Interface elements were used to

simulate the materials response under monotonic loading. These interface elements were placed over the initially undamaged material in front of the initial crack so that the crack could grow only in the symmetric plane of the SCB specimen. The mesh for the model is shown in Figure 2.7. The researchers also evaluated the factors affecting the mixtures' ability to resist fatigue cracking. Six asphalt mixtures were tested, representing a combination of factors such as binder type, binder modifier, aggregate type, and air void content. The loading rate was also varied, as well as the initial notch length. The SCB test was conducted at three low temperatures (-30°, -18°, and -6°C). Results indicated a strong dependence of low temperature cracking resistance on the test temperature. Additionally, significant effects of aggregate type, air void content, binder grade and modifier type were reported. The effects of loading rate and initial notch depth were observed only for the warmest test temperature. The authors also noted that the test was conducted with satisfactory repeatability, as indicated by the low coefficient of variation (Li and Marasteanu 2006).

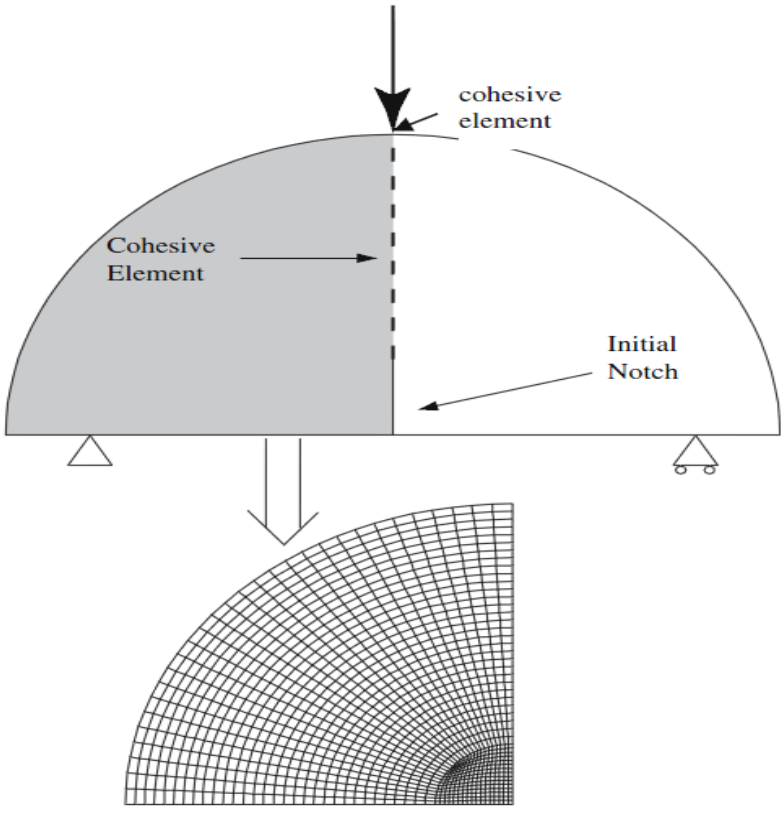

Figure 2.7 2D Finite element mesh of SCB specimen (Li and Marasteanu 2006)

Huang et al. (2005) compared the ability of the semi-circular bend test to characterize the tensile strength of HMA mixtures with indirect tension testing (IDT). Comparisons of the SCB and IDT results of 16 mixtures were conducted both analytically and numerically through the use of FE modeling, using ABAQUS software. Results from the study indicated the SCB test was capable of providing consistent results. The authors also noted several advantages of the semi-circular bending configuration, such as ease of sample preparation and load frame configuration highlighted as distinct advantages of the test method (Huang et al. 2005).

Li and co-workers (2009) used the SCB fracture test to evaluate the performance of asphalt mixture resistance to a low temperature fracture. The test was performed at three low temperatures (-30°C, -18°C, -6°C), two loading rates (0.00015 mm/s and 0.005 mm/s) and an initial notch length (30 mm and 50 mm). Fracture energy was calculated from the experimental data by using the following equation:

$$G_f = \frac{W_0 + mg\delta_0}{A_{lig}} \tag{2.23}$$

where,
W_0 = the area below the measured load deformation curve;
m = weight of the specimen;
g = acceleration due to gravity, 9.81 m/s2;
δ_0 = deformation at the final failure of the specimen; and
A_{lig} = area of a ligament.

Experimental results showed the dependence of a low temperature fracture resistance on the test temperature. Results of the analysis showed that fracture resistance of asphalt mixtures is significantly affected by types of aggregate and air void content; the cracking resistance of asphalt mixtures is related to the significance of binder grade and modifier type. The authors also found that the loading rate and initial notch length delivered a significant effect on the fracture energy at the highest test temperature; however the effect was strongly diluted at the two lower temperatures.

Wu and co-workers (2009) evaluated a finite element analysis technique using the embedded discontinuity method (EDM) to model cracking in HMA mixes. The SCB bending test was chosen as an example to evaluate the EDM in the study. In EDM, the elemental displacement field may be decomposed into the elastic part u^e and the cracking part u^c (Wu et al. 2009):

$$u = u^e + u^c \quad (2.24)$$

where,
u^e = elastic displacement which is smooth across the element; and
u^c = cracking displacement, which is discontinuous and has a jump along the embedded crack interface.

Figure 2.8 shows an example element in EDM. The elemental displacement fields are interpolated from nodal displacements using classic finite element shape functions (Wu et al. 2009):

$$u = \sum_{\alpha \in A} N_\alpha u_\alpha = \sum_{\alpha \in A} N_\alpha (u_\alpha^e + u_\alpha^c) = \sum_{\alpha \in A} N_\alpha u_\alpha^e + \sum_{\alpha \in A} N_\alpha w \quad (2.25)$$

where,
α = subscript indicates node number; and
N = finite element shape function.

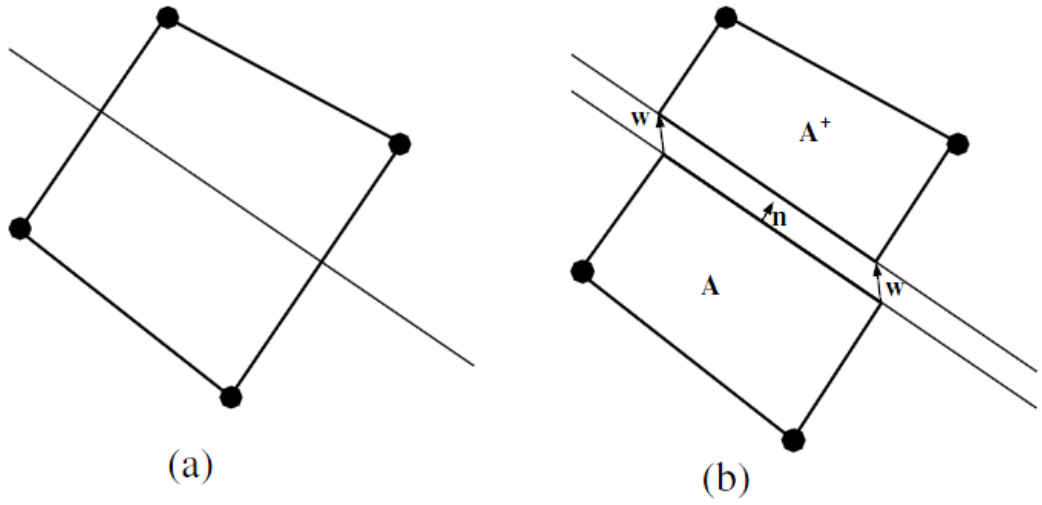

Figure 2.8 Finite element with a crack with uniform opening: (a) without cracking; and (b) with uniform displacement jump across the crack line (Sancho et al. 2007).

The cohesive crack model was used to describe the HMA cracking development (Wu et al. 2009):

$$t = f(\tilde{w}) \frac{w}{\tilde{w}} \quad (2.26)$$

where,
t = the residual traction acting across the crack faces;
w = the crack opening displacement vector; and
$\tilde{w}$ = the historical maximum magnitude of w.

The scalar function *f* defines the classical softening function under pure opening mode (Wu et al. 2009):

$$f(\tilde{w}) = f_t \exp\left(-\tilde{w} \cdot \frac{f_t}{G_f}\right) \quad (2.27)$$

where,
f_t = the tensile strength; and
G_f = the specific cohesive fracture energy.

Results indicated that EDM is a very promising finite element analysis technique, yet additional research is necessary to make the analysis more robust (Wu et al. 2009). Aragao and Kim (2010) conducted a comprehensive study by combining an SCB test and an FE method to characterize fracture properties of asphalt mixtures, subjected to a wide range of loading rates at intermediate temperature conditions. A high-speed camera with a digital image correlation system was used to monitor the local fracture behaviors at the initial notch tip of the SCB specimens. The SCB fracture tests are simulated by means of a finite element method, based on viscoelasticity and cohesive zone fracture theory. Dynamic frequency sweep tests were conducted to identify the linear viscoelastic material properties of the mixture, identified using the generalized Maxwell model:

$$G'(\omega) = G_\infty + \sum_{i=1}^{n} \frac{G_i \omega^2 \rho_i^2}{\omega^2 \rho_i^2 + 1} \quad (2.28)$$

where,
G' (ω) = storage shear modulus;
ω = angular frequency;
G = long-time equilibrium modulus;
G_i = spring constants in the generalized Maxwell model;
ρ_i =relaxation time; and
n = number of Maxwell units in the generalized Maxwell model.

The shear relaxation modulus can be expressed in the time domain as follows:

$$G(t) = G_\infty + \sum_{i=1}^{n} G_i e^{-\frac{1}{\rho_i}} \quad (2.29)$$

where,
G(*t*) = shear relaxation modulus in time domain; and
t = loading time.

Assuming the Poisson's ratio of the mixture is time-independent and that the mixture is isotropic, the following expression relating the G(t) to E(t) can be written as:

$$E(t) = 2 \cdot G(t) \cdot (1 + V) \tag{2.30}$$

where,
E(t) = relaxation modulus in normal direction; and
ν = Poisson's ratio.

Material fracture properties were obtained by defining the cohesive strength and fracture energy. The experimental and predicting results matched well and revealed the rate-dependent fracture characteristics of asphalt mixtures at intermediate temperatures. Figure 2.9 presents the constructed finite element mesh and the boundary conditions, used to model the SCB fracture testing of HMA specimens.

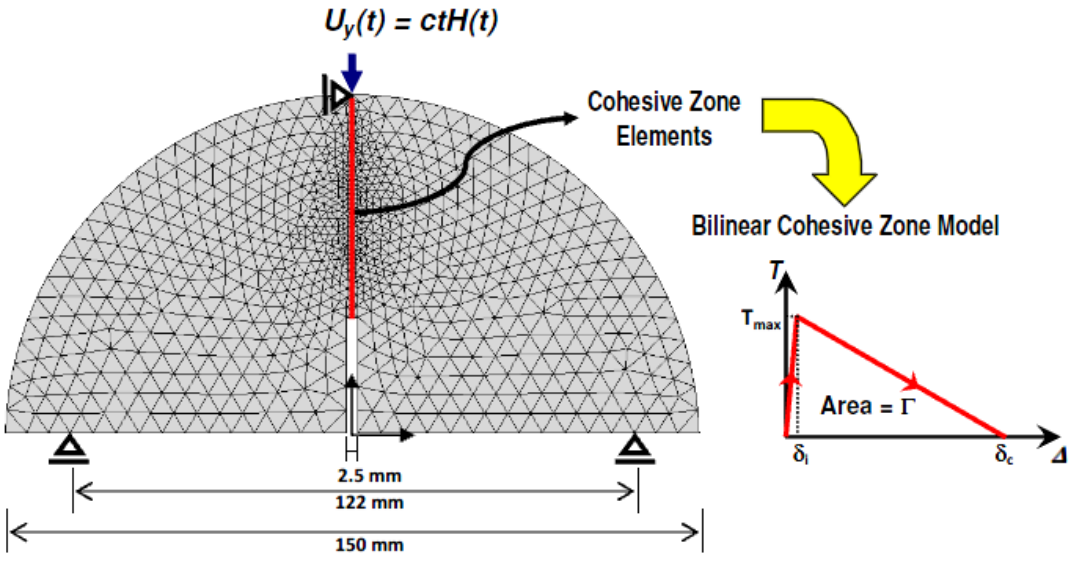

Figure 2.9 A finite element mesh and its boundary conditions to model the SCB testing (Aragao and Kim 2010)

Erkens and co-workers (2002a) introduced the asphalt concrete response (ACRe) material model, implemented in the finite element package CAPA-3D. The ACRe model was utilized to provide insights to the fracture processes occurring within an SCB specimen during testing. The model, based on the theory of rate dependent consistent plasticity is described as (Erkens et al. 2002a):

$$f = \frac{J_2}{P_a^2} - \frac{\left[-\alpha\left(\frac{I_1-R}{P_a}\right)^n + \gamma\left(\frac{I_1-R}{P_a}\right)^2\right]}{\sqrt{(1-\beta\cos(3\theta))}} = 0 \quad (2.31)$$

$$\cos(3\theta) = \frac{3\sqrt{3}}{2}\frac{J_3}{(J_2)^{\frac{3}{2}}} \quad (2.32)$$

where,
I_1 = the first stress invariant;
J_2 = the second deviator stress invariant;
J_3 = the third deviator stress invariant;
Pa = atmospheric pressure = -0.1 MPa; and
α, β, γ n R= model parameters, depending on material characteristics.

A constant displacement rate of 6 mm/sec was applied at the top of the 3D FE model for 100 time steps, using the dynamic analysis option of CAPA-3D in the study. The localization of tension and compressive damage along the diameter of the specimen occurs in the final stages of the test, as shown in Figure 2.10. Since the tensile deformation is much larger than the compressive damage, the compressive damage can be neglected.

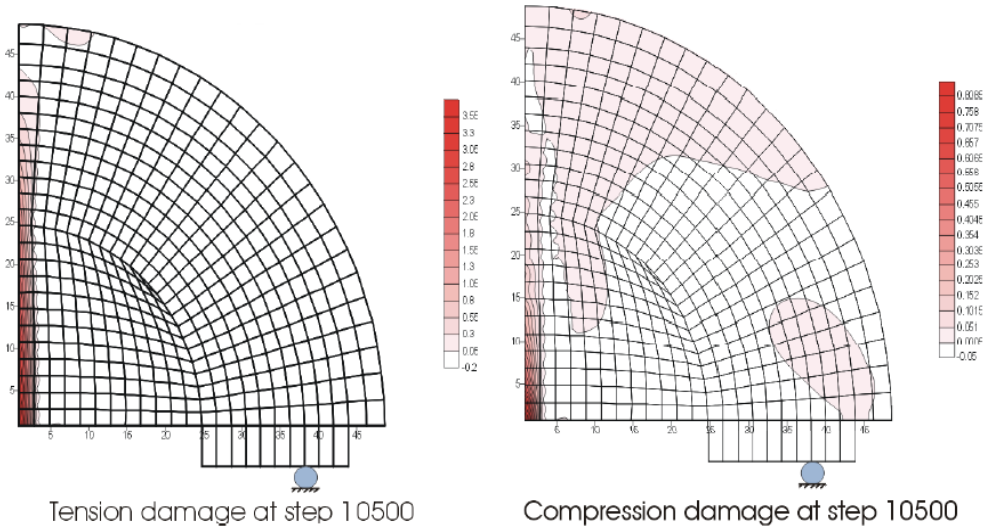

Figure 2.10 Damage localization (Erkens et al. 2002a)

2.3 X-ray CT Imaging Analysis of HMA

X-ray computed tomography (CT) is a nondestructive imaging technology, capable of acquiring a 3D or 2D image of the internal structure of a solid object, such as asphalt concrete. The directing planar X-rays pass through the specimen, along several different paths and from different directions, and are ultimately captured by the detector. The attenuations of X-rays

within a specimen are recorded for calculating the linear attenuation coefficients, which may be used to represent the spatial locations of the different components of the specimen. After finishing the collection of attenuations for a full rotation of the specimen, it is vertically moved downward for scanning the next slice.

X-ray CT has been frequently applied in recent years to characterize cracks or any damage in HMA by measuring the internal structure distribution of specimens, such as the locations of aggregates, as well as mastic and air voids. Image analysis techniques of X-ray CT images can be used to quantify damage parameters by measuring the cracking growth in mixtures under uniaxial loading. In order to obtain a more accurate internal structure distribution, 2D cross-sectional CT images are necessary to reconstruct 3D visualization images of the specimens. 2D cross-sectional CT images were obtained in order to measure air void distribution and crack size in asphalt specimens at different depths. After capturing 2D cross-sectional images, a 3D visualization image of the sample may be reconstructed for importing to a computer in order to simulate the performance of the asphalt mixture under various loading and environmental conditions. As a benefit of this non-destructive technology, the intact sample may still be used for engineering properties tests, such as the dynamic modulus test and the flow number test. Hence, X-ray CT is an effective technology to study the relationship between asphalt microstructure and engineering properties.

Masad and co-workers (1998) recommended that X-ray CT image analysis procedures be used to quantify the internal structure of asphalt concrete. Internal structure is quantified in terms of aggregate orientation, aggregate contacts, and air void distribution in specimens compacted in the SGC and LKC. An X-ray CT was used to obtain images from four specimens. All specimens were cut vertically into three vertical sections, using a diamond saw. Two images were captured subsequently from the two faces of each cut. A total of six images were acquired for each specimen. Before the analysis, air voids, asphalt binder, and aggregates phases were defined by choosing threshold gray intensity. The aggregates display different colors, depending on the mineral composition; it is difficult to separate the aggregates from the other two phases. In order to solve this issue and to isolate the air voids, the authors transformed the original image into a binary image of black and white phases, as shown in Figure 2.11. The white area represents the region of air void. The black area composes the region of the other two phases.

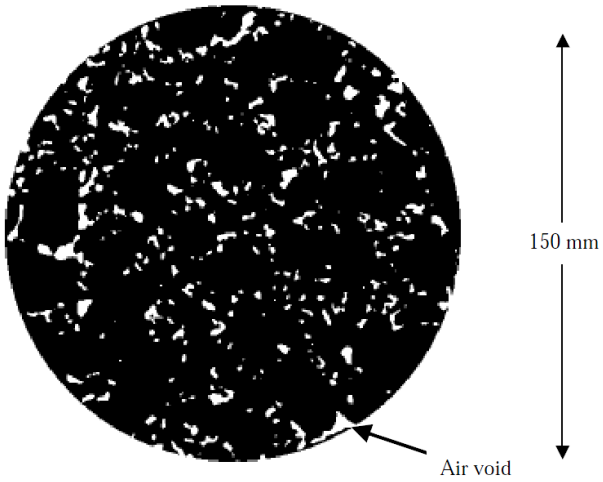

Figure 2.11 Image threshold to isolate air voids (white) (Masad et al. 1998)

Wang and co-workers (2001) used X-ray CT images and a virtual sectioning technique to reconstruct three-dimensional structures and to obtain cross-sectional images needed for the damage quantification. The specimen was moved downward in order to scan slices along a certain height; these slices were obtained and stacked to produce a 3D volume structure. Figure 2.12 presents several cross-sectional images.

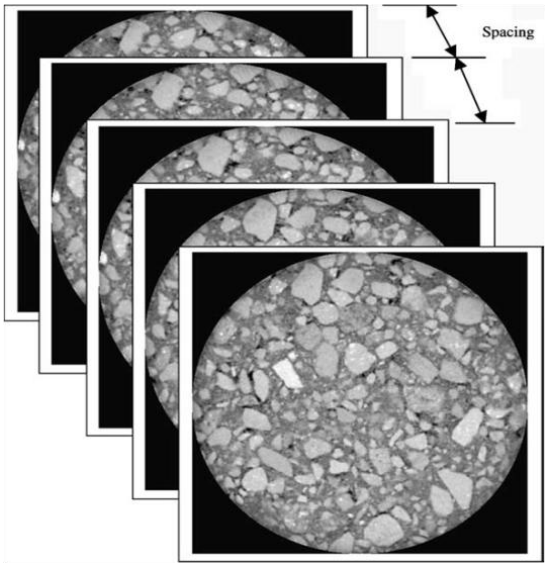

Figure 2.12 Cross-sectional images produced by XRT imaging (Wang et al. 2001)

Figure 2.13 presents the 3D visualization of an asphalt concrete specimen, where 81 slices (sectional images) were stacked to produce a 3D volume depiction. In addition, Wang and co-workers (2001) reported that tomography imaging carries a resolutions issue that in the

transverse directions (i.e., horizontal and vertical), the resolutions are significantly different. This result is due to the spacing between adjacent image sections, which is much larger than shown in the image resolution. In order to acquire smooth transitions and inherent connections between the images, an interpolation technique between the sectional images is recommended by the authors.

An X-ray CT technique was applied to measure the internal structure in asphalt mixes by Masad and co-workers (2002). Both experimental and analytical methods were employed to quantify the structure air voids in the study. An X-ray CT system and image analysis techniques were used to measure air void sizes at different depths within asphalt mixes. Horizontal images of the internal structure of asphalt mix specimens were captured by means of an X-ray CT system. Figure 2.14 shows an X-ray CT image of an asphalt concrete specimen with a diameter of 150 mm.

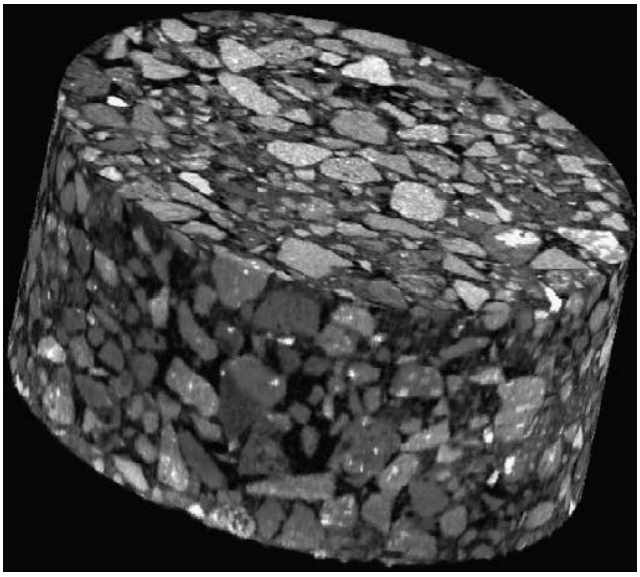

Figure 2.13 Visualization in 3D of an Asphalt Concrete Specimen (Wang 2001)

In 2007, Adhikari and You used X-ray CT imaging technology to characterize the aggregate orientation, aggregate gradation, mastic distribution, and air void distribution in an asphalt mixture. The dynamic modulus of sand mastic and asphalt mixtures were measured with uniaxial compression tests in the laboratory, using three temperatures and six loading frequencies. From the X-ray CT images, the locations of aggregate, air voids, and mastic were predicted based on the grayscale intensities, which ranged from 0 to 255. Corresponding to

different densities of these three phases (aggregate, air voids, and mastic) within the asphalt mix, the X-ray images consisted of 256 intensity levels of gray. The air void threshold value was chosen from 0-124; the mastic threshold value was from 125–203; and the aggregate threshold value was 126–255. Figure 2.15 shows the color segmentation applied to separate air voids, aggregate and mastic drawn from the gray intensity of images.

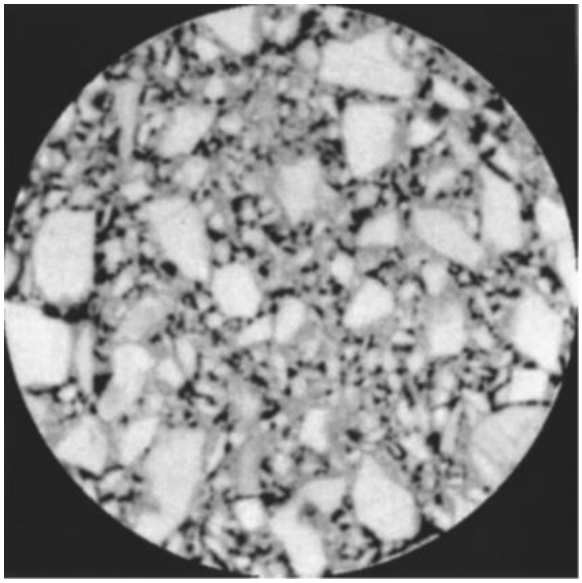

Figure 2.14 Horizontal Cross-Sectional X-ray CT image of Asphalt Concrete Specimen (Masad et al. 2002)

The study simulated three replicates of 3D Distinct Element Modeling (DEM) and six replicates of 2D DEM. For the purpose of acquiring accurate air void distribution, 2D images were visualized through vertical orientation. The aggregate elastic modulus and mastic properties were used as input parameters in this simulation. By recording the responses of the asphalt mastic, and mixture modules under a compressive load strain, this study calculated the dynamic moduli. The results from experimental measurements compared with the 2D and 3D predictions. Adhikari and You found that the 3D distinct element models have the ability to predict the mixture moduli during a range of temperatures and loading frequencies. The 3D models prediction was for superior to that of the 2D models. The modeling of asphalt mixture from a 2D to a 3D approach demonstrated significant progress.

Kassem et al (2008) employed X-ray CT and ground penetrating radar (GPR) to examine the quality of the compaction of thick asphalt layers within full-depth pavements in Texas. Air void distribution and uniformity in asphalt pavement cores from two different structural asphalt pavement sections were detected and analyzed. One incorporated a stone-filled (SF) Superpave mix and the other incorporated a traditional, dense-graded material. The X-ray CT images were separated into three phases: air voids, aggregate, and mastic by threshold. The threshold images were analyzed to determine the average percent of air voids using macros that were developed in an image processing software Image-Pro software (Media Cybernetics, Inc., MD). The three dimensional air voids distribution within the SF mix, corresponding to the results in Figure 2.16(a) is shown visually in Figure 2.16(b). The GPR and X-ray CT results displayed a good agreement, showing that the use of GPR and X-ray CT to evaluate the compaction of asphalt pavement is effective.

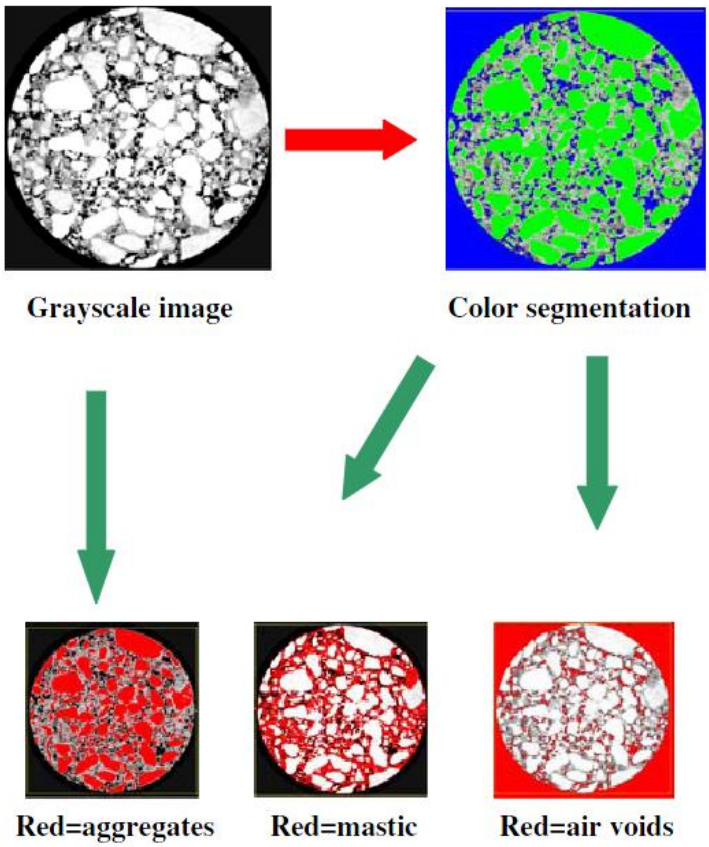

Figure 2.15 Color segmentation on X-ray CT gray scale images (Adhikari and You 2007)

Adhikari and You (2011) applied an X-ray CT technique to develop a three-dimensional (3D) discrete-element model of asphalt mixture. In order to get ideal images for an asphalt mixture, the researchers used X-ray CT equipment, with 420 kV of energy and 2.1 mA. A spherical resolution of 0:20 mm pixel was used in the X-ray CT images. The scanning obtained 2D X-ray CT images that were assembled to 3D images. Locations of aggregates, mastic, and air voids were acquired from the image-processing technique based on grayscale intensities, which ranged from 0 to 255. The air void level index was chosen as 0–124. The threshold index of an aggregate size larger than 1.18, 0.6, and 0.3 mm was selected as 202–255, 193–255, and 188–255, respectively (Adhikari and You 2011). Figure 2.17 shows the segmentation process to separate air voids, aggregate, and sand mastic.

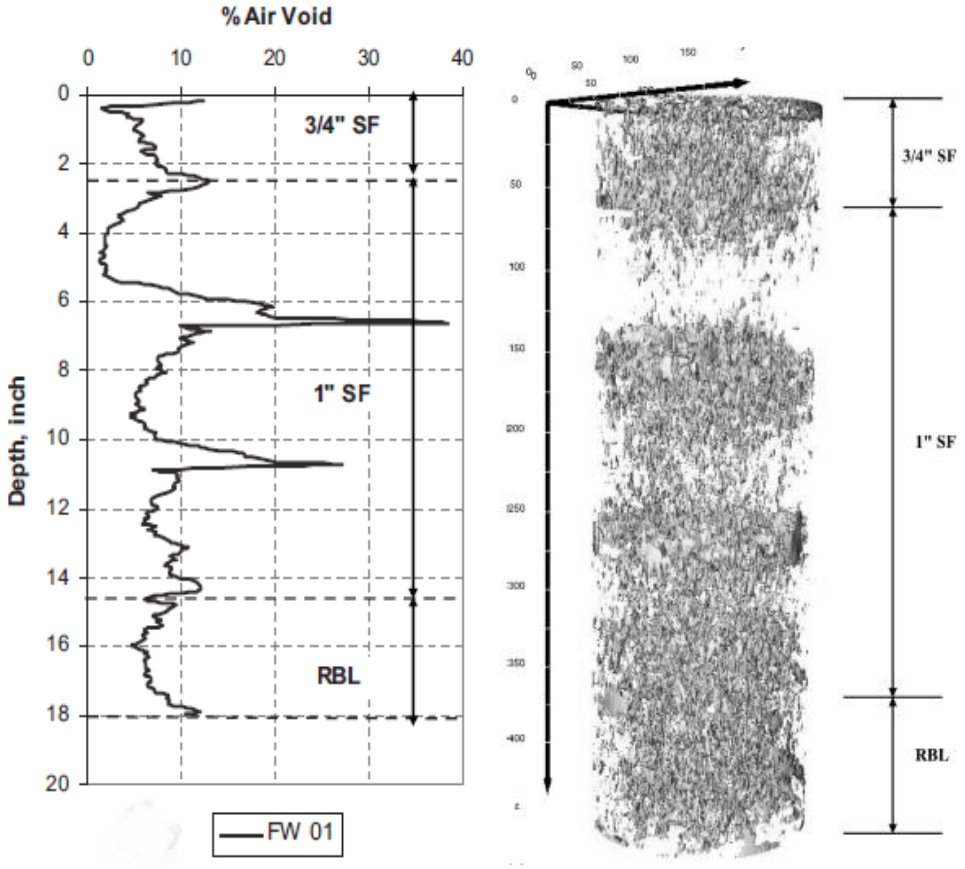

(a) (b)

Figure 2.16 Three-dimensional images of air void and the percentage air voids distribution plot (a), and GPR data (b) (Kassem et al. 2008)

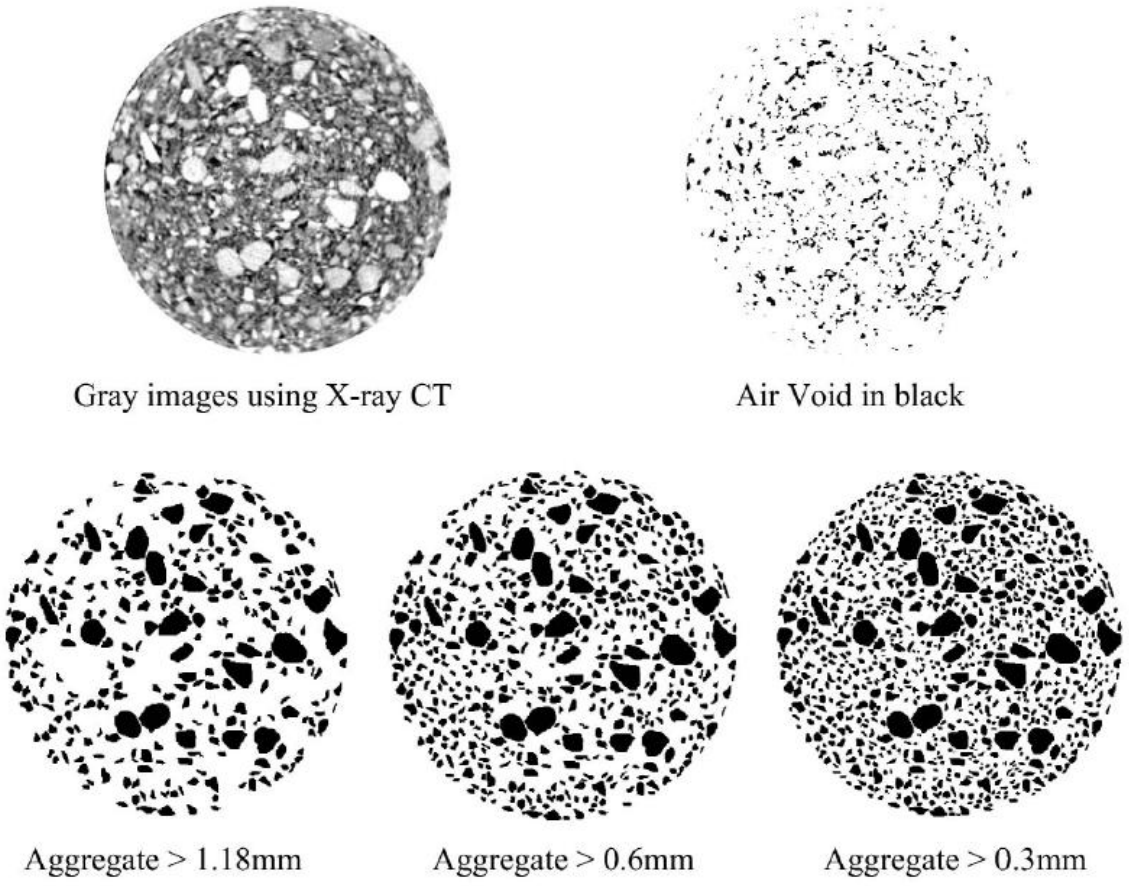

Figure 2.17 The X-ray CT images of asphalt specimen with air void before and after the segmentation (Adhikari and You 2011).

2.5 Constitutive Modeling of HMA

When a vehicle travels on top of a HMA pavement layer, three different types of strain develop in the material: elastic recoverable strain, viscous recoverable strain, and irrecoverable strain. Elastic strain is associated with the ability of HMA to respond to the applied load and to recover instantaneously the energy released during deformation. On the other hand, viscous strain involves a time-dependent deformation of HMA. Only part of the viscous strain is recoverable and is time-dependent. Scarpas and co-workers (1997) divided the total strain into elastic and viscoplastic components, with the purpose of showing a phenomenological approach for materials that exhibit plastic and creep deformation. The study and simulated the initiation and development of pavement distresses under various loading conditions. Damage evolution and

temperature effects were also considered in determining ultimate strength in the study. As shown in the Figure 2.18, the total strain can be separated into four components as follows:

$$\varepsilon = \varepsilon^{e} + \varepsilon^{p} + \varepsilon^{ve} + \varepsilon^{vp} \tag{2.33}$$

where,
ε = total strain;
ε^{e} = elastic strain, which is recoverable and time-independent;
ε^{p} = plastic strain, which is irrecoverable and time-independent;
ε^{ve} = viscoelastic strain, which is recoverable and time-dependent; and
ε^{vp} = viscoplastic strain, which is irrecoverable and time-dependent.

Assuming small strain deformations, the total strain (ε_{ij}) of asphalt concrete mix, subjected to an applied stress, can be decomposed into a recoverable viscoelastic strain (ε_{ij}^{vp}) and an irrecoverable strain (ε_{ij}^{nve}) (Abu Al-Rub et al. 2009):

$$\varepsilon_{ij} = \varepsilon_{ij}^{nve} + \varepsilon_{ij}^{vp} \tag{2.34}$$

Based on Schapery's theory (1969), the one-dimensional, recoverable strain subjected to an applied stress σ^{τ}can be described as follows (Abu Al-Rub et al., 2009):

$$\varepsilon^{nve}(t) = g_0 D_0 \sigma^{t} + g_1 \int_0^{t} \Delta D(\psi^{t} - \psi^{t}) \frac{d(g_2 \sigma^{t})}{d(\tau)}\, d\tau \tag{2.35}$$

where,
D_0 = instantaneous elastic compliance;
ΔD = transient compliance; and
g_0, g_1 , and g_2 = nonlinear parameters related to stress or strain level.

The reduced time ψ^{t} is a combined function of a stress/strain shift factor, a temperature shift factor, and other environment shift factors shown as (Abu Al-Rub et al. 2009):

$$\psi^{t} = \int_0^{t} \frac{d\xi}{a_T a_s a_e} \tag{2.36}$$

where,
a_T = temperature shift factor;
a_s = strain or stress shift factor; and
a_e = environment shift factor.

The three-dimensional isotropic constitutive relations can be separated into two parts: deviatoric stress part S_{ij} and volumetric stress part σ_{ij}, given as (Abu Al-Rub et al. 2009):

$$\varepsilon_{ij}^{nve} = \frac{1}{2G}\, S_{ij} + \frac{\sigma_{kk}}{9K}\delta_{ij} = \frac{1}{2}JS_{ij} + \frac{1}{3}B\sigma_{kk}\delta_{ij} \qquad (2.37)$$

where,
G = shear moduli;
K = bulk moduli;
J = shear compliances; and
B = bulk compliances;

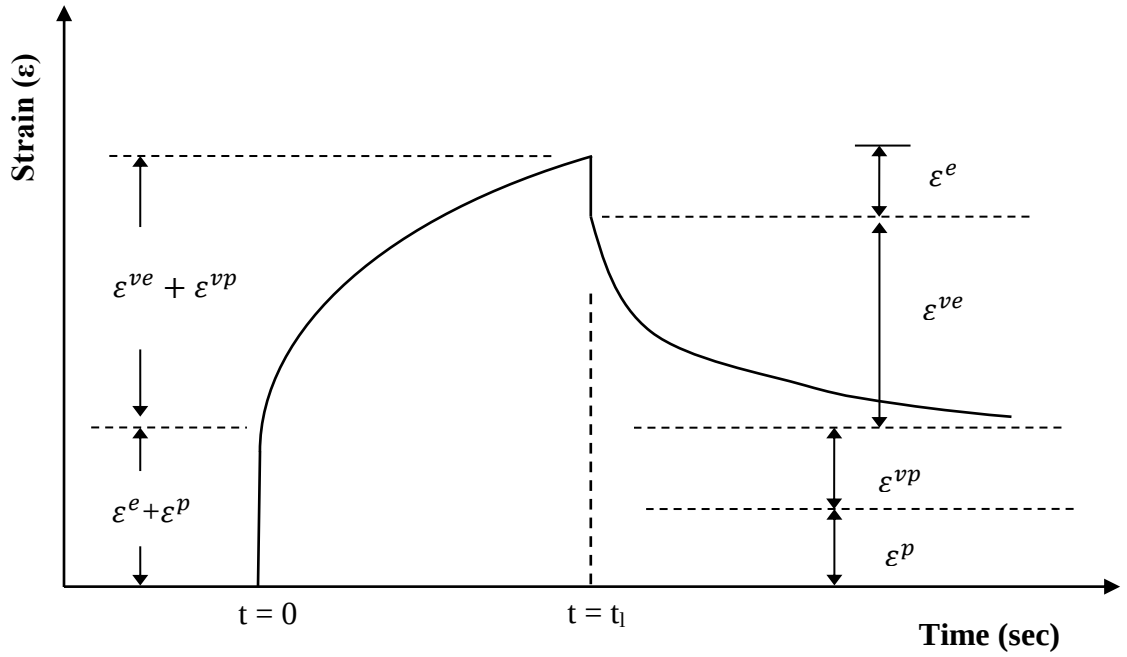

Figure 2.18 Schematic of the Strain Components in the Elasto-Visco-Plastic Material (Dessouky et al. 2005)

Applying Schapery's theory, the deviatoric and volumetric strain components can be written as follows (Lai and Bakker, 1996):

$$e_{ij}^{nve,t} = \frac{1}{2}g_0{}^t J_0 S_{ij}^t + \frac{1}{2}g_1{}^t \int_0^t \Delta J^{(\psi^t - \psi^t)} \frac{d\left(g_2^\tau S_{ij}^\tau\right)}{d\tau}\, d\tau \qquad (2.38)$$

$$\varepsilon_{kk}^{nve,t} = \frac{1}{3}g_0{}^t J_0 S_{ij}^t + \frac{1}{3}g_1{}^t \int_0^t \Delta B^{(\psi^t - \psi^t)} \frac{d\left(g_2^\tau \sigma_{kk}^\tau\right)}{d\tau}\, d\tau \qquad (2.39)$$

where,
$e_{ij}^{nve,t}$ = the deviatoric strain tensor;
$\varepsilon_{kk}^{nve,t}$= the volumetric strain tensor;
J_0 = instantaneous shear compliances; and
B_0 = instantaneous bulk compliances.

The deviatoric strain $e_{ij}^{nve,t}$ and volumetric strain $\varepsilon_{kk}^{nve,t}$ components can be represented as follows (Huang et al., 2007):

$$e_{ij}^{nve,t} = \frac{1}{2}\left[g_0{}^t J_0 + g_1^t g_2^t \sum_{n=1}^{N} J_n - g_1^t g_2^t \sum_{n=1}^{N} J_n \frac{1-\exp(-\lambda_n \Delta\psi^t)}{\lambda_n \Delta\psi^t}\right] S_{ij}^t -$$

$$\frac{1}{2} g_1{}^t \sum_{n=1}^{N} J_n \left[\exp(-\lambda_n \Delta\psi^t)\, q_{ij,n}^{t-\Delta t} - g_2^{t-\Delta t} \frac{(1-\exp(-\lambda_n \Delta\psi^t))}{\lambda_n \Delta\psi^t} S_{ij}^{t-\Delta t}\right] \quad (2.40)$$

$$\varepsilon_{kk}^{nve,t} = \frac{1}{3}\left[g_0{}^t J_0 + g_1^t g_2^t \sum_{n=1}^{N} B_n - g_1^t g_2^t \sum_{n=1}^{N} B_n \frac{1-\exp(-\lambda_n \Delta\psi^t)}{\lambda_n \Delta\psi^t}\right] \sigma_{kk}^t -$$

$$\frac{1}{3} g_1{}^t \sum_{n=1}^{N} B_n \left[\exp(-\lambda_n \Delta\psi^t)\, q_{kk,n}^{t-\Delta t} - g_2^{t-\Delta t} \frac{(1-\exp(-\lambda_n \Delta\psi^t))}{\lambda_n \Delta\psi^t} \sigma_{kk}^{t-\Delta t}\right] \quad (2.41)$$

Erkens and co-workers (2002b) developed a three-dimensional, strain rate sensitive, temperature and loading-history-dependent, constitutive model for HMA. The model was used to study the dynamic response of pavements subjected to impulse loads. An FE model was utilized for study of the initiation and propagation of damage in two flexible pavement structures under repeated loading conditions. Two main phases of material response, softening and hardening, were considered in the model (Figure 2.19). Nonlinear Newton-Raphson methodology was utilized to evaluate incremental volumetric and deviatoric plastic strain. The updated stress was computed by means of both trial stress and stress correction. The simulations may explain the influence of geometry and material characteristics on pavement damage patterns.

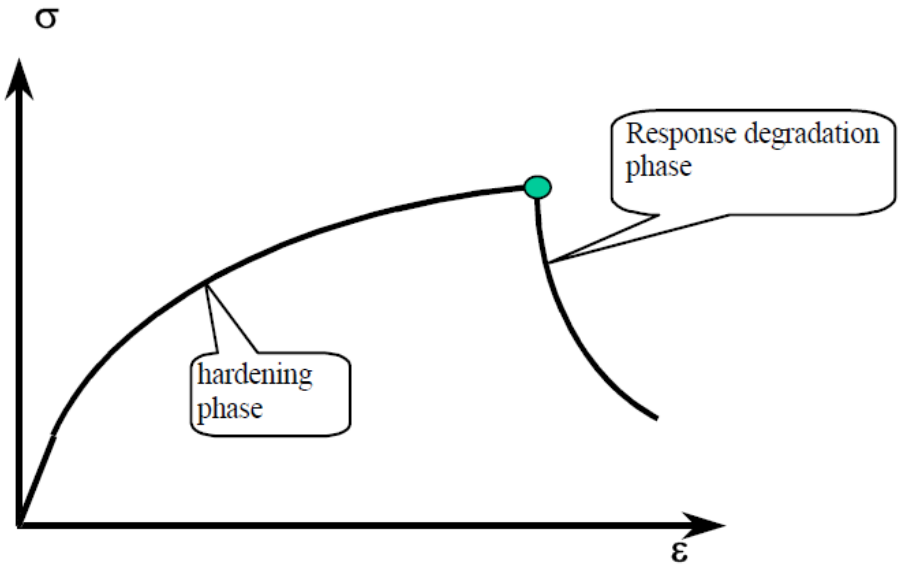

Figure 2.19 Schematic of main phases of material model response (Erkens et al. 2002b)

Based on the Hierarchical Single surface (HISS) plasticity-based model, Huang et al. (2002) developed the following viscoplastic, constitutive equations which considered the temperature and loading rate to be affecting factors:

$$F = \frac{J_2}{P_a^2} + \left[\alpha_{ps}\left(\frac{J_1}{P_a}\right)^n + \gamma\left(\frac{J_1}{P_a}\right)^2\right] * (1 - \beta \cdot \cos 3\theta)^{-m} = 0 \quad (2.42)$$

$$\cos 3\theta = \frac{3\sqrt{3}}{2} \cdot \frac{J_3}{J_2^{3/2}} \quad (2.43)$$

where,
Pa = the atmospheric pressure;
α_{ps} = the hardening of growth function; and
α_{ps}, β, γ, m and n = material parameters defining the yield surface.
J_1, J_2 and J_3 = first, second and third invariant of stress, respectively.

The modified HISS model to account for temperature effects is shown as following (Huang et al. 2002):

$$F = F(\sigma_{ij}, \alpha, \theta) \quad (2.44)$$

where,
σ_{ij} is the stress tensor component;
α is the hardening function; and
θ is the temperature.

Tashman et al. (2005) developed a microstructure-based, viscoplastic, continuum model to study the permanent deformation of asphalt concrete (AC). In the model, strain rate dependency, confining pressure dependency, dilation, aggregate friction, anisotropy, and damage were considered to be the factors, effecting the permanent deformation of AC at high temperatures. The effective viscoplastic strain can be obtained by integrating the effective strain rate, given as follows:

$$\dot{\bar{\varepsilon}}_{vp} = \frac{[\sqrt{X} - \beta(1-Y)]}{\sqrt{\frac{3}{2}X + 3\beta Y\sqrt{X} + 3\beta^2 + \frac{3}{2}\beta^2 Y^2}} \sqrt{\dot{\varepsilon}_{ij}^{vp}\,\dot{\varepsilon}_{ij}^{vp}} \quad (2.45)$$

$$X = \frac{1}{3} - \frac{4}{9}\sqrt{24}\mu\left(\frac{\Delta}{3+\Delta}\right)^2 \quad (2.46)$$

$$Y = \frac{4}{3}\sqrt{24}\lambda\left(\frac{\Delta}{3+\Delta}\right)^2 \quad (2.47)$$

where,

λ and μ = anisotropy coefficients that reflect the effect of the aggregate anisotropic distribution on the confining and shear stresses, respectively;
β = aggregate interlocking and dilation; and
Δ = anisotropy of aggregate distribution.

Mathematical modeling of HMA response to loading demands the prediction of strain accumulation under a variable loading time and temperature. Viscous deformation depends on three parameters, which are the stress level, time, and temperature. Al-Qadi and Elseifi (2004) described the isotropic viscoelastic behavior of HMA under variable loads, using a time-hardening model:

$$\dot{\varepsilon}^c = A\sigma^n t^m \tag{2.48}$$

where,
$\dot{\varepsilon}^c$ = creep strain rate;
σ = constant stress;
t = time; and
A, m, n = fitting parameters function of the temperature.

To determine the fitting parameters of Equation (2.48), a newly-developed laboratory variable creep load test was developed. This test consists of applying 10 different load levels to the specimen while holding each load for a period of 60 sec. A recovery rest period of 350 sec was set between each load level to allow the material to recover some of the viscous deformation. Laboratory-determined material characteristics were incorporated into a 3D FE model to predict pavement response to vehicular loading. Results of the FE viscoelastic model were in agreement with field measurements; the FE model successfully simulated retardation of HMA responses in the transverse direction and rapid recovery of HMA in the longitudinal direction. Moreover, the developed model allowed a prediction of permanent deformation at the surface and a partial recovery after load application.

While an asphalt mixture behaves as a viscoplastic material, coarse aggregate particles are assumed to behave elastically in a heterogeneous modeling approach. The linear elastic model for the coarse aggregate particles is as follows:

$$\sigma_{ij}(t) = C^E_{ijkl} . \varepsilon_{kl}(t) \tag{2.49}$$

where,
$\sigma_{ij}(t)$ = stress as a function of time;
$\varepsilon_{kl}(t)$ = strain as a function of time;

C_{ijkl}^{E}= elastic modulus which is not time-dependent; and
t = time of interest.

The linear viscoelastic constitutive model for the asphalt matrix:

$$\sigma_{ij}(t) = \int_0^t C_{ijkl}^{VE}.(t-\tau)\frac{\partial \varepsilon_{kl}}{\partial \tau}d\tau \tag{2.50}$$

where,
C_{ijkl}^{VE}(t) = viscoelastic stress relaxation modulus which is time-dependent;
τ= time-history integration variable.

The linear viscoelastic stress relaxation modulus can be expressed as a Prony series:

$$C_{ijkl}^{VE}(t) = C_{ijkl}^{\infty} + \sum_{p=1}^{M} C_{ijkl}^{p} \exp\left(-\frac{C_{ijkl}^{p}}{\eta_{ijkl}^{p}}t\right) \tag{2.51}$$

where,
C_{ijkl}^{∞} and C_{ijkl}^{p}= spring constants in the generalized Maxwell model;
η = dashpot constants in the generalized Maxwell model; and
M = the number of dashpots.

Masad and co-workers (2007) developed an elastoviscoplastic model to describe the constitutive behavior of HMA at high temperatures. The rate form of the constitutive equation is obtained as follows:

$$\dot{\sigma}_{ij} = D_{ijkl}\left(\dot{\varepsilon}_{kl} - \dot{\varepsilon}_{kl}^{vp}\right) \tag{2.52}$$

where,
$\dot{\sigma}_{ij}$ = Stress rate tensor;
D_{ijkl} = Fourth-order time dependent viscoelastic stiffness tensor;
$\dot{\varepsilon}_{kl}$ = Strain rate tensor; and
$\dot{\varepsilon}_{kl}^{vp}$ = Viscoplastic component.

The viscoplastic component, which dominates the material response at high temperatures, is defined through the following flow rule:

$$\dot{\varepsilon}_{ij}^{vp} = \dot{\gamma}^{vp}\frac{\partial g}{\partial \sigma_{ij}} \tag{2.53}$$

where,
$\dot{\gamma}^{vp}$= viscoplastic multiplier that is nonzero only when plastic deformation occurs; and
g= viscoplastic potential function.

$$\dot{\varepsilon}_{ij}^{vp} = \Gamma\langle\phi(f)\rangle\frac{\partial g}{\partial\sigma_{ii}} \tag{2.54}$$

where,
$\Gamma\langle\phi(f)\rangle$ specifies the magnitude of $\dot{\varepsilon}_{ij}^{vp}$;
Γ = viscosity parameter; and
ϕ = overstress function that is typically taken as a power function of *f*.

"$\langle . \rangle$" is McCauley brackets, imply that

$$\langle\phi(f)\rangle = \begin{cases} 0, & \phi(f) \leq 0 \\ \phi(f) = f^N, & \phi(f) > 0 \end{cases} \tag{2.55}$$

where,
N = rate sensitivity parameter to be determined experimentally.

The yield function *f* is defined as follows:

$$f = \bar{F}\left(\sigma_{ij}\right) - k = 0 \tag{2.56}$$

where,
$\bar{F}\left(\sigma_{ij}\right)$= stress-dependent function.

The developed model incorporated critical microstructure properties, such as anisotropy and material damage. In addition, a yield surface based on the Drucker-Prager model was used to describe stress-dependency of the material. The Drucker-Prager model is given in the form:

$$f = \tau - \alpha I_1 - k = 0 \tag{2.57}$$

where,
τ = deviatoric shear stress;
I_1 = hydrostatic stress;
α = a parameter that reflects the material frictional properties of the material; and
k = a hardening parameter that reflects the combined effect of the cohesive and frictional properties.

The model was fitted to results of triaxial compression and extension tests, conducted on three contrasting types of mixtures. The model was then adapted a FE model to simulate the mix behavior at high temperatures. Results showed that the tensile strength of the mixes was much lower than its compressive strength. In addition, the effect of aggregate type on the mix performance against permanent deformation was clearly detected.

Dai and You (2007) presented a micromechanic FE framework to predict the viscoelastic properties of the asphalt mixtures. In the two-dimensional (2D) mixture microstructure, aggregates (elastic) and mastic (viscoelastic) were divided into different subdomains. The viscoelastic mastic was combined with elastic aggregates to predict the viscoelastic properties of asphalt mixtures in their study. The generalized Maxwell model was applied for viscoelastic asphalt mastic. The linear constitutive behavior for this Maxwell model can be expressed as (Dai and You, 2009):

$$\sigma_{ij} = E_{\infty}\varepsilon_{ij} + \int_0^t E_t \frac{d\varepsilon_{ij}(\tau)}{d\tau} d\tau \tag{2.58}$$

where,
E_1 = the relaxed modulus; and
E_t = the transient modulus as a function of the time.

The volumetric constitutive relationship was expressed as the combination of volumetric stress σ_{kk} and strain ε_{kk} :

$$\sigma_{kk}(\xi) = 3K_{\infty}\varepsilon_{kk}(\xi) + \int_0^{\xi} 3K_t(\xi - \xi') \frac{d\varepsilon_{kk}(\xi')}{d\xi'} d\xi' \tag{2.59}$$

where,
K_{∞}= the relaxed bulk modulus; and
$K_t(\xi - \xi')$ = the transient bulk modulus.

The formulation of the deviatoric behavior is:

$$\hat{\sigma}_{ij}(\xi) = 2G_{\infty}\hat{\varepsilon}_{ij}(\xi) + \int_0^{\xi} 2G_t(\xi - \xi') \frac{d\hat{\varepsilon}_{ij}(\xi')}{d\xi'} d\xi' \tag{2.60}$$

where,
G_{∞} = the relaxed shear modulus; and
$G_t(\xi - \xi')$ = the transient shear modulus.

A displacement-based incremental FE modeling scheme with a constant strain rate over each increment was developed in the following format (Dai and You 2009):

$$\Delta\sigma = K \cdot \Delta\varepsilon + \Delta\sigma^R \tag{2.61}$$

where,
$\Delta\sigma$ = incremental stress;
$\Delta\varepsilon$ = incremental stain;
K = incremental stiffness; and
$\Delta\sigma^R$ = the residue stress vector.

The incremental formulations of the volumetric and deviatoric behavior are (Dai and You 2009):

$$\Delta\sigma_{kk} = 3\left[K_{\infty} + \sum_{m=1}^{N} \frac{K_m \rho_m}{\Delta\xi}\left(1 - e^{-\frac{\Delta\xi}{\rho_m}}\right)\right]\Delta\varepsilon_{kk} + \Delta\sigma_{kk}^{R} \quad (2.62)$$

$$\Delta\hat{\sigma}_{ij} = 2\left[G_{\infty} + \sum_{m=1}^{N} \frac{G_m \rho_m}{\Delta\xi}\left(1 - e^{-\frac{\Delta\xi}{\rho_m}}\right)\right]\Delta\hat{\varepsilon}_{ij} + \Delta\hat{\sigma}_{ij}^{R} \quad (2.63)$$

where,
K_m = the bulk constants of the spring in the mth Maxwell element;
G_m = the shear constants of the spring in the mth Maxwell element; and
ρ_m = the spring constant.

2.6 Cohesive Modeling Technique

Cohesive zone model (CZM) was introduced by Dugdale (1960) and Barenblatt (1962). This model has been used increasingly for fracture modeling in many areas in order to study the fracture mechanisms in various materials. Figure 2.20 shows the CZM applied in a macro-crack domain. The domain, Ω, is divided into two domains, Ω1 and Ω2, and the CZM is inserted at the interface. The CZM approach is only suitable for predicting the crack propagation when a crack growth path is predictable. The cohesive zone model confines the fracture into a small zone. The non-zero traction stress, T, acting on the two opposite crack surfaces, is a function of a separation, Δ, which provides a phenomenological description of crack propagation. This nonlinear constitutive behavior of a cohesive crack is derived through a cohesive energy potential ϕ in the form:

$$T = \frac{\partial \emptyset}{\partial \Delta} \quad (2.64)$$

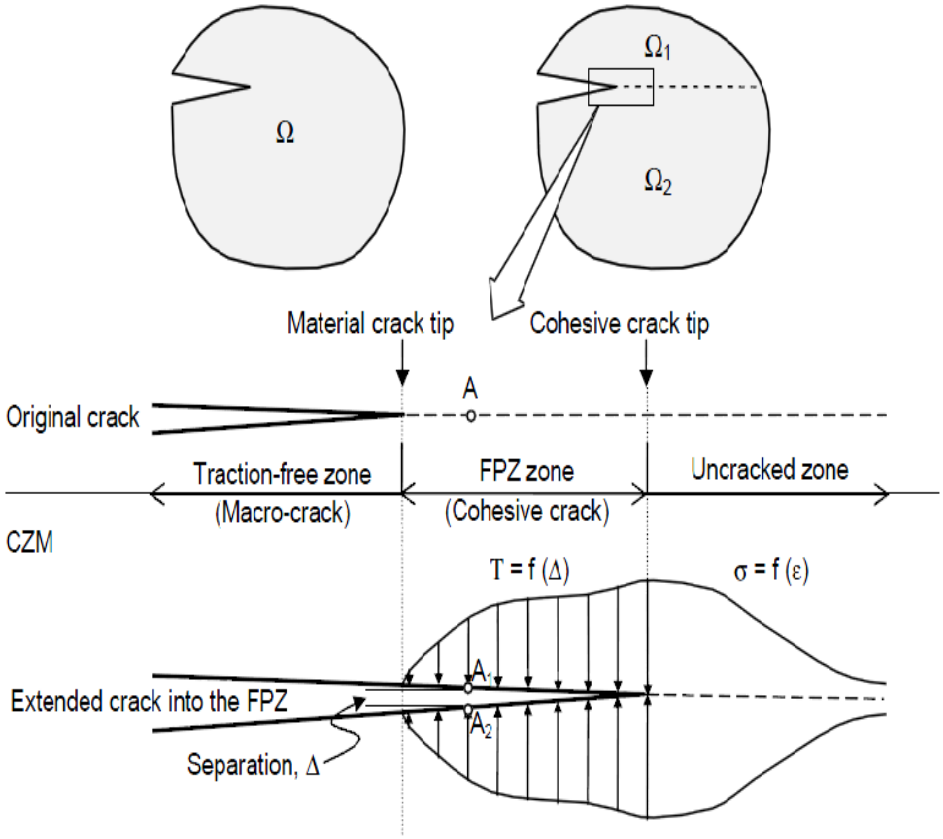

Figure 2.20 Crack formation in a fracture process zone with a cohesive zone model (Baek 2010)

A traction-separation law (TSL) explains the relationship between traction and separation in the CZM. The CZM can be described as the process of fracture in three aspects: (1) the strength of local material; (2) the amount of the cohesive energy potential; (3) the form of the cohesive energy potential; i.e., the shape of the T-Δ curve. Figure 2.21 illustrates a constant and exponential function of the TSL. The cohesive strength, T_0, keeps constant until Δ reaches a critical separation, Δc, whereas $T = T_0$. After the traction reaches the peak point, it starts to decrease and then vanishes at Δc. The fracture energy Γc, which represents the amount of dissipated energy per unit crack extension, can be computed based on the area under the T-Δ curve, as shown in Figure 2.21. The integration formulation of Γc can be written as:

$$\Gamma c = \int T(\Delta) d\Delta \tag{2.65}$$

where,
T is a function of separation, Δ.

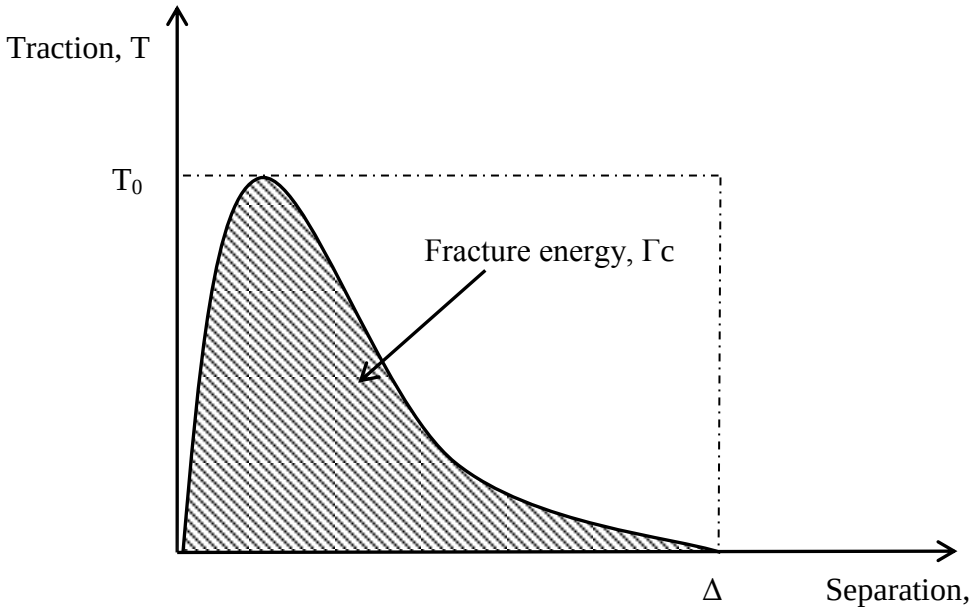

Figure 2.21 Traction–Separation Relationship for Cohesive Crack

Ortiz and Pandofi (1999) proposed a computationally-convenient, exponential form of cohesive energy potential, ϕ:

$$\phi = \exp(1)\, T_0 \Delta_C \left[1 - \left(1 + \frac{\Delta}{\Delta_c}\right) \exp\left(-\frac{\Delta}{\Delta_c}\right)\right] \tag{2.66}$$

$$\Delta = \sqrt{\alpha^2\left({\Delta_T}^2 + {\Delta_B}^2\right) + {\Delta_N}^2} \tag{2.67}$$

where,
α = the weight assigned to two sliding displacements;
Δ_T, Δ_B and Δ_N = opening displacement;
Δ_c = the critical separation Δ when T =T_0;
T is the work conjugate of Δ which can be expressed as:

$$T = \sqrt{\alpha^{-2}\left({T_T}^2 + {T_B}^2\right) + {T_N}^2} \tag{2.68}$$

where,
T_T, T_B and T_N = the tractions on the directions corresponding to displacements Δ_T, Δ_B and Δ_N.

Based on the theory of fracture mechanics, Soares et al. (2003) presented a numerical scheme in which the binder and the aggregates are considered to be distinct materials. CZM was utilized to crack propagation of HMA during the indirect tension test (IDT) in the study. Finite element meshes were generated from cross-sections of sawn, cylindrical, asphalt specimens. CZ elements were defined as the interface between the binder and the aggregates. Therefore, the crack can

propagate along a predefined path. The path definition and mesh generation are illustrated in Figure 2.22.

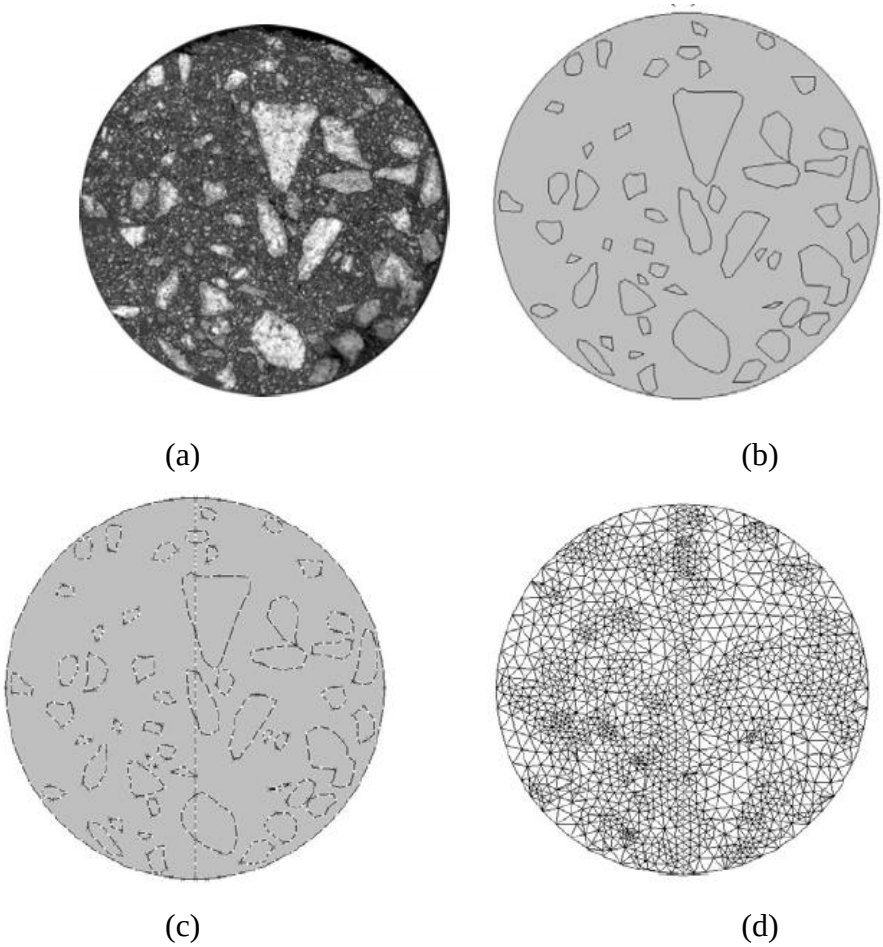

(a) (b)

(c) (d)

Figure 2.22 Steps in the finite element mesh generation: (a) Image Digitalization; (b) Geometry c) Crack Path definition; (d) FE Mesh (Soares et al. 2003)

Paulino et al. (2004) developed an intrinsic CZM, based on the energy potential for HMA. The intrinsic CZM was calibrated with a single-edge notched beam (SENB) test and validated with the IDT test. Since mesh regeneration at the crack front is not needed, the intrinsic CZM is not only more efficient in computation, but also robust enough to be applied in FE modeling. Song et al. (2006) studied the fracture behavior of asphalt concrete, using an intrinsic CZM to simulate the mixed-mode crack propagation in the SENB test. The cohesive parameters were calibrated with the test. An exponential cohesive law was applied to govern the separation and traction response along the cohesive zone and ahead of a crack tip, as illustrated in Figure 2.23. CZ elements were accomplished by applying the user element capability of the ABAQUS software.

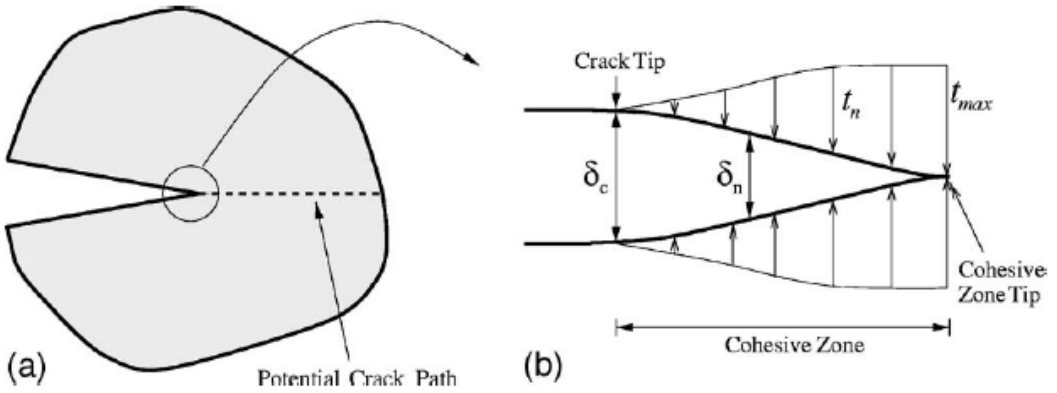

Figure 2.23 (a) Potential crack path definition in cohesive zone; (b) Displacement jump δ_n and corresponding traction t_n along a cohesive surface (Song et al. 2006)

In order to simulate damage growth due to cracks in viscoelastic media, Allen and Searcy (2001) proposed a nonlinear viscoelastic cohesive zone model, which can reflect nonlinear viscoelastic damage growth in the asphalt mixtures. The study assumed that the constitutive relations within the body can be simply represented by combining an elastic model of the coarse aggregate particles, as well as a viscoelastic model of the asphalt matrix that is composed of asphalt mastic, fine aggregates, and air voids. The model has the ability to predict viscoelastic damage evolution, material softening, and final fracture failure of highly inelastic asphalt concrete mixtures. The three-dimensional, traction-displacement relationship for the nonlinear, viscoelastic, cohesive zone model is as follows (Allen and Searcy 2000, 2001):

$$T_i(t) = [1 - \alpha(t)]\left[\frac{1}{\delta_i} + \int_0^t C^{cz}(t-\tau)\frac{\partial u_i}{\partial \tau}d\tau\right] \quad (2.69)$$

where,
$i = n$ (normal direction), t (tangential direction), or r (radial direction);
T_i = cohesive zone traction;
u_i = cohesive zone displacement;
δ_i = cohesive zone material length parameter;
$\alpha(t)$ = cohesive zone damage evolution function; and
$C^{cz}(t)$ = viscoelastic stress relaxation modulus of the cohesive zone.

Kim et al. (2007) developed a nonlinear, viscoelastic, cohesive zone model to explain the randomly oriented interface fracture, which causes damage evolution in the asphalt mixtures. Heterogeneous asphalt concrete mixture models with three phases were utilized to simulate the asphalt behavior in their study: coarse aggregate particles, asphalt matrix, and the cohesive zone

phase within the asphalt matrix and along the boundaries between matrix and particle boundaries. Figure 2.24 is a schematic view of a general heterogeneous elastic-viscoelastic body, containing discrete cracks and potential paths of crack propagation. The cohesive zone phase successfully modeled the nonlinear viscoelastic damage in the sample by employing interface elements, as shown in Figure 2.25. These interface elements were randomly oriented in the sample to simulate crack initiation and propagation.

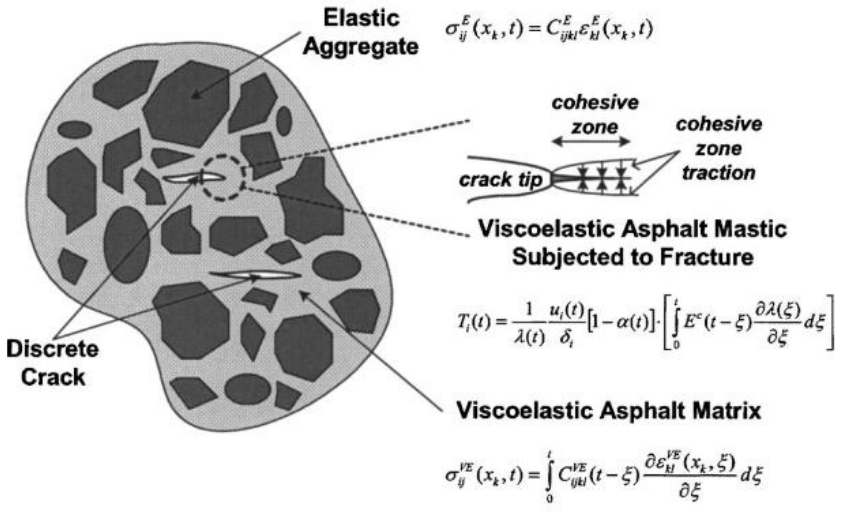

Figure 2.24. A general elastic-viscoelastic body containing discrete cracks and potential cracking paths (Kim et al. 2007)

Baek and Al-Qadi (2006) simulated a modified SENB test by using the FE method with the cohesive elements, based on the bilinear CZM in ABAQUS. The effects of HMA properties on crack initiation time and crack propagation rate were studied by the authors. The study successfully simulated the fracture behavior of HMA was at -10 ˚C, by assuming that the viscous behavior of the HMA was negligible on the overall HMA fracture. A damage value, which can indicate the degradation of the initial stiffness of the material, is used to define the degree of softening in cohesive elements and to trace crack formation. The damage value ranging from 0.0 (no damage) to 1.0 (full damage) is defined as follows:

$$D = \frac{\Delta_m^c(\Delta_m^{max}-\Delta_m^0)}{\delta_m^{max}(\Delta_m^f-\Delta_m^0)} \quad (2.70)$$

where,
D = damage value;

Δ^c = critical separation at which traction T=0;
Δ^0 = damage initiation separation at which traction T is peak; and
Δ^{max} = actual maximum separation.
Δ_m= mixed mode separation combining three separations equally, written in Equation (2.71):

$$\Delta_m = \sqrt{(\Delta_1)^2 + (\Delta_2)^2 + (\Delta_3)^2} \tag{2.71}$$

where,
Δ_1, Δ_2 and Δ_3 = separations in normal, first and second tangential directions, respectively; and
Δ_m^0 = the damage initiation separation corresponding to the onset of damage initiation in a mixed mode, shown in Equation (2.72) (Camanho and Davila 2002):

$$\Delta_m^0 = \begin{cases} \Delta_1^0 \Delta_2^0 \sqrt{\frac{1+\beta^2}{(\Delta_2^0)^2 + (\beta \Delta_1^0)^2}} & \Delta_1 > 0 \\ \Delta_2^0 & \Delta_1 \leq 0 \end{cases} \tag{2.72}$$

where,
β = mixed mode ratio =$\Delta_1/(\Delta_2)^2+(\Delta_3)^2$.

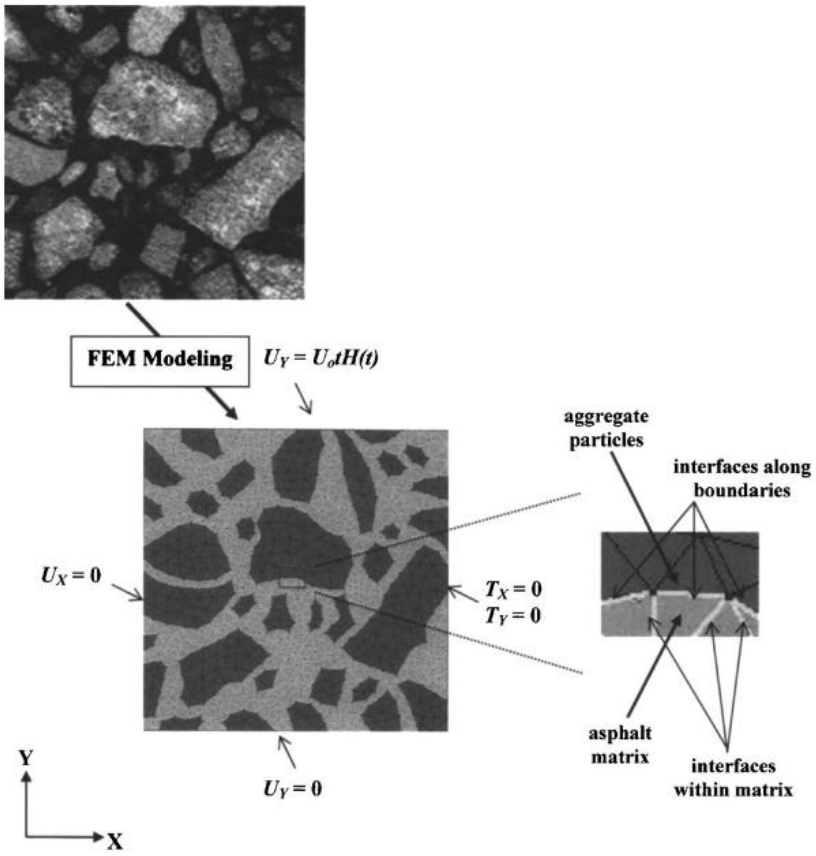

Figure 2.25 Finite element modeling and interface elements orientation of the sample (Kim et al. 2007)

Baek (2010) proposed that the TSL consists of ascending and descending parts to represent initial material stiffness and softening behaviors due to material damage. The bilinear TSL whose softening curve follows a linear function for Modes I, II, and III was utilized in this study. In Figure 2.26(a), the bilinear TSL is used only for tension loading in mode I; and no softening occurs in compression. In Figure 2.26(b), the same bilinear TSL is used for tension and compression loading modes II and III, regardless of the direction of fracture. The material has the elastic behavior before damage occurs at point A in Figure 2.26(a). In mode I, the traction T increases, as separation Δ increases utile $T = T_0$ in the tension zone. The traction T can be obtained by using the Equation (2.73) based on the assumption that T_0 is the tensile strength of the material (Baek 2010):

$$T_i = T_i^0 \left(\frac{\Delta}{\Delta^0}\right)_i = \left(\frac{T^0}{\Delta^0}\right)_i \Delta_i = \left(\frac{E\varepsilon^0}{\Delta^0}\right)_i \Delta_i = \left(\frac{E}{\frac{\Delta^0}{\varepsilon^0}}\right)_i \Delta_i = \left(\frac{E}{L_e}\right)_i \Delta_i = K_i \Delta_i \quad (2.73)$$

where,
T =traction;
Δ = separation;
E = material modulus;
ε = strain;
L_e = element length;
K = material stiffness;
Superscript o denotes a value corresponding to cohesive strength; and
Subscript i denotes normal and two tangential directions.

Baek (2010) also indicated that the fracture dissipation energy, W, can be obtained, based on traction-separation responses. The quadratic damage initiation and linear damage evolution are in a two-dimensional cohesive element, where the corresponding material stiffness is (Baek 2010):

$$T = (1 - D)K^0\Delta \quad (2.74)$$

where,
K^0 = stiffness of undamaged material.

The dissipation of energy can be calculated as an area under the T-Δ curve and the degraded K line. The dissipated energy corresponding to Δ_{max} is written as follows (Baek 2010):

$$W_i = \int_0^{\Delta_i^{max}} T_i(\Delta_i)d\Delta_i - \frac{1}{2}(1 - D)K^0\left(\Delta_i^{maxi}\right)^2 \quad (2.75)$$

where,
W = the dissipation of energy in each fracture mode;
T = a nonlinear function of Δ;

D is a stiffness degradation parameter corresponding to Δ^{max}; and
Subscript i indicates fracture mode.

The term of $T_i(\Delta_i)d\Delta_i$ denotes the total fracture energy of the cohesive element, and the second term represents a partial energy that is still stored in the cohesive element. The current dissipation energy of the mixed mode fracture can be calculated by summing three dissipated energies obtained in each fracture mode in the following Equation (2.76) (Baek 2010):

$$W = \sum_{i=1}^{3} W_i = \sum_{i=1}^{3} \left\{ \int_0^{\Delta_i^{max}} T_i(\Delta_i) d\Delta_i - \frac{1}{2}(1-D)K^0\left(\Delta_i^{maxi}\right)^2 \right\} \quad (2.76)$$

The total dissipation energy is calculated by using the following Equation (77) (Baek 2010):

$$W = \frac{K^0 \Delta_m^0 \Delta_m^c \left(\Delta_m^{max} - \Delta_m^0\right)}{2\left(\Delta_m^c - \Delta_m^0\right)} \quad (2.77)$$

where,
D = damage value;
K^0 = stiffness of undamaged material;
Δ_m^c = critical separation in a mixed mode;
Δ_m^0 = damage initiation separation in a mixed mode; and
Δ_m^{max} = maximum separation in a mixed mode.

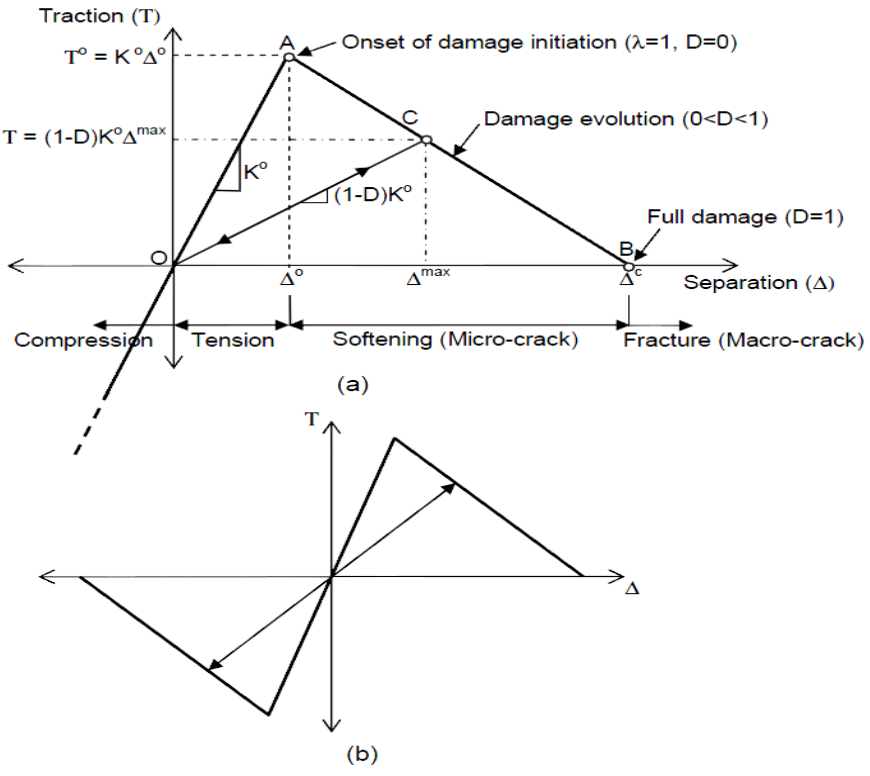

Figure 2.26 Schematic of typical bilinear traction separation laws for (a) Mode I and (b) Modes II and III (Baek 2010)

2.4 References

Abaqus. (2007). Abaqus/Standard User's Manual Version 6.7, ABAQUS, Inc., Palo Alto, CA.

Abu Al-Rub, R., Masad, E., and Chien-Wei Huang (2009). Improving the Sustainability of Asphalt Pavements through Developing a Predictive Model with Fundamental Material Properties, Report No. 2. Government Accession No. 3. Recipient's Catalog No. SWUTC/09/476660-00007-1.

Adhikari ,S., and You, Z., (2007). Distinct Element Modeling of the Asphalt Mixtures: from Two-dimensional to Three-dimensional Models. Transportation Research Board, National Research Council, Washington, D.C.

Allen, D. H., and Searcy, C. R. (2000). Numerical aspects of a micromechanicalmodel of a cohesive zone." J. Reinf. Plast. Compos., 19:3,240–248.

Allen, D. H., and Searcy, C. R. (2001). A micromechanical model for a viscoelastic cohesive zone. Int. J. Fract., 107:2, 159–176.

Archilla, AR., Diaz, LG., Carpenter, SH. (2007). Proposed Method to Determine the Flow Number from Laboratory Axial Repeated Loading Tests in Bituminous Mixtures. Transportation Research Board 86th Annual Meeting. National Research Council, Washington, D.C.

Aragao, F., and Kimn, Y-R. (2010) Characterization of Fracture Properties of Asphalt Mixtures Based on Cohesive Zone Modeling and Digital Image Correlation Technique. Paper presented at the 91st Transportation Research Board Annual Meeting, Washington, D.C.

Alavi, A.H., Ameri, M., Gandomi, A.H., Mirzahosseini, M.R. (2010). Formulation of flow number of asphalt mixes using a hybrid computational method, Construction and Building Materials.

Al-Qadi, I.L., Elseifi, M.A., and Yoo, P.J. (2004). In-Situ validation of mechanistic pavement finite element modeling. Proceedings of the 2nd International Conference on Accelerated Pavement Testing, Minneapolis.

Al-Khateeb, G., Shenoy, A., Gibson, N., and Harman, T. (2006). A new simplistic 1 model for dynamic modulus predictions of asphalt paving mixtures. Journal of the Association of Asphal Paving Technologists, Vol. 75, pp. 1254–1293.

Baek, J. and Al-Qadi, I. L. (2006). Finite element method modeling of reflective cracking initiation and propagation: Investigation of the effect of steel reinforcement interlayer on retarding reflective cracking in hot-mix asphalt overlay. Transportation Research Record, No. 1949, pp. 32 – 42.

Barenblatt, G. I. (1962). The mathematical theory of equilibrium cracks in brittle fracture. Advances in Applied Mechanics. Vol. 7. pp. 55 – 129.

Bausano, J., Williams, C. (2007). A new approach to calculating flow number.

Bari, J. and Witczak, M.W. (2004). An Evaluation of the Effect of Lime Modification on Dynamic Modulus Stiffness of HMA for Use with the New NCHRP 1-37A M-E Pavement Design Guide Procedures. Transportation Research Board of the National academies, Washington, D.C pp 10-19.

Bari, J., and Witczak, M.W. (2006). Development of a New Revised Version of the Witczak E* 31 Predictive Model for Hot Mix Asphalt Mixtures. Journal of the Association of Asphalt Paving 32 Technologists, Vol. 75, pp. 381-423.

Biligiri, K.P., Kaloush, K.E., Mamlouk, M.S., and Witczak, M.W. (2007). Rational Modeling of Tertiary Flow for Asphlat Mixutres. Journal of the Transportation Research Board No.2001, pp 63-72.

Bonaquist, R.F., Christensen, D.W., and Stump, W. (2003). Simple Performance Tester for Superpave Mix Design: First-Article Development and Evaluation. National Cooperative Highway Research Program (NCHRP) Report 513, Transportation Research Board, National Research Council, Washington, D.C.

Bonaquist, R., and Christensen, D.W. (2005). A Practical Procedure for Developing Dynamic Modulus Master curves for Pavement Structural Design. Journal of the Transportation Research Board, 1929, Washington, D.C., 208-217.

Braz, D., Da Motta, L.M.G., Lopes, R.T., (1999). Computed tomography in the fatigue test analysis of an asphaltic mixture. Appl. Radiat. Isot. 50 (4), 661–671.

Birgisson, B., Shola,G. and Roque, R., (2004). Evaluation of Predicted Dynamic Modulus for Florida Mixtures. Transportation Research Board, National Research Council, Washington, D.C. pp, 200-207.

Camanho, P. P. and Dávila, C. G. (2002). "Mixed-mode decohesion finite elements for the simulation of delamination in composite materials," NASA/TM-2002-211737, National Aeronautics and Space Administration, Hampton, VA.

Collop, C., Scarpas, A. T., Kasbergen, C., and de Bondt, A. (2003). Development and finite element implementation of a stress dependent elasto-visco-plastic constitutive model with damage for asphalt. Transportation Research Record 1832, Transportation Research Board, Washington, D.C., 96-104.

Cundall, P. A. (1971). A computer model for simulating progressive large scale movements in blocky rock systems. Proc., Int. Symp. Rock Fracture, ISRM, Vol. II-8, Nancy, France, 129–136.

Dai, Q., Sadd, M.H., Parameswaran, V., and Shukla, A. (2005). Prediction of Damage Behaviors in Asphalt Materials Using a Micromechanical Finite-Element and Image Analysis. Journal of Engineering Mechanics, ASCE, Vol. 131, No. 7, pp. 668-677.

Dai, Q. and You, Z. (2009). Micromechanical Finite Element Framework for Predicting Viscoelastic Properties of Heterogeneous Asphalt Mixtures. Materials and Structures, Springer Netherlands, Vol. 41(6), pp.1025-1037, ISSN: 1359-5997 , 1871-6873.

Dai, Q. (2010). Prediction of Dynamic Modulus and Phase Angle of Stone-Based Composites using Micromechanical Finite Element Approach. Journal of Material in Civil Engineering, ASCE, 22 (6), 618-627.

Deshpande, V. S., and Cebon, D. (1999). Steady-state constitutive relationship for idealized asphalt mixes. Mechanics of Materials, 31, 271-287.

Dharamveer Singh, Musharraf M. Zaman, and Sesh Commuri. (2010). Evaluation of Predictive Models for Estimating Dynamic Modulus of HMA Mixes used in Oklahoma. Transportation Research Board Annual Meeting 2010.

Dougan, C., Stephens, J., Mahoney, J. and Hansen, G., (2003). E*-Dynamic Modulus Test Protocol – Problems and Solutions. Report Number: CT-SPR-0003084-F03-3 Connecticut Department of Transportation and Federal Highway Administration, 2003.

Dugdale, D. S. (1960). Yielding of steel sheets containing slits. Journal of Mechanics and Physics of Solids, Vol. 8, No. 2, pp. 100 – 104.

Elseifi, M.A., Al-Qadi, I.L., and Flinstch, G.W. (2003). Quantitative Effect of Elastomeric Modification on Binder Performance at Intermediate and High Temperatures. Journal of Materials in Civil Engineering, ASCE, Vol. 15, No. 1, 32-40.

Elshelby, J.D. (1957). The Determination of the Elastic Field of an Ellipsoidal Inclusion, and Related Problems. Proceedings of the R. Soc. London, Ser. A, 241, pp. 376-396.

Dessouky, S., Eyad Masad, E. and Little, D. (2005). Mechanistic Model to Predict The Impact of The Aggregate Matrix On The Permanent Deformation of Asphalt Mixtures. Texas Transportation Institute. Report No. FHWA/TX-05/0-1707-6.

ERES Consultants and Fugro-BRE Inc. (2002). Introduction to mechanistic-empirical design of new and rehabilitated pavements. Reference Manual, NHI Course No. 131064.

Erkens, S., Liu, X., Scarpas, A., Molenaar, A., and Blaauwendraad, J. (2002a). Asphalt concrete response: Experimental determination and finite element implementation. Proc., 9th Int. Conf. on Asphalt Pavements, ISAP, Minn.

Erkens, S., Liu, X. and Scarpas, A. (2002b). 3D finite element model for asphalt concrete response simulation. The International Journal of Geomechanics, 2(3), 305-330.

Guide for Mechanistic-Empirical Design of New and rehabilitated Pavement Structures (2003). NCHRP 1-37A Project, Transportation Research Board of the National academies, Washington, D.C.

Huang, Y. H. (1967). "Deformation and volume change characteristics of a sand asphalt mixture under constant direct triaxial compressive stresses." Highway Research Record 178, 60-74.
Huang, B., Mohamad, L., and Wathugala, W. (2002). "Development of a thermo-viscoplastic constitutive model for HMA mixtures." Journal of the Association of Asphalt Paving Technologists, 71, 594-618.

Huang, C.W., Masad, E., Muliana, A., and Bahia, H. (2007). Nonlinear viscoelastic analysis of asphalt mixes subjected to shear loading. Mechanics of Time Dependent Materials, 11, 91-110.

Huang, B., Shu, X., and Zuo, G.(2005). Laboratory Evaluation of Semi-Circular Bending Tensile Strength Test for HMA Mixtures. Journal of the Transportation Research Board, 84th Annual Meeting Compendium of Papers CD-ROM.

Hofman, R., Oosterbaan, B., Erkens, S.M.J.G., Van der Kooij, J., (2003). Semi-Circular Bending Test to Assess the Resistance Against Crack Growth. Paper presented at the proceedings of the 6th International Rilem Symposium in Zurich, Switzerland, pp. 257-263.
Itasca Consulting Group. _2004a_. PFC 2D Version 3.1, Minneapolis.

Kaloush, K. and Witczak, M. (2001). Simple Performance Test for Permanent Deformation of Asphalt Mixtures. 2002 Annual Transportation Research Board Meeting, Washington, D.C.

Kassem, E., Walubita, L., Scullion, T., Masad, E., and Wimsatt, A. (2008). "Evaluation of Full Depth Asphalt Pavement Construction Using X-ray Computed Tomography and Ground Penetrating Radar," Journal of Performance of Constructed Facilities, ASCE, Vol. 22, No. 6, pp. 408-416.

Kassem, E., Masad, E., Bulut, R., Lytton, R. (2009). Measurements of the Moisture Diffusion Coefficient of Asphalt Mixtures and its Relationship to Mixture Composition, International Journal of Pavement Engineering, Vol. 10, No. 6, pp. 389-399.

Khanum, T., Mulandi, J.N., and Hossain, M. (2008). Implementation of the 2002 AASHTO Design Guide for Pavement Structures in KDOT. Final Report KSU-04-4, Kansas Department of Transportation.

Khaleel, M., Zbib, H., Nyberg, E., (2001). Constitutive modeling of deformation and damage in superplastic materials. International Journal of Plasticity 17, 277–296.

Kim, Y. and Lee, H. (2006). Determination of Dynamic Modulus of Cold In-place Recycling Mixture with Foamed Asphalt using New Simple Performance Testing Equipment. 2007 Transportation Research Board 2007 Annual Meeting. Washington, D.C. No. 07-1322.

Kim, Y., Allen, D.H. and Little, D.N. (2007). A Computational Constitutive Model for Predicting Nonlinear Viscoelastic Damage and Fracture Failure of Asphalt Concrete Mixtures. International Journal of Geomechanics, 102-110.

Krishna P. Biligiri, Kamil E. Kaloush, Michael S. Mamlouk and Matthew W. Witczak. 2007. "Rational Modeling of Tertiary Flow for Asphalt Mixtures", Transportation Research Record TRR 2001, Journal of Transportation Research Board of the National Academies, Washington, D. C.January 2007, pp. 63-72.

Kvasnak, A., Robinette, C. J., and Williams, R. C. (2007). A Statistical Development of a Flow Number Predictive Equation for the Mechanistic-Empirical. Pavement Design Guide, Transportation Research Board.

Lai, J. and Bakker, A. (1996). 3D schapery representation of non-linear viscoelasticity and finite element implementation. Computational Mechanics, 18, 182-191.

Li, X.J., and Marasteanu, M.O. (2010). Using Semi Circular Bending Test to Evaluate Low Temperature Fracture Resistance for Asphalt Concrete. Journal of Experimental Mechanics, Vol. 50, pp. 867-876.

Liu, Y. and You, Z (2010). Accelerated Discrete Element Modeling of Asphalt-Based Materials with the Frequency-Temperature Superposition Principle. Journal of Engineering Mechanics doi:10.1061/(ASCE)EM.1943-7889.0000234.

Lu, Y., and Wright, P. J. (1998). Numerical approach of visco-elastoplastic analysis for asphalt mixtures. Journal of Computers and Structures, 69, 139-157.

Wang, L.B., Frost, J.D., G.Z Voyiadjis. T.P. Harman (2001). Quantification of damage parameters using X-ray tomography images, Mechanics of Materials 35 (2003) 777–790.

Masad, E., Muhunthan, B., Shashidhar, N., and Harman, T. (1998). Quantifying Laboratory Compaction Effects on the Internal Structure of Asphalt Concrete. Transportation Research Board 1998 Annual Meeting, Washington, DC.

Masad, E., Jandhyala, V.K., Dasgupta, N., Somadevan, N., and Shashidhar, N. (2002). Characterization of Air Void Distribution in Asphalt Mixes Using X-ray Computed Tomography. Journal of Materials in Civil Engineering, ASCE, Vol. 14, No. 2, 122-129.

Masad, E., Dessouky, S., and Little, D. (2007). Development of an Elastoviscoplastic Microstructural-Based Continuum Model to Predict Permanent Deformation in Hot Mix Asphalt. International Journal of Geomechanics, ASCE, Vol. 7, No. 2, pp. 119-130.

Mohammad, L.N., Wu, Z., Obulareddy, S., and Cooper, S., (2006). Permanent Deformation Analysis of HMA Mixtures Using Simple Performance Tests and The 2002 Mechanistic-Empirical Pavement Design Software. Accepted for Publication, Journal of the Transportation Research Board.

Molenaar, A., Scarpas, A., Liu, X., Erkens, S. (2002). Semi-Circular Bending Test; Simple But Useful? Journal of Asphalt Paving Technologists, Vol. 71, pp. 794-815.

Mull, M.A., Othman, A., and Mohammad, L. (2006). Fatigue Crack Growth Analysis of HMA Employing the Semi-Circular Notched Bend Specimen. Journal of the Transportation Research Board, 85th Annual Meeting Compendium of Papers CD-ROM.

Murakami, S. (1988). Mechanical modeling of material damage. Journal of Applied Mechanics. ASME 55 (2), 280–286.

NCHRP Project 9-19 June 2001 Quarterly Progress Report.

Ortiz, M. and Pandofi, A. (1999). Finite deformation irreversible cohesive elements for the three dimensional crack propagation analysis. International Journal for Numerical Methods in Engineering 44, 1267–1282.

Panoskaltsis, V. (2005). Mechanics of Asphalt Concrete: Analytical and Computational Studies. PhD dissertation, Case Western Reserve University, Cleveland, Ohio, USA.

Paulino, G. H., Song, S. H., and Buttlar, W. G. (2004). Cohesive zone modeling of fracture in asphalt concrete. Proceedings of the 5th International RILEM Conference–Cracking in Pavements: Mitigation, Risk Assessment, and Preservation, (C. Petit, I. L. Al-Qadi, and A. Millien, eds.), Limoges, France, pp. 63 – 70.

Paris, P., and Erdogan, F. (1963). A Critical Analysis of Crack Propagation Laws. Transaction of The ASME, Journal of Basic Engineering, 85(D), No. 4.

Perzyna, P. _1966_. "Fundamental problems in viscoplasticity." Adv. Appl. Mech., 9, 253–377.

Perzyna, P. (1984). Constitutive Modeling of Dissipative Solids for Postcritical Behavior and Fracture. Journal of Engineering Materials and Technology, ASME, 106, 410 - 419.

Rodezno, M.C., Kaloush, K.E. and Corrigan, M.R. (2009). Development of a Flow Number Predictive Model. Transportation Research Board 2010 Annual Meeting, Washington, DC. pp 79-87.

Sancho, J.M., et al., An embedded crack model for finite element analysis of concrete fracture. Engineering Fracture Mechanics, 2007. 74: p. 75-86.

Scarpas, A., Al-Khoury, R., Van Gurp, C., Erkens, S., (1997). Finite element simulation of damage development in asphalt concrete pavements. In: Proceedings of the 8th International Conference on Asphalt Pavements, University of Washington, Seattle, WA, pp. 673–692.

Scarpas, A., Al-Khoury, R., Van Gurp, C., and Erkens, S. M. (1997). Finite element simulation of damage development in asphalt concrete pavements. Proc., eighth International Conference on Asphalt Pavements, University of Washington, Seattle, WA, 673-692.

Shu, X., and Huang, B. (2008). Dynamic Modulus Prediction of HMA Mixtures Based on the Viscoelastic Micromechanical Model. Journal of Materials in Civil Engineering. ASCE, Vol. 20, No. 8, pp. 530-538.

Sides, A., Uzan, J., and Perl, M. (1985). A comprehensive visco-elastoplastic characterization of sand-asphalt under compression and tension cyclic loading. ASTM Journal of Testing and Evaluation, 13, 59-59.

Soares, J. B., Colares de Freitas, F. A., and Allen, D. H. (2003). Crack modeling of asphaltic mixtures considering heterogeneity of the material. Proceedings of the 82nd Annual Meeting of the Transportation Research Board (CD-ROM), Transportation Research Board, Washington, D.C.

Song, S. H., Paulino, G. H., and Buttlar, W. G. (2006). A bilinear cohesive zone model tailored for fracture of asphalt concrete considering viscoelastic bulk material. Engineering Fracture Mechanics, Vol. 73, No. 18, pp. 2829 – 2849.

Goh , S. W. and You, Z.. (2009). A simple stepwise method to determine and evaluate the initiation of tertiary flow for asphalt mixtures under dynamic creep test. Construction and Building Materials. 23:3398–340.

Tashman, L.,Masad, E., Little,D.,and Zbib,h.,(2005). A microstructure-Based Viscoplastic Model for Asphalt Concrete. Journal International jounrnal of plasticity. Vol 21,No 9,1659-1685.

Witczak, M.W., Kaloush, K., Pellinen, T., El-Basyouny, M., and Von Quintus, H.(2002). Simple Performance Test for Superpave Mix Design. NCHRP Report 465, Transportation Research Board, Washington, D.C.

Wu, R., Denneman, E., Harvey, J. (2009). Evaluation of Embedded Discontinuity Method for Finite Element Analysis of Cracking of Hot-Mix Asphalt Concrete. Transportation Research Board 2009 Annual Meeting, Washington, DC. ISBN: 9780309142687.

Yang, E., Ping, W. Virgil, Xiao, Y. and Qiu,Y. (2011). A Simplified Predictive Model of Dynamic Modulus for Characterizing Florida Hot Mix Asphalt Mixtures Transportation Research Board of the National academies, Washington, D.C. pp.3-18.

Zelelew H., Paugh C., and Corrigan M. (2010). Warm-Mix Asphalt Laboratory Permanent Deformation Performance in the State of Pennsylvania: A Case Study. 2011 Annual Transportation Research Board Meeting, Washington, D.C.

You, Z., Adhikari, S., and Dai, Q. (2008). Three-Dimensional Discrete Element Models for Asphalt Mixtures. Journal of Engineering Mechanics, ASCE, Vol. 134(12), pp.1053-1063.

You, Z., Adhikari ,S., Kutay ,E. (2009). Dynamic modulus simulation of the asphalt concrete using the X-ray computed tomography images. Materials and Structures 42:617–630.

CHAPTER 3 – MODELING AND EVALUATION OF THE CRACKING RESISTANCE OF ASPHALT MIXTURES USING THE SEMI-CIRCULAR BENDING TEST AT INTERMEDIATE TEMPERATURES[1]

3.1 Introduction

One of the major distresses that directly affect the serviceability and quality of flexible pavement structures is cracking. Cracking appears at the pavement surface as longitudinal cracks, transverse cracks, and a combination of both that extend over the width of the pavement and creates hazardous conditions for the road users. Water infiltration through the cracks may subsequently cause weakening and deterioration of the base and/or subgrade. Cracking is also the main cause of many pavement distresses (e.g., stripping in hot-mix asphalt [HMA] layers, loss of subgrade support, etc.). The rehabilitation of pavement damage caused by cracking failure is usually costly. Therefore, it has been suggested that cracking, especially fatigue cracking, should be primarily addressed by adequate mixture and pavement design procedures as well as proper construction practices.

In order to avoid premature failure of asphalt mixtures through a cracking-related mechanism, it is necessary to characterize the fracture and fatigue-resistance properties of the designed mixture in the laboratory prior to installation. Several laboratory test methods were suggested to characterize asphalt mixture fracture resistance with various degrees of success. This includes, among others, the dissipated creep strain energy (DCSE) test, the four-point bending fatigue test, the disk-shaped compact tension (DCT) test, and the Texas overlay tester (OT). However, many of these laboratory procedures are too complex and time-consuming for regular use in state-related design and QA activities. In addition, the observed variation in the results and the empirical nature of some of these tests may prevent the development of methodical conclusions about the fracture resistance of the materials. In this study, an experimental and theoretical evaluation of the SCB test is conducted for the prediction of the cracking performance of asphalt mixtures.

1This chapter previously appeared as Modeling and Evaluation of the Cracking Resistance of Asphalt Mixtures Using the Semi-Circular Bending Test at Intermediate Temperatures, 2012. It is reprinted by permission of Taylor & Francis.

3.2 Objective and Scope

The objective of this study is to conduct a comprehensive evaluation of the SCB test and to utilize the results to evaluate a number of asphalt mixtures' resistance to fatigue and cracking failure. To achieve this objective, a number of asphalt mixtures including mixtures with a high content of reclaimed asphalt pavement (RAP) were tested. The cracking and fatigue performances predicted from the SCB test were compared to the DCSE test. Results of the experimental program were then used to validate a 3D FE model, which was used to interpret and to analyze the failure mechanisms in the SCB test.

3.3 Background

Cracking mechanisms in asphalt mixtures have been studied since the 1960s. Various test methods were proposed to predict the fracture behavior of HMA mixtures, including the single edged notched beam (SENB) test, the SCB test, the indirect tensile test (IDT) fracture parameter, and the DCT test. Each of these test procedures has unique advantages and disadvantages (Li and Marasteanu 2010). The SCB test is based on fracture mechanics and the J-integral, which considers the elasto-plastic/visco-plastic relationship of HMA mixtures, rather than the stress intensity factor (K) commonly used in linear elastic fracture mechanics (Mull et al 2006). The SCB test configuration has been favored by many researchers due to the ease of sample preparation including cores removed from the field and the quick and simple testing procedure (Li and Marasteanu 2010, Adamson et al. 1996).

Molenaar et al. (2002) evaluated the usefulness of the SCB test in characterizing the fracture resistance of HMA mixtures. The researchers evaluated the advantages and disadvantages of the semi-circular specimen in determining the tensile properties of HMA mixtures. Finite Element Method (FEM) was used to illustrate, while there are some compressive stresses, the dominant failure mechanism is tension located at the bottom of the specimen. However, the authors recognized that the strain rates will not be constant over the height of the specimen. This behavior makes it difficult to determine a modulus of the mixtures. The researchers used CAPA 3D FEM software to model the behavior of un-notched SCB specimens. Results of the modeling suggest that the dominant mode of failure in SCB specimens is fracture, making the test viable for evaluation of a mixture's fracture resistance (Molenaar et al. 2002).

Arabani and Ferdowsi (2009) conducted a study to compare the SCB test to a suite of static and dynamic tests commonly used to describe tensile strength, fracture and fatigue properties of asphalt mixtures. The study showed that the SCB test could be used to characterize the tensile strength of asphalt mixtures. Additionally, the SCB fracture parameter had good correlation with fracture parameters obtained from stiffness modulus testing via the Nottingham Asphalt Tester (NAT) (Arabani and Ferdowsi 2009). Huang et al. (2005) compared the ability of the semi-circular bend test to characterize the tensile strength of HMA mixtures with IDT. Comparisons of the SCB and IDT results of 16 mixtures were conducted both analytically and numerically through the use of FE modeling using ABAQUS software. Results from the study indicated the SCB test was capable of providing consistent results. The authors also noted several advantages of the semi-circular bending configuration; ease of sample preparation and load frame configuration were highlighted as distinct advantages of the test method (Huang et al. 2005).

Mull et al. (2002) evaluated the use of the semi-circular bend configuration to characterize the fatigue crack propagation of HMA mixtures. Three HMA mixtures were evaluated for fatigue susceptibility using SCB fracture parameters and scanning electron microscopy to identify fatigue damage species associated with each mixture. The research found that the SCB specimen is suitable for both static and fatigue fracture characterization (Mull et al. 2002). Li and Marasteanu (2010) evaluated the ability of the SCB test to evaluate low temperature fracture resistance of HMA. The researchers also evaluated the factors affecting the mixtures' ability to resist fatigue cracking. Six asphalt mixtures were tested representing a combination of factors such as binder type, binder modifier, aggregate type, and air void content. The loading rate was also varied as well as the initial notch length. The SCB test was conducted at three low temperatures (-30°, -18°, and -6°C). Results indicated strong dependence of low temperature cracking resistance on the test temperature. Additionally, significant effects of aggregate type, air void content, binder grade and modifier type were reported. The effects of loading rate and initial notch depth were only observed for the warmest test temperature. The authors also noted the test was conducted with satisfactory repeatability as indicated by the low coefficient of variation (Li and Marasteanu 2010).

Adamson et al. (1996) combined the use of the weight function approach with the finite element method to develop relationships to evaluate both the flexure and fracture properties of

quasi-brittle materials, such as asphalt mixtures, using semi-circular bend geometries (Adamson et al. 1996). Aragao and Kim simulated the SCB test of a fine aggregate matrix (FAM) using 2D finite element and cohesive modeling technique (2010). FAM was selected in this study to ensure testing repeatability and to be able to incorporate experimental test results in a microstructural modeling approach that simulates damage in HMA. Results of this study showed that a bilinear cohesive modeling approach was successful in simulating the results of this test. Two material parameters (cohesive strength and fracture energy) that are load-related were used to simulate the behavior in the vicinity of the crack tip.

3.4 Background Experimental Program

3.4.1 The SCB Test Method

Cracking potential was evaluated using the SCB test procedure suggested by Mohammad and co-workers (2005), Figure 3.1. The critical strain energy release rate, also called the critical value of J-integral (J_c) was used to describe the mixture's resistance to fracture:

$$J_c = -\left(\frac{1}{b}\right)\frac{dU}{da} \tag{3.1}$$

where,
J_c= critical strain energy release rate (kJ/mm^2);
b = sample thickness (mm);
a = notch depth (mm);
U = strain energy to failure (N.mm); and
dU/da = change of strain energy with notch depth.

To determine the critical value of J-integral (J_c) using Equation (3.1), semi-circular specimens with at least two different notch depths should be tested to determine the change of strain energy with notch depth (dU/da). In this study, three notch depths of 25.4 mm, 31.8 mm, and 38 mm were tested to confirm that the measurements and calculations are within the linear viscoelastic region by fitting a regression line to the change of strain energy with notch depth, Figure 1b.

The semi-circular specimen was loaded monotonically until fracture failure under a constant cross-head deformation rate of 0.5 mm/min. in a three-point bending load configuration. The load and deformation were continuously recorded. A test temperature was selected at 25°C to correspond to the intermediate temperature range at which most of the traffic load is applied.

High J_c values are desirable for fracture-resistant mixtures. A threshold of a minimum J_c of 0.65 kJ/m^2 has been suggested as a failure criterion for this test (Wu et al. 2005).

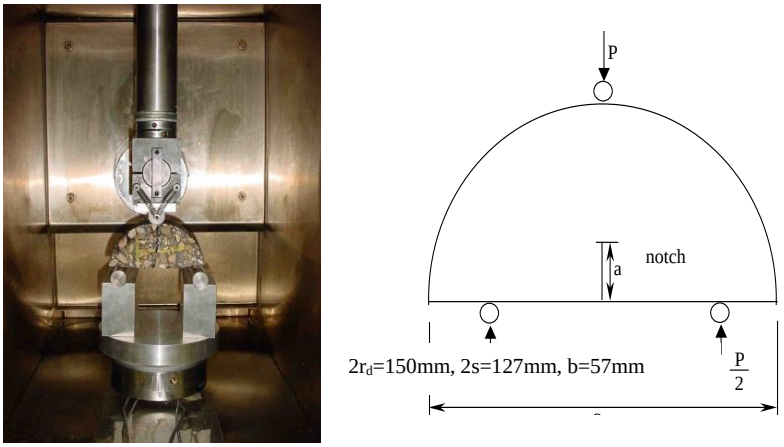

(a)

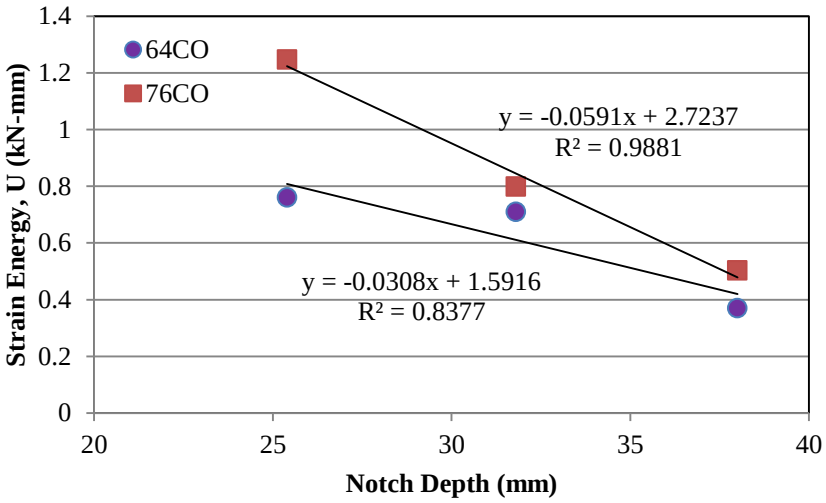

(b)

Figure 3.1 Semi-Circular Bending Test Setup

3.4.2 Sample Fabrication

Gyratory specimens, 150 mm diameter, were compacted to a height of 57 mm and an air void content of 7 ± 0.5%. The circular specimens were then cut along the center diameter of the specimen yielding two semi-circular halves. To reduce effect of mixture variation between specimens, each half of the specimen was designated with the same notch depth (i.e., 25.4 mm, 31.8 mm, or 38.1 mm). Four semicircular specimens were tested at each notch depth. The

tolerance on the notch depth is ±1.0 mm, while the notch width is 3.0 ± 0.5 mm. Figure 3.2 shows the steps used in the SCB sample preparation.

Step 1: Prepare gyratory-compacted samples

Step 2: Cut specimens along the center diameter

Step 3: Create notch with desired depth

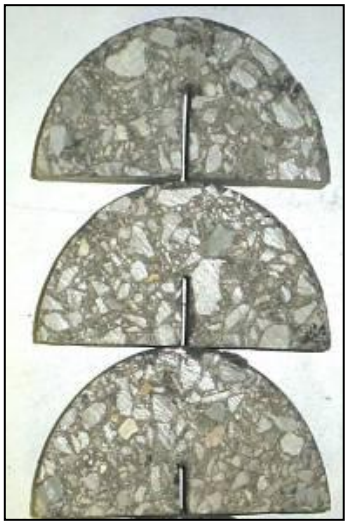

Step 4: Repeat procedure for three notch depths

Figure 3.2 Semi-Circular Bending Specimen Preparation Steps

3.4.3 The Dissipated Creep Strain Energy Test

The DCSE test threshold represents the energy that the mixture can tolerate before it fractures. The evaluation of DCSE of an HMA mixture involves two individual laboratory tests to be performed on the same specimen. Two laboratory tests, the indirect resilient modulus (M_R) test and the indirect tensile strength (ITS) test, were conducted at 10°C on the same specimen to calculate the dissipated strain energy. Triplicate specimens of 150 mm in diameter and 50 mm in

thickness were used. The test specimens were conditioned at 10°C for four hours before a 200-cycle haversine load with a 0.1 sec loading period and a 0.4 sec rest period in each loading cycle was applied along the diametrical plane on the specimen.

The DCSE calculation used in this study was introduced by Roque et al. (2002, 2004). DCSE is defined as the fracture energy (FE) minus the elastic energy (EE). The fracture energy is defined as the area under the stress-strain curve up to the point where the specimen begins to fracture. The elastic energy is the energy resulting in elastic deformation. Therefore, M_R, calculated from the resilient modulus test, is used to calculate the EE. DCSE calculation can be summarized as follows:

$$DCSE = FE - EE \tag{3.2}$$

A minimum DCSE of 0.75 kJ/m^3 is recommended to ensure acceptable cracking performance of the mixture (Roque et al. 2002).

3.4.4 Test Materials

Table 3.1 presents a description of the evaluated mixtures. Five mixtures were prepared according to the same mix design. A 19 mm Superpave mixture meeting Louisiana Department of Transportation and Development (LADOTD) specifications ($N_{initial}$ = 8-, N_{design} = 100-, N_{max} = 160-gyrations), was designed according to AASHTO PP 28, "Standard Practice for Designing Superpave HMA" and Section 502 of the 2006 Louisiana Standard Specifications for Roads and Bridges. The optimum asphalt cement content was determined based on volumetric (VTM = 2.5 - 4.5 percent, VMA ≥ 12%, VFA = 68% -78%) and densification (% G_{mm} at $N_{initial} \leq 89$, %G_{mm} at $N_{max} \leq 98$) requirements. The design asphalt content was held at 4% for all the mixtures. Siliceous limestone aggregates and coarse natural sand were used in mix preparation.

In this study, the cracking performance of two mixtures containing RAP was evaluated using SCB as compared to two conventional mixes containing 0% RAP (64CO and 76CO). The first mixture was a PG 76-22 HMA containing 15% RAP (76RAP15). The second mixture was a PG 64-22 HMA containing 40% RAP. Since mixtures containing high content of RAP are expected to be susceptible to fatigue cracking, the mixture containing 40% RAP was treated with an engineered rejuvenating additive consisting of de-metalized oil and resin to soften the RAP binder and to reduce the stiffness of the mixture (64RAP40). Four replicates were conducted for

each notch depth and for three notch depths for each mix (25.4, 31.8, and 38.1 mm). Therefore, the adopted SCB test procedure requires 12 specimens to be tested; test duration is approximately 10 minutes per specimen and around 4 hours per mixture.

Table 3.1 Description of the Evaluated Mixes

Mixture Abbreviation	**Description**
64CO	Conventional HMA mixture with PG 64-22
70CO	Conventional HMA mixture with Styrene-Butadiene Styrene Polymer-Modified PG 70-22
76CO	Conventional HMA mixture with Styrene-Butadiene Styrene Polymer-Modified PG 76-22
76RAP15	HMA mixture with Styrene-Butadiene Styrene Polymer Modified PG 76-22 and 15% RAP
64RAP40	HMA mixture with PG 64-22 HMA containing 40% RAP and engineering additives

3.5 Results of the Experimental Program

Repeatability of the SCB and DCSE tests in terms of coefficient of variation (CV) is presented in Table 3.2. As shown in this table, the repeatability of the SCB testing process was acceptable with an average CV of 18.9% for all mixes. Figure 3.3 illustrates typical test results from the SCB test for the 70CO mix (notch depth = 38 mm). As shown in this figure, the vertical load applied on the sample gradually increases as the displacement-controlled through the actuator is progressively increased. The specimen resists the applied displacement up to the fracture point and then starts failing; after that, the required load to induce the prescribed displacement gradually decreases until total failure of the specimen is reached. To assist in the analysis of the data, polynomial models were fitted to the measurements, see Figure 3.3. While there is no practical use for these models, they allow reducing fluctuation in the measurements and noises in

the raw data. The coefficients of determination for these models were greater than 0.9 for all cases.

Table 3.2 Repeatability of SCB and DCSE Test Results

Mixture	SCB	DCSE
	CV (%)	CV (%)
64CO	5.4	18.4
70CO	21.1	14.2
76CO	16.6	12.7
76RAP15	26.4	31.6
64RAP40	24.8	22.4
Average (%)	18.9	19.9

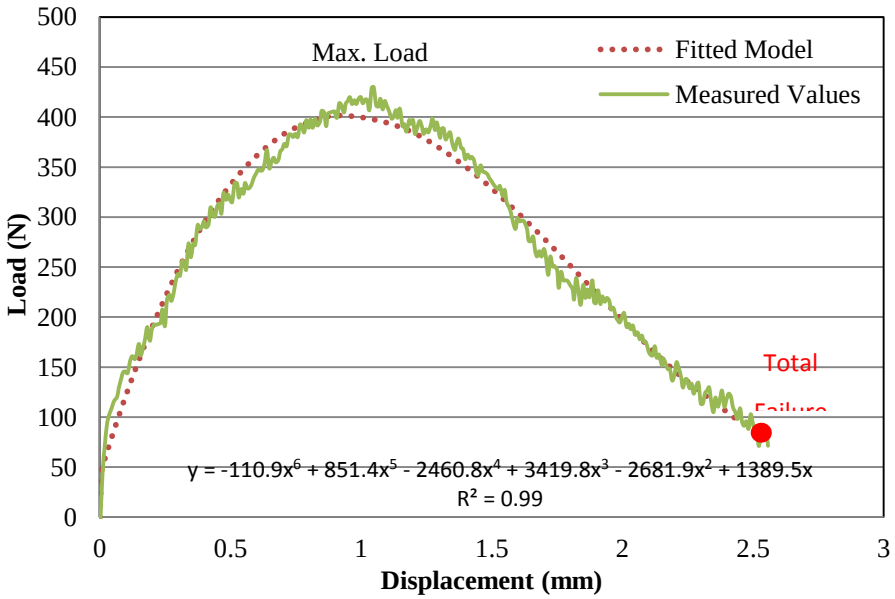

Figure 3.3 Typical Results from the Semi-Circular Bending Test (70CO)

Figures 3.4 (a and b) compare the SCB test results for the 64CO to the 64RAP40 and for the 76CO to the 76RAP15, respectively. As shown in Figure 4a, SCB test results predict that the mix prepared with high RAP content will fail at a lower level of displacement, which is indicative that the mix with high RAP is more brittle than the conventional mix and has reduced elongation capabilities. In addition, the maximum load measured for the mix with high RAP content was greater than the conventional mix. Testing conducted for the NCHRP Project 9-12 study reported that recycled mixtures with a RAP content greater than 20% have a lower fatigue life than virgin

mixtures (McDaniel et al. 2000). Similar trends were observed for the mix prepared with 15% RAP (76RAP15) as compared to the conventional mix prepared with virgin materials and polymer-modified binder (76CO), Figure 4b.

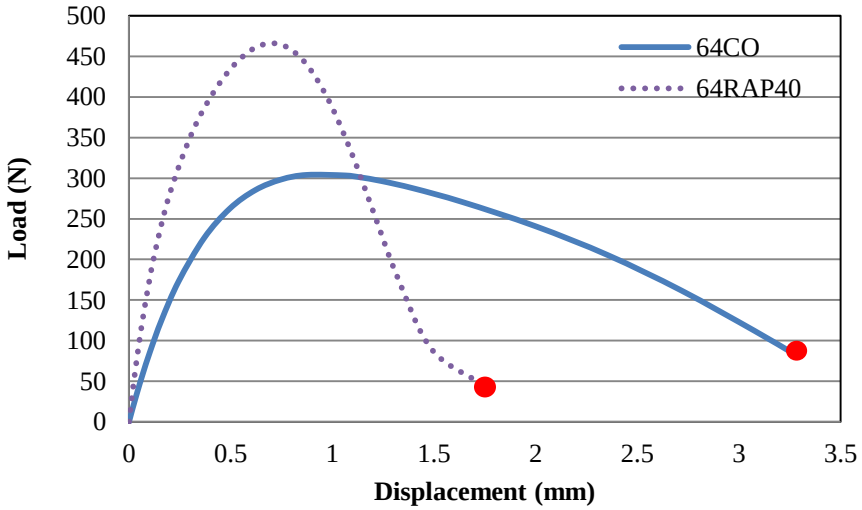

(a)

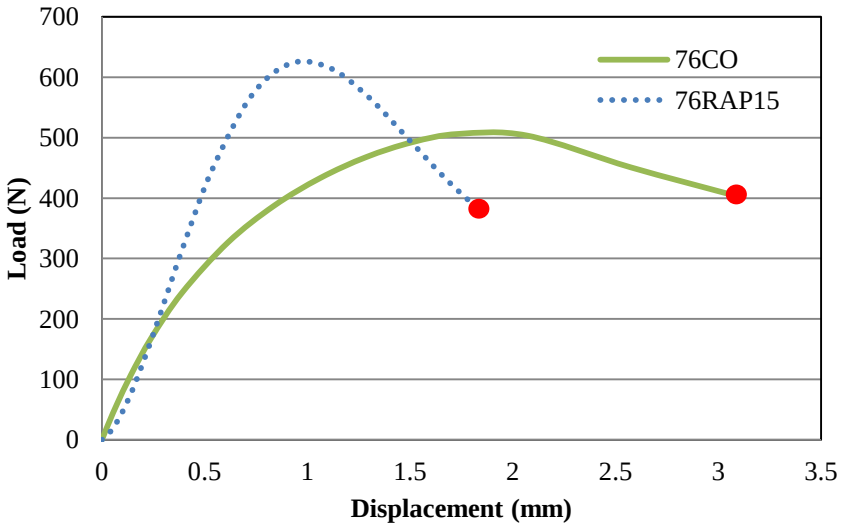

(b)

Figure 3.4 Comparison of the Semi-Circular Bending Test Results for Mixes with and without RAP

3.5.1 Fracture Performance

Figure 3.5 presents a comparison of the critical strain energy rate (J_c) data for the mixtures evaluated in this study. Error bars representing a 19% variation from the mean values are shown in these figures. As shown in this figure, two mixtures did not satisfy the failure criterion used in

the SCB test: 64CO and 64RAP40. These results should be discussed in light of the general assumption introduced by the critical strain energy rate. In the SCB test, cracking resistance of a mixture is described either by its high stiffness characteristics (e.g., 76RAP15) or through its high elongation properties (e.g., 76CO). However, a poor cracking performance may be observed if the mix does not keep a balance between the two properties (i.e., stiffness and elongation properties) as noted for mix 64CO, which had low stiffness characteristics while acceptable elongation properties. As shown in Figure 3.5, the mix prepared with the engineered rejuvenating additive and high RAP content (64RAP40) outperformed the conventional mix prepared with the same binder grade and virgin materials (64CO) given its high stiffness characteristics, Figure 3.4a. It was also observed that the PG76 mixture containing 15% RAP (76RAP15) outperformed the conventional PG76 mixture (76CO) prepared with virgin materials; however, both mixes satisfied the cracking criterion for this test, which is set at a minimum J_c of 0.65 kJ/m^2.

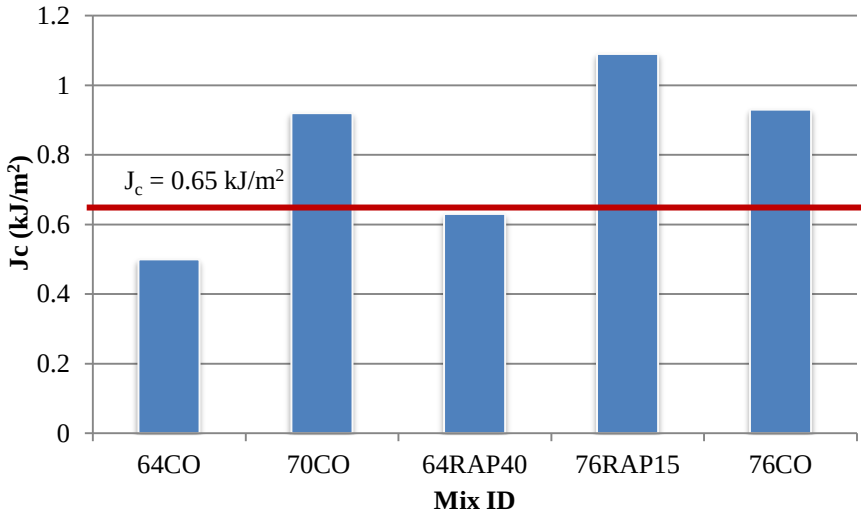

Figure 3.5 SCB test results for cracking performance

The fracture resistance of the prepared mixes was predicted from the results of the DCSE test, Figure 3.6. Mixtures that exhibit lower DCSE values are more susceptible to cracking than HMA mixtures having higher values when mixtures are exposed to similar environmental and loading conditions. The results of the DCSE, shown in Figure 3.6, indicated that all mixtures met the 0.75 kJ/m^3 cracking criterion except for the 64RAP40 prepared with high RAP content and the engineered additive rejuvenator.

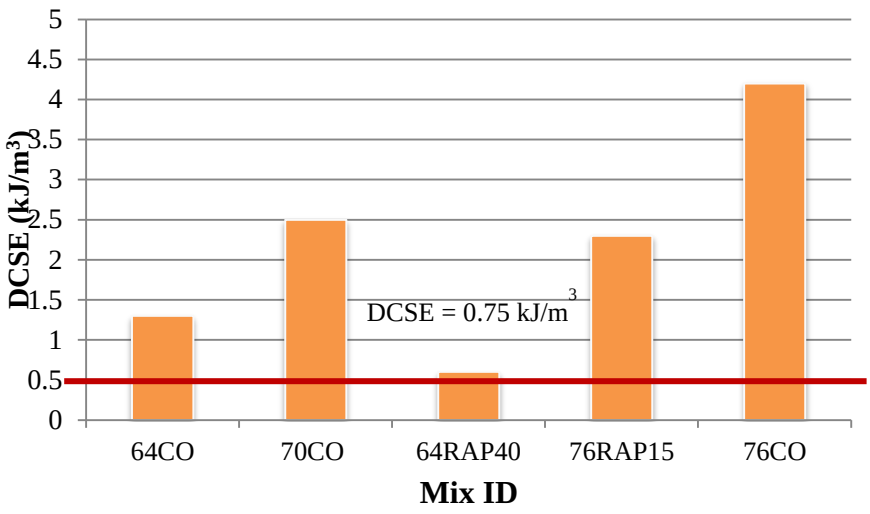

Figure 3.6 DCSE test results

Figures 3.5 and 3.6 allow one to compare the DSCE and SCB test results. Results of the DCSE test agreed with the results of the SCB test with the exception of mix 64CO, which failed the fracture criterion in the SCB test but satisfied the criterion set for the DCSE test. This may be due that the DCSE test mainly describes the mix crack initiation properties rather than its crack propagation characteristics as it is the case in the SCB test. Nevertheless and as compared to the other mixes, the 64CO mix performed poorly in both test setups. It is also noted from Figures 3.5 and 6 that the asphalt mixtures prepared with polymer-modified PG 76-22, and PG 76-22 with low percentages of RAP were the overall best performers against cracking failure in the experimental program.

3.6 Theoretical Investigation

Results of the experimental program were investigated using a 3D FE approach. The 3D FE model, which accurately simulated the SCB test procedure, was used to achieve two main objectives: (1) identify the main failure mechanisms during the SCB testing process; and (2) study damage propagation in the SCB test. The commercial software ABAQUS version 6.9-1 was used for FE modeling of the SCB test procedure (ABAQUS Theory Manual 2010). Figure 3.7a illustrates the general layout of the FE model. Loading consisted of a displacement rate of 0.5 mm/min on the top of the specimen. The model is simply supported on the bottom sides of the model.

Cohesive zone elements with a bilinear traction-separation law were used in the FE model to simulate the cracking zone in the SCB test. Cohesive zone elements have been successfully applied by other investigators to simulate HMA cracking behavior and to avoid modeling the singularity at the crack tip (7, 13 - 14). Bilinear cohesive elements used in the FE model assumed linear elastic traction-separation behavior followed by linear propagation of damage as illustrated in Figure 3.7b (ABAQUS Theory Manual 2010). As shown in Figure 7b, the constitutive behavior of cohesive element is defined by the cohesive strength (T_o), the stiffness in the elastic region (K), and the cohesive fracture energy (Γ_c), which represents the area under the traction-separation curve. In the elastic region prior to δ_o, no damage occurs in the material and the deformation is recoverable. As displacement is increased in the specimen, the damage initiation point (δ_o, T_{max}) is reached. Once this point is reached, damage gradually progresses in the specimen while the damage variable (SDEG) monotonically increases from 0 to 1. Once a cohesive element is completely damaged (SDEG = 1), it is removed from the simulation and damage progresses through the specimen.

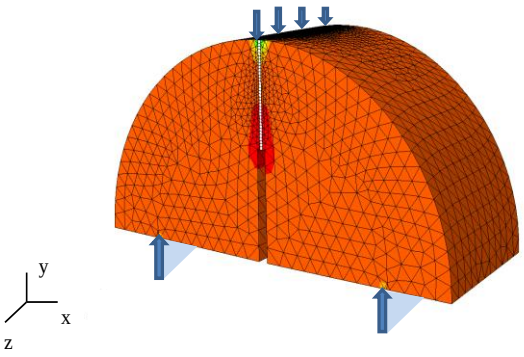

(a)

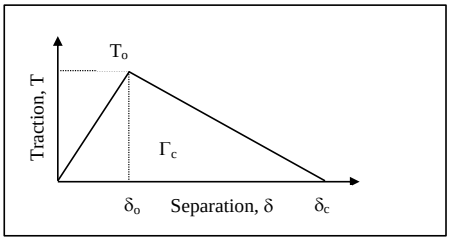

(b)

Figure 3.7 General Layout of the FE Model and Constitutive Behavior of the Cohesive Zone Element

3.6.1 HMA Constitutive Behavior

The viscoelastic behaviors of the prepared mixtures were characterized by laboratory testing using the dynamic modulus test in accordance with AASHTO T342-11. Dynamic modulus testing was conducted using triplicate samples at five temperatures (-10, 4.4, 25, 37.8, and 54.4^{o}C) and six frequencies (0.1, 0.5, 1, 5, 10, and 25 Hz). The air void content of the prepared samples was controlled between 7 ± 0.5%. The CV of the test results was less than 20% for all test temperatures and frequencies. Complex modulus experimental data were used to develop extended master curves at a reference temperature of 25^{o}C in accordance with the procedure suggested by Bonaquist and Christensen (2005) and successfully adopted by Al-Qadi et al. (2008) to simulate HMA viscoelastic behavior. This procedure employs the sigmoidal function to describe the rate dependency of the complex modulus master curve as follows, Figure 8:

$$\log(E^*) = \delta + \frac{(Max - \delta)}{1 + e^{\beta + \gamma\left\{\log(t) - \frac{\Delta E_a}{19.14714}\left[\left(\frac{1}{T}\right) - \left(\frac{1}{295.25}\right)\right]\right\}}} \tag{3.3}$$

where,
E* = complex modulus (MPa);
t = loading time (sec);
T = temperature in ° Rankine;
ΔE_a, δ, β and γ = fitting parameters; and
Max = limiting maximum modulus (MPa).

After fitting the sigmoidal model presented in Equation (3.3) to the measured data, this model was used to extend the master curve to very low and high frequencies not attainable in the laboratory. To describe the isotropic, linear viscoelastic behavior of HMA in the FE model, a generalized Maxwell solid model was used and fitted to the sigmoidal model (Figure 3.9). The model consists of a spring and n-Maxwell elements connected in parallel (Al-Qadi et al. 2008):

$$G(t) = G_0 - \sum_{i=1}^{N} g_i \left[1 - e^{-t/\tau_i}\right] \tag{3.4}$$

where,
G(t) = shear relaxation modulus at time t (MPa);
G_0 = glassy instantaneous shear relaxation modulus (MPa);
g_i = material constants referred to as relaxation strengths; and
τ_i = relaxation times (sec).

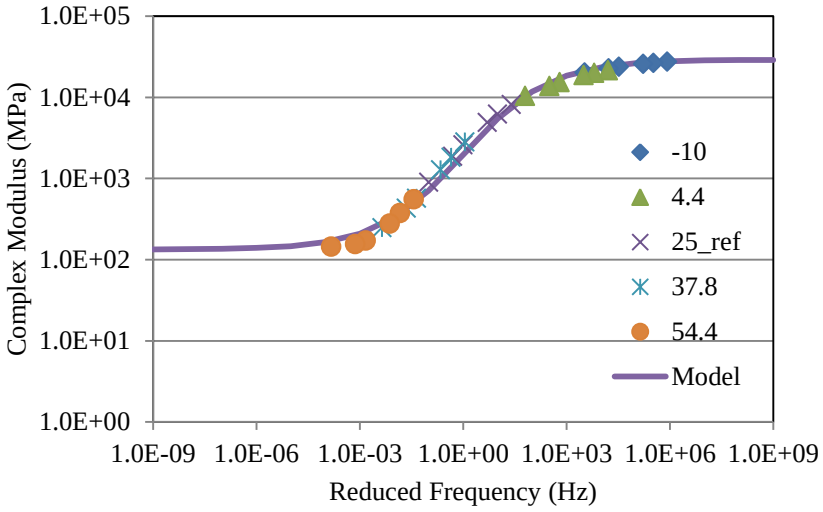

(a) 64CO

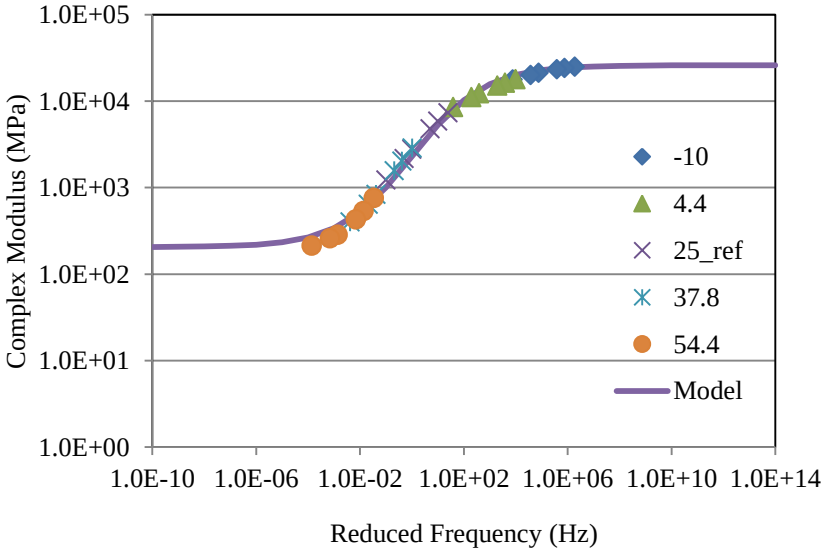

(b) 76CO

Figure 3.8 Extended Master curves for (a) the 64CO mixture and (b) the 76CO mixture (numbers on the series indicate the test temperatures in ^{o}C)

To fit Equation 3.4 to the sigmoidal model, a built-in module in the FE commercial software ABAQUS, was used (ABAQUS Theory Manual 2010). Variations of the normalized shear modulus with time were fitted to Equation 3.4 through a nonlinear least squares curve fitting process. Eleven to thirteen Prony series terms were used to obtain an accurate fit. Figures 3.9 (a and b) present a comparison between the input data (sigmoidal model) and the Prony series

model for two mixes. Based upon this analysis, the viscoelastic properties of HMA were defined at 25°C in the FE model.

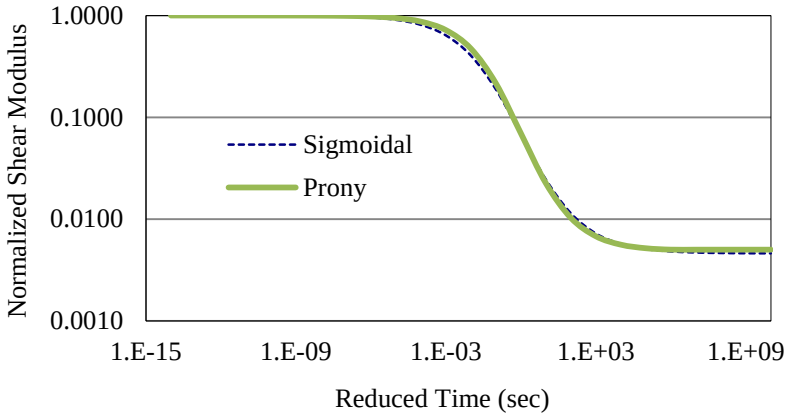

(a) 64CO

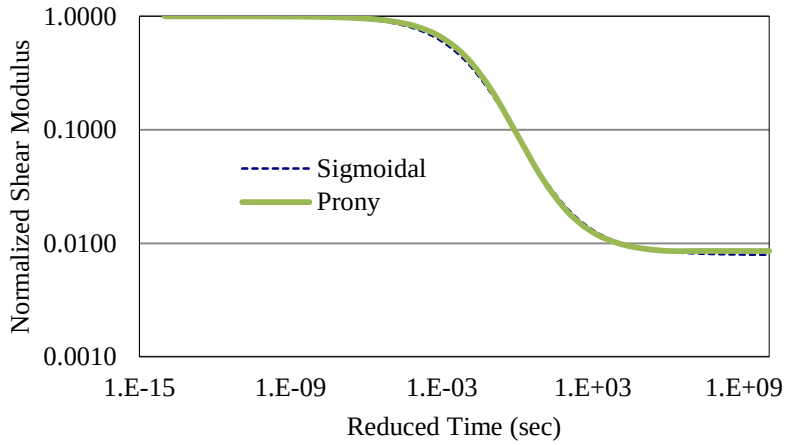

(b) 76CO

Figure 3.9 Fitting of the master curve to a prony series expansion for (a) 64CO and (b) 76CO

3.6.2 Cohesive Zone Element Constitutive Behavior

As suggested by Aragao and Kim (2010), parameters of the cohesive zone elements were obtained by fitting results of the FE model to the SCB experimental data. In this process, the cohesive strength (T_o) and the cohesive fracture energy (Γ_c) were repetitively varied until an acceptable match was achieved between experimental measurements and simulation output. Parameter K was selected sufficiently large to ensure linear elastic behavior in the undamaged phase. Figure 3.10 presents a comparison between measured and predicted SCB test results for

the 70CO and the 76CO mixes. As shown in this figure, a good agreement was achieved between measured and FE-predicted SCB test results. Based on these results, one may consider that the FE model provides an acceptable representation of the SCB test. Results of the FE model was used to identify the main failure mechanisms and to study damage propagation in the SCB test.

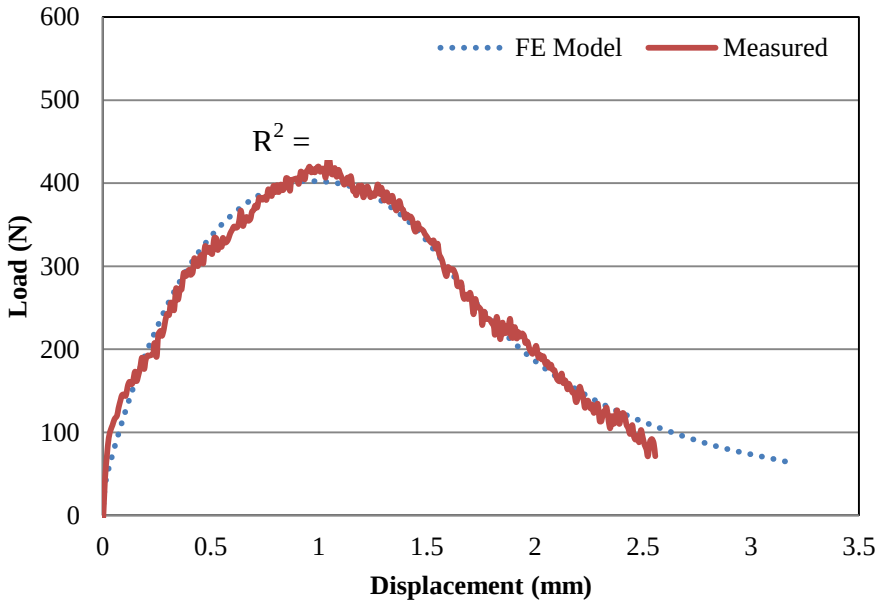

(a) 70CO

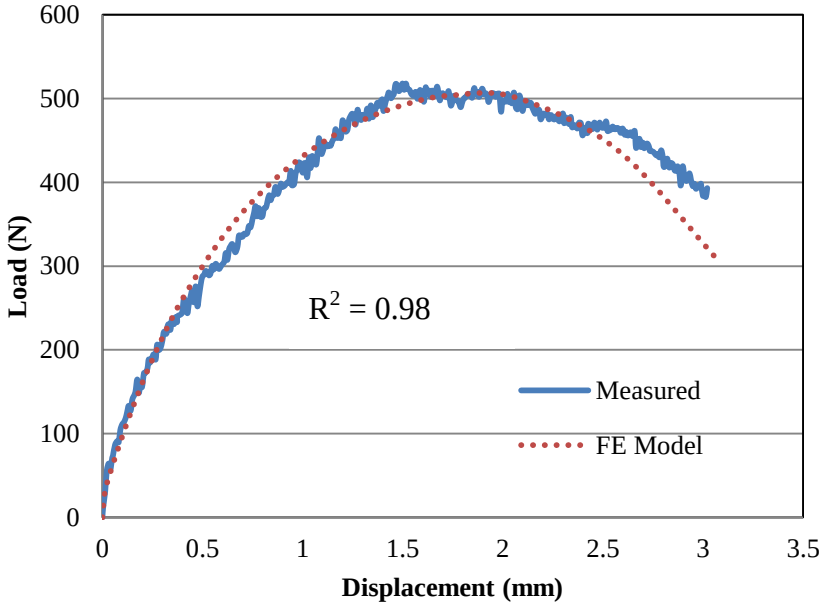

(b) 76CO

Figure 3.10 Comparison of FE and experimental SCB test results

3.6.3 FE Model Results and Analysis

Evolution of damage in the SCB was investigated using the results of the FE model. Figure 11 illustrates the damage propagation during the test process as predicted by the FE model for the 38.0-mm notch depth specimen. Damage describes the degradation of material stiffness through the testing process once the propagation criterion is satisfied. As shown in Figure 3.11, damage starts to propagate locally at the notch tip, Stage 1. Once total damage of the cohesive element is reached in the vicinity of the notch tip, damage progresses upward, Stage 2. As the applied displacement is increased, damage gradually progresses upward until total failure is reached, Stage 3.

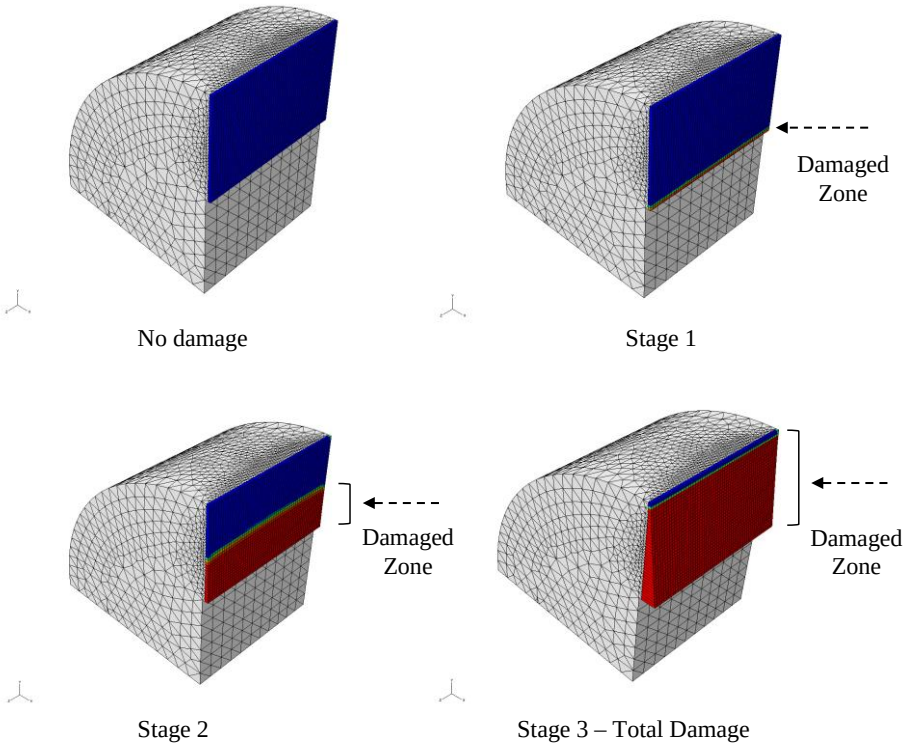

Figure 3.11 Damage Evolution in the SCB Test

Figure 3.12 shows the variation of horizontal stress, (S_{xx}) vertical stress (S_{yy}), and shear stress (S_{xy}) with time during the SCB test at mid-notch depth in the specimen. SDEG is a dimensionless scalar damage variable used to describe the evolution of damage in the element and captures the combined effects of all active failure mechanisms in the specimen. It initially has a value of 0 and then gradually increases until it reaches a terminal value of 1. As shown in

this figure, full damage of the element (SDEG ≈ 1.0) located at mid-notch depth in the specimen occurred after around 60 sec of the start of the test. Damage in the element was caused by a combination of vertical and horizontal stresses (S_{xx} and S_{yy}) acting on the element; however, the effect of shear (S_{xy}) on the progress of damage was negligible.

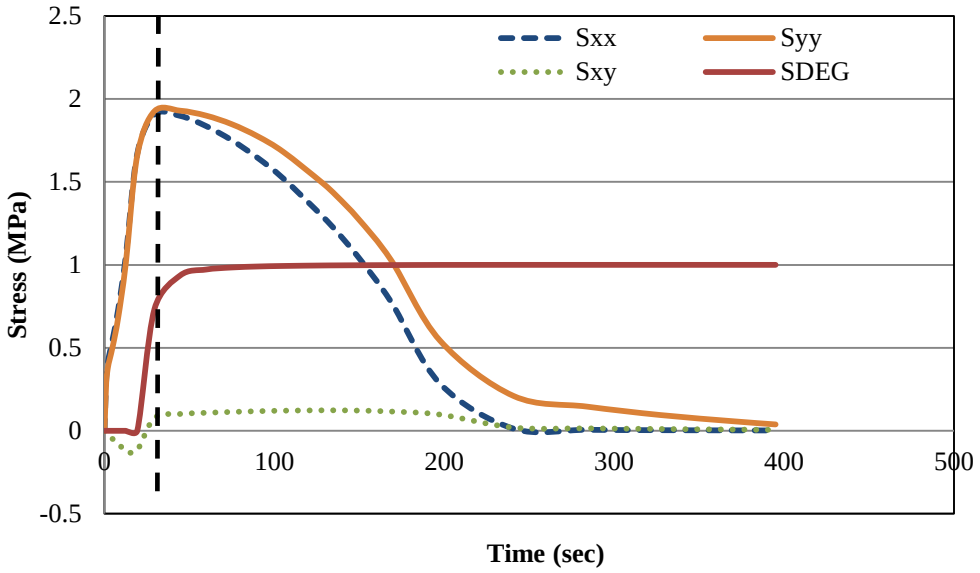

(a) 64CO

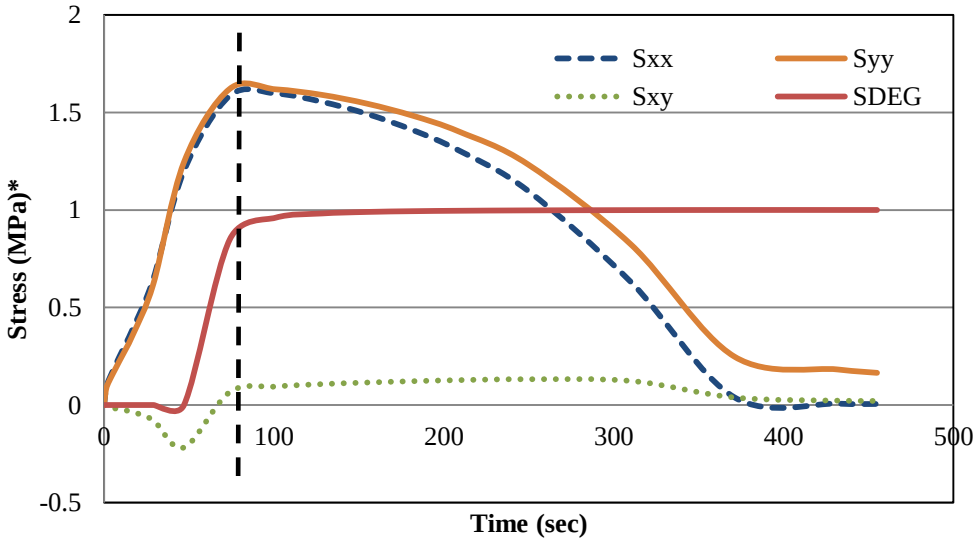

(b) 76CO

Figure 3.12 Progress of damage and stresses in the SCB test for (a) 64CO and (b) 76CO - * SDEG is a dimensionless scalar damage variable.

3.7 Summary and Conclusions

The SCB test configuration has been favored by many researchers due to the ease of sample preparation including cores removed from the field and the quick and simple testing procedure. It offers the potential of assessing the cracking resistance of the mix in the design phase and in QA activities. The objective of this study was to conduct a comprehensive evaluation of the SCB test and to utilize this test to evaluate a number of asphalt mixtures against cracking failure. Results of the experimental program were also used to validate a 3D FE model, which was used to interpret and to analyze the failure mechanisms in the SCB test. Based on the results of this study, the following conclusions may be drawn:

- SCB test results predicted that the mix prepared with high RAP content is more brittle than a comparable conventional mix and provides high stiffness characteristics. The critical strain energy rate successfully described the fracture performance of the evaluated mixes and was able to differentiate between them in terms of cracking resistance. Mixes prepared with polymer-modified binders were the best performers in this test against fracture.
- Results of the SCB were in agreement with the DCSE test and identified the mixes with high RAP content and the one prepared with straight unmodified binder as possible poor cracking performers in the field.
- The SCB test process as well as the propagation of damage were successfully simulated using 3D FE and cohesive elements. The presented modeling approach was in good agreement with measured test results for all mixes.
- Based on the results of the FE model, damage propagates in the vicinity of the notch and is mainly caused by a combination of vertical and horizontal stresses in the specimen. The effect of shear was negligible in progressing damage in the specimen.

3.8 Acknowledgements

This research was partially funded by the Louisiana Board of Regents - Research Competitiveness Subprogram (RCS). The assistance of the Louisiana Transportation Research Center (LTRC) and B. Vallabhu in preparing the asphalt concrete specimens is greatly appreciated.

3.9 References

ABAQUS Theory Manual (2010), Version 6.9-1. Habbit, Karlsson & Sorenson, Inc., Pawtucket, RI.

Adamson, R.M., Dempsey, J.P., and Mulmule, S.V. (1996). Fracture Analysis of Semi-Circular and Semi-Circular-Bend Geometries. International Journal of Fracture, Vol. 77, pp. 213-222, 1996.

Al-Qadi, I.L, Elseifi, M.A., Yoo, P.J., Dessouky, S.H., Gibson, N., Harman, T., D' Angelo, J., and Petros, K. (2008). Accuracy of Current Complex Modulus Selection Procedure from Vehicular Load Pulse in NCHRP 1-37A Mechanistic-Empirical Pavement Design Guide. Transportation Research Record: Journal of the Transportation Research Board, No. 2087, Washington, D.C., 2008, 81-90.

Arabani, M. and Ferdowsi, B. (2009). Evaluating the Semi-Circular Bending Test for HMA Mixtures. International Journal of Engineering A: Basics, Vol. 22, No.1, pp. 47-58, 2009.

Aragao, F. and Kim, Y.R. (2010). Characterization of Fracture Properties of Asphalt Mixtures Based on Cohesive Zone Modeling and Digital Image Correlation Technique. Paper presented at the 91st Transportation Research Board Annual Meeting, Washington, D.C.

Aragao, F.T., Kim, Y.R., Lee, J., and Allen, D.H. (2011). Micromechanical Model for Heterogeneous Asphalt Concrete Mixtures Subjected to Fracture Failure. Journal of Materials in Civil Engineering, ASCE, Vol. 23, No. 1, pp.30-38.

Baek, J. (2010). Modeling Reflective Cracking Development in Hot-Mix Asphalt Overlays and Quantification of Control Techniques, Ph.D. Dissertation, University of Illinois, Urbana-Champaign.

Bonaquist, R., and Christensen, D.W. (2005). A Practical Procedure for Developing Dynamic Modulus Master curves for Pavement Structural Design. Journal of the Transportation Research Board, 1929, Washington, D.C., pp. 208-217.

Huang, B., Shu, X., and Zuo, G. (2005). Laboratory Evaluation of Semi-Circular Bending Tensile Strength Test for HMA Mixtures. Journal of the Transportation Research Board, 84th Annual Meeting Compendium of Papers CD-ROM.

Li, X.J., and Marasteanu, M.O. (2010). Using Semi Circular Bending Test to Evaluate Low Temperature Fracture Resistance for Asphalt Concrete. Journal of Experimental Mechanics, Vol. 50, pp. 867-876.

McDaniel, R. S., Soleymani, H., Anderson, R. M., Turner, P., and Peterson, R., (2000). Recommended Use of Reclaimed Asphalt Pavement in the SuperPave Mixture Design Method. NCHRP Final Report (9-12), TRB, Washington, D.C.

Molenaar, A., Scarpas, A., Liu, X., Erkens, S. (2002). Semi-Circular Bending Test; Simple But Useful? Journal of Asphalt Paving Technologists, Vol. 71, pp. 794-815.

Mull, M.A., Othman, A., and Mohammad, L. (2006). Fatigue Crack Growth Analysis of HMA Employing the Semi-Circular Notched Bend Specimen. Paper No. 06-1665 presented at the 85th Annual Meeting of the Transportation Research Board.

Roque, R., Birgisson, B., Zhang, Z., Sangpetngam, B. and Grant, T., (2002). Implementation of SHRPP Indirect Tension Tester to Mitigate Cracking in Asphalt Pavements and Overlays, Final Report Submitted to Florida Department of Transportation, University of Florida, Gainesville.

Roque, R., Birgisson, B., Drakos, C. and Dietrich, B., (2004). Development and Field Evaluation of Energy-Based Criteria for Top-Down Cracking Performance of Hot-Mix Asphalt, Journal of the Association of Asphalt Paving Technologists, Vol. 73, Baton Rouge, Louisiana.

Wu, Z., Mohammad, L.N., Wang, L.B., Mull, M.A. (2005). Fracture Resistance Characterization of Superpave Mixtures Using the Semi-Circular Bending Test. Journal of ASTM International, Vol. 2, No. 3.

CHAPTER 4 –A CRACK PROPAGATION MODEL FOR ASPHALT MIXTURES BASED ON THE CYCLIC SEMI-CIRCULAR BENDING TEST[2]

4.1 Introduction

Cracking is a major failure mechanism in asphalt pavements that is caused by repeated traffic loading through a fatigue-related mechanism and thermal stress build-up at low temperature (Elseifi et al. 2012). It directly affects the ride quality and structural capacity of flexible pavements. In order to avoid premature failure of asphalt mixtures through a cracking-related mechanism, it is necessary to characterize the fracture and fatigue-resistance properties of asphalt mixtures in the laboratory during the design process. Several laboratory test methods have been introduced to characterize the fracture and fatigue resistances of hot-mix asphalt (HMA) including the dissipated creep strain energy test (DCSE), the disk-shaped compact (DSC) tension test, the four-point bending fatigue test, and the semi-circular bending (SCB) test.

The semi-circular bend test configuration has been favored by many researchers due to the ease of sample preparation including cores removed from the field and the quick and simple testing procedure (Li and Marasteanu 2010, Adamson et al. 1996). It offers the potential of assessing the fracture resistance of asphalt mixes in the laboratory in the design phase as well as in quality assurance (QA) testing activities. In this test method, a semi-circular gyratory-compacted specimen is notched at mid-span and is subjected to a monotonically increasing load until failure under a constant cross-head deformation rate of 0.5 mm/min. Based on the procedure introduced by Mohammad and co-workers, the critical strain energy release rate (J_c) is calculated and is used to describe the mixture's resistance to fracture (Wu et al. 2005).

While the use of SCB has been successful to characterize the fracture resistance of HMA, only limited attempts were found in the literature to assess the fatigue resistance of HMA in the laboratory using this test setup. Fracture and fatigue resistances of asphalt mixes can be different as the former is tested under a monotonically increasing load while the latter is associated with a cyclic load, which causes progressive and localized damage in the material. The objective of this study is twofold. First, a fatigue crack propagation model was developed based on the cyclic

[2] Presented at the 92nd Transportation Research Board Annual Meeting, 2013.

SCB test and the generalized J-integral approach. Second, the effect of creep deformation on the SCB test results obtained at intermediate temperature was investigated. To achieve these objectives, the necessary theoretical formulation is introduced based on fracture mechanics principles. Results of the model were validated based on laboratory testing of asphalt mixtures using a cyclic SCB test.

4.2 Background

4.2.1 Fatigue in HMA

Fatigue cracking is caused by repeated axle load applications usually lower than the strength of the material. It is a progressive localized damage due to fluctuating stresses and strains in the material and a build-up of irrecoverable strains (Hsu and Tseng 1996). Upon application of a load to the pavement, the material responds to the load, and tends to return to its original condition after passage of the load. However, when the load is removed, induced strains are only partly recovered and permanent strains progressively accumulate over time. Fatigue cracking usually starts at the bottom of the HMA layer, which represents the location of the greatest tensile strain in case of fully-bonded conditions between the different layers. However, cracking may also start at the pavement surface in case of thermal fatigue cracking or surface initiated top-down cracking (Hsu and Tseng 1996, Svasdisant et al. 2002).

Fatigue cracking is a three phase process consisting of crack initiation, progressive stable crack growth (i.e., crack propagation), and an ultimate failure stage, in which the crack growth rate increases rapidly as global instability is approached. The crack initiation phase is composed of two stages of micro-cracking and formation of macro-cracks, and is defined by the number of load repetitions required to form a visible damaged zone at the bottom of the layer (Uzan 1997). In the case of fatigue cracking induced by traffic loading, the original damage occurs primarily at the bottom of the HMA layers and grows upwards. The crack propagation phase, which is the phase simulated in the SCB test, represents the stage where the crack propagates to the surface through the entire thickness of the HMA layers. The crack propagation phase in asphalt pavements has been described by the empirical power law developed by Paris and Erdogan (1963):

$$\frac{da}{dN} = C\Delta K^m \quad (4.1)$$

where,
a = crack length;
N = number of loading cycles;
ΔK = range of stress intensity factor; and
C and m = material constants.

Since the stress intensity factor was developed for homogeneous and elastic materials, Rice (1968) introduced the path-independent contour integral J-integral, which considers the elasto-plastic/visco-plastic relationship of materials. It is equal to the generalized strain energy strain energy release rate (G) under mode I opening mode (Molenaar 2012). It can be determined from the following equation:

$$J = G = \frac{K_I^2}{E'} \tag{4.2}$$

where,
J = J-integral
K_I = stress intensity factor; and
E' = E (for plane stress conditions).

Mun and Lee (2011) used the generalized J-integral to study the crack propagation behavior of HMA under cyclic loading conditions. Results showed that the J-integral is suitable to predict the viscoelastic crack propagation in HMA mixtures under different loading magnitudes and frequencies. Kuai et al. (2009) developed a model to predict the crack propagation of asphalt concrete based on the generalized J-integral approach using the disk-shaped compact (DSC) test. Based on Schapery's earlier work for nonlinear viscoelastic materials, the J-integral was computed from a hereditary integral using the following equation (Schapery 1984):

$$J = \int_0^t D(t-\tau)\frac{\partial\left(P(\tau)\cdot G(a)\right)^2}{\partial\tau}\,d\tau \tag{4.3}$$

where,
D(t) = creep compliance;
P = loading function;
G = the parameter related to the dimensionless geometry function; and
τ = retardation time.

Results from Kuai et al. (2009) showed a good agreement between DSC and the crack propagation model developed based on Equation (4.3). Compared to the stress intensity factor K, the J-integral is a more accurate approach to describe the fatigue crack propagation of asphalt mixtures. Mull et al. (2006) studied the application of the SCB test configuration to characterize

the fatigue crack propagation of HMA mixtures. In this study, the value of J-Integral was calculated from the areas enclosed in the hysteresis loops using Equation (4.4):

$$J = \frac{1}{b}\left(\frac{\partial p}{\partial a}\right) \quad (4.4)$$

where,
P = potential energy which is the area between the loading curve and unloading curve of hysteresis loop;
b = specimen thickness; and
a = crack length.

4.2.2 Semi-Circular Bending Test

Starting from the early 1960s, numerous studies have evaluated cracking of asphalt mixtures in the laboratory. The SCB test is a laboratory procedure that evaluates the fracture resistance of HMA and steady-state propagation of a notch into an asphalt specimen. While it has been favored by many researchers due to its simple and quick test procedure and its use of a semi-cylindrical sample that can originate from a field core or from gyratory-compacted specimens, it has been exclusively used to study the fracture resistance of asphalt mixes (Elseifi et al. 2012). A brief description of the methods used to estimate the fracture resistance of asphalt mixes based on the SCB test is provided. A more thorough review has been presented elsewhere (Elseifi et al. 2012).

Molenaar et al. (2002) evaluated the usefulness of the SCB test in characterizing the fracture resistance of HMA mixtures. The SCB test was used to characterize the fracture resistance of HMA mixtures based on two parameters:

$$\sigma_t = 4.8\frac{F}{D} \quad (4.5)$$

$$M_r = 1.84\frac{F}{V} \quad (4.6)$$

where
σ_t = maximum tensile stress at the bottom of the specimen;
M_r = resilient modulus;
F = load per unite width of the specimen at failure;
D = specimen diameter; and
V = vertical deformation.

Arabani and Ferdowsi (2009) compared the SCB test to the indirect tensile strength test (ITS) and the Triaxial Hveem test, which are used to determine tensile strength, fracture resistance, and

fatigue properties of asphalt mixtures. The apparent fracture toughness was calculated as follows:

$$K_1 = \sigma_0 \sqrt{\pi a} Y_1 \quad (4.7)$$

$$\sigma_0 = \frac{F_{max}}{DL} \quad (4.8)$$

where,
K_1 = apparent fracture toughness;
Y_1 = normalized intensity factor;
F_{max} = maximum force at failure;
D = specimen diameter; and
L = specimen thickness.

Li and Marasteanu (2010) evaluated low temperature fracture resistance of HMA using the fracture energy. In their study, fracture energy (G_f) was calculated as follows (Li and Marasteanu 2010):

$$G_f = \frac{W_0 + mg\delta_0}{A_{lig}} \quad (4.9)$$

where,
W_0 = fracture work which is the area under the measured load-deformation curve;
m = weight of the specimen;
g = gravity acceleration;
δ_0 = deformation at the final stage of failure; and
A_{lig} = ligament area.

The procedure adopted in this study was developed by Mohammad and co-workers (2005), which is based on fundamental fracture mechanics principles (Anderson 2005). In this method, the fracture resistance of asphalt mixtures is estimated in the SCB using the critical strain energy release rate (J_c). In order to determine the value of J_c, load-vertical deflection curves are obtained by testing specimens with three notch depths (25.4, 31.8 and 38.0 mm) in the SCB test. The area under the load-vertical deflection curve, up to the maximum load, represents the strain energy to failure, U_f (Figure 4.1a). As shown in Figure 4.1b, the average values of U for each notch depth are plotted versus notch depth to obtain the slope (dU/da) from a regression line. The critical strain energy rate (J_c) can then be computed using the following equation (Wu et al. 2005):

$$J_c = -\left(\frac{1}{b}\right)\frac{dU_f}{da} \qquad (4.10)$$

where,
b = thickness of specimen;
a = crack length; and
U_f = the area under the load-vertical deflection curve, which represents the strain energy to failure (Figure 4.1).

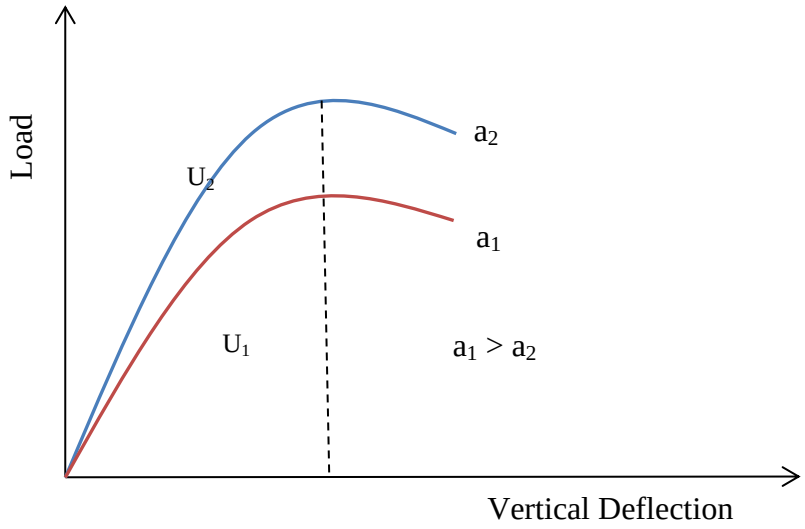

(a)

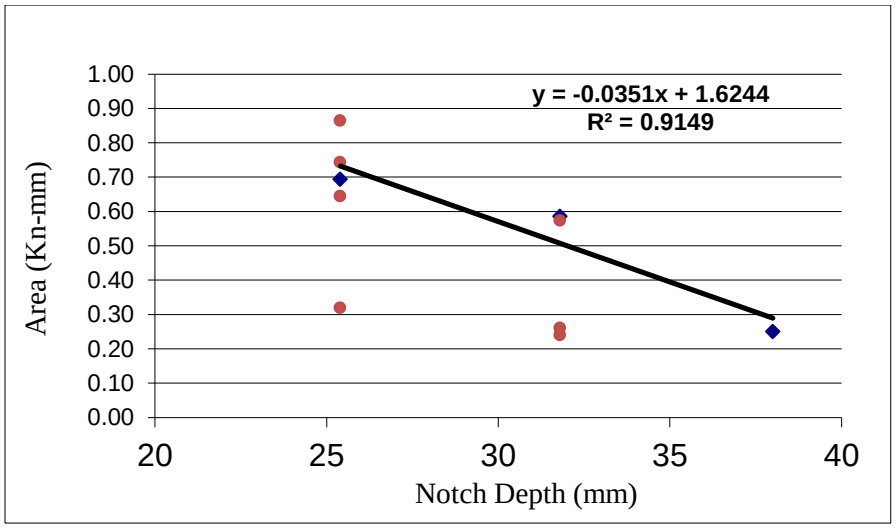

(b)

Figure 4.1 Critical strain energy release rate calculations (a) load-vertical deflection curves and (b) strain energy versus notch depth

Bayomy and co-workers (2005) determined the critical strain energy release rate, J_c, from a simple three-point bending fracture test using notched semi-circular HMA specimens. An un-

notched 3D FE model was used to predict J_c. Results showed that as the J_c increased, the stiffness increased in the evaluated mixtures. Based on these results, it was determined that the J_c could be used as an indicator of HMA resistance to fracture. Huang et al. (2005) compared the ability of the semi-circular bend test to characterize the tensile strength of HMA mixtures with IDT. Comparisons of the SCB and IDT results of 16 mixtures were conducted both analytically and numerically through the use of FE modeling. Results from the study showed that the SCB test was capable of providing consistent results. The authors also noted several advantages of the SCB test configuration; ease of sample preparation and load frame configuration were highlighted as distinct advantages of the test method (Huang et al. 2005). Table 4.1 summarizes the approaches used to characterize the fracture resistance of asphalt mixes based on the SCB test method.

Table 4.1 SCB Approaches for Fracture Resistance Evaluation of HMA

Sources	**Parameters**	**Equation**
Huang et al. (2005)	Tensile Strength	$\sigma_x = 3654 \cdot \frac{P_{ult}}{D \cdot t}$
Bayomy et al. (2006)	Critical Strain Energy Release Rate	$J_c = \left\lvert \frac{d}{da}\left(\frac{U}{b}\right) \right\rvert$
Mun and Lee (2011)	Change in the J-integral	$C(\Delta J)^P = \frac{dN}{da}$
Li and Marasteanu (2010)	Fracture Energy (G_f)	$G_f = \frac{W_0 + mg\delta_0}{A_{lig}}$
Mohammad et al. (2005)	Critical Strain Energy Release Rate	$J_c = -\left(\frac{1}{b}\right)\frac{dU_f}{da}$

4.3 Experimental Program

The cyclic SCB test was conducted to evaluate the fatigue cracking potential of asphalt mixtures. The proposed crack propagation model was based on Equations (4.2) and (4.3), which necessitates solving the hereditary integral to calculate J-integral as demonstrated in the following sections. In addition, to investigate the effects of creep deformation, the monotonic fracture resistance test was conducted.

4.3.1 Cyclic SCB Test

The SCB test setup utilized in this study is shown in Figure 4.2; it consists of a three-point bending load configuration, which is loaded at mid-span. Based on the test procedure suggested by Mohammad and co-workers (2005), test temperature was selected to be 25°C to correspond to the intermediate temperature range at which most of the traffic load that is responsible for fatigue damage, is applied. The stress-controlled cyclic SCB test was conducted by applying a haversine compressive load on a notched specimen with a loading frequency of 0.5 Hz. The maximum load was set at 670 N and the minimum load was set at 10% of the maximum load. Cyclic testing was conducted until the crack propagates to pre-defined crack lengths, at which the numbers of cycles for propagation are recorded.

4.3.2 Monotonic SCB Test

Based on the approach developed by Mohammad and co-workers (2005), the semi-circular specimen was loaded monotonically until failure under a constant cross-head deformation rate of 0.5 mm/min. The load and deformation are continuously recorded. Three notch depths (25.4 mm, 31.8 mm, and 38 mm) were tested to validate that the calculation and measurements are within the linear viscoelastic region. Typical test results of the monotonic SCB test are shown in Figure 4.1. Based on the results of this test, the critical strain energy release rate (J_c) was calculated according to Equation (4.10) and as illustrated in Figure 4.1.

4.3.3 Specimen Preparation

The SCB test specimens were obtained by cutting circular gyratory-compacted samples along their center diameter. The gyratory SCB specimens with 150 mm diameter were compacted to a 57 mm in height and an air void ratio of 7 ± 1.0 %. Three notches (25.4 mm, 31.8 mm, and 38 mm) were cut using a special saw blade with 3.0 mm thickness. The tolerance was ±1.0 mm on the notch depth and ± 0.5 mm on the notch width. Four semi-circular specimens were prepared and tested for each notch depth.

Figure 4.2 Semi-Circular Bending Test Setup

4.3.4 Test Materials

The experimental program consisted of two sets of test materials. For the cyclic study and as shown in Table 4.2, three mixtures consisting of a control, a crumb rubber (CR) modified asphalt mixture, and a chemically modified crumb rubber (CMCR) asphalt mixture, were tested. The three mixes had a nominal maximum aggregate size of 19.0 mm and were prepared according to AASHTO PP 28 and the Virginia Department of Transportation (VDOT) specifications for a high traffic surface mixture. Aggregate gradation was kept constant for three mixes and the asphalt binder content was maintained at 4.85%.

In the creep deformation study and as shown in Table 4.2, five mixtures including three conventional mixes (64CO, 70CO and 76CO) and two mixtures containing reclaimed asphalt pavement (RAP), (76RAP15 and 64RAP40), were prepared according to AASHTO PP 28 and the Louisiana Department of Transportation and Development (LADOTD) specifications ($N_{initial}$ = 8-, N_{design} = 100-, N_{final} = 160-gyrations). The mixture containing 40% RAP was treated with a rejuvenating engineered additive consisting of de-metalized oil and resin to soften the RAP binder and reduce the stiffness of the mixture (64RAP40). Four replicates, which meet the volumetric (VTM = 2.5 - 4.5 percent, VMA $\geq$ 12%, VFA = 68% -78%) and densification (%G_{mm} at $N_{initial} \leq 89$, %G_{mm} at $N_{final} \leq 98$) requirements, were tested.

Table 4.2 Description of the evaluated mixes

Study	Mixture Abbreviation	Description
Cyclic SCB	CO	Conventional HMA with PG 70-28
	CR	HMA mixture with Crumb-Rubber Modified PG 70-22
	CMCR	HMA mixture with Chemically Modified Crumb Rubber PG 76-28
Effects of Creep Deformation	64CO	Conventional HMA mixture with PG 64-22
	70CO	Conventional HMA mixture with Styrene-Butadiene Styrene Polymer-Modified PG 70-22
	76CO	Conventional HMA mixture with Polymer-Modified PG 76-22
	76RAP15	HMA mixture with Polymer Modified PG 76-22 and 15% RAP
	64RAP40	HMA mixture with PG 64-22 HMA containing 40% RAP and engineering additives

4.4 Model Formulation and Validation

4.4.1 The Strain Energy Release Rate for Nonlinear Elastic Materials

The fracture energy, E_f, can be used as a parameter to evaluate the fracture resistance of asphalt mixtures. It is defined as the work required to create a unit of new fracture surface:

$$E_f = \frac{dW_f}{dA} \tag{4.11}$$

where,
E_f = fracture energy;
W_f = facture work required to create new surfaces; and
A = crack area =Thickness*(Radius-a) for three dimensional specimens.

According to the theorem of Griffith energy balance, in order for the crack to increase in area dA, sufficient potential energy in the material are needed (Anderson 2005). Under equilibrium conditions, the Griffith energy balance is given by:

$$-\frac{dU}{dA} = \frac{dW_f}{dA} \tag{4.12}$$

where,
U = internal strain energy.

Rice (1968) proposed that the strain energy release rate in a nonlinear elastic material is equal to the value of the path-independent integral (J-integral):

$$J = -\frac{dU}{dA} = \frac{dW_f}{dA} \tag{4.13}$$

where,
U = internal strain energy; and
A = crack area =Thickness*(Radius-a) for three dimensional specimens.

4.4.2 The Viscoelastic Solution of J-Integral

A path-independent J-integral was introduced by Rice (1968) with the purpose of studying the crack in a nonlinear material. Consider a counterclockwise path, Γ, around the crack tip, the J-integral is defined by:

$$J = \int_{\Gamma}\left(wdy - T_i\frac{\partial u_i}{\partial x}ds\right) \tag{4.14}$$

where,
w = strain energy density;
T_i = components of the traction vector;
u_i = components of displacement vector; and
ds = length increment along the contour Γ.

Schapery (1984) defined a pseudo-elastic strain for solving viscoelastic problems with elastic solutions based on the Hooke's law:

$$\varepsilon_{ij}^{e}(t) = \frac{\sigma_{ij}(t)}{E_R} \tag{4.15}$$

where,
E_R = reference modulus; and
ε_{ij}^{e} = pseudo-strain.

The constitutive relationship between the strain and creep compliance is given by:

$$\varepsilon_{ij}(t) = \int_0^t D(t-\tau)\frac{d\sigma_{ij}(\tau)}{d\tau}\,d\tau \tag{4.16}$$

where,
D(t) = creep compliance.

The creep compliance, D(t), was computed from known E(t) using the approach developed by Park and Schapery (1999). Substituting Equation (4.15) into Equation (4.16), a nonlinear viscoelastic constitutive equation can be written as:

$$\varepsilon_{ij}(t) = E_R \int_0^t D(t-\tau) \frac{d\varepsilon_{ij}^e(\tau)}{d\tau} \, d\tau \tag{4.17}$$

where,
E_R = reference modulus; and
ε_{ij}^e = pseudo-strain.

Based on the viscoelastic correspondence principle, a generalized time-dependent J integral can be defined by developing a pseudo-elastic J-integral J_e:

$$J_e = \int_\Gamma \left(w^e dy - T_i \frac{\partial u_i^e}{\partial x} ds \right) \tag{4.18}$$

where,
w^e = pseudo-strain energy density $w^e = \int \sigma_{ij} \, d\varepsilon_{ij}^e$;
u_i^e = pseudo displacement vector; and
J_e = pseudo-elastic J integral which equals to energy release rate G.

Based on Schapery's approach (1984), Kuai and co-workers (2009) developed a generalized J-Integral, which can convert the viscoelastic problem into an elastic problem. Based on this approach, the generalized J-integral for the viscoelastic material is given as:

$$J = E_R \int_0^t D(t-\tau) \frac{\partial J_e}{\partial \tau} \, d\tau = \int_{t_0}^t D(t-\tau) \frac{\partial K_I{}^2}{\partial \tau} \, d\tau \tag{4.19}$$

where,

$$K_I = K_n \frac{P(\tau)}{T \cdot \sqrt{R}} \tag{4.20}$$

K_n is a normalized average stress intensity factor, which can be mathematically expressed as (Kuruppu 2000):

$$K_n = 70.4\left(\frac{a}{R}\right)^2 - 51.1\frac{a}{R} + 16.7 \tag{4.21}$$

where,
T = thickness of specimen;
a= notch depth;
K_I= Mode I stress intensity factor;
K_n= normalized stress intensity factor;
R= radius of specimen; and
$P(\tau)$ = loading function.

Therefore, the viscoelastic solution of J-integral, J_v, can be calculated by plugging Equation (4.20) into Equation (4.19) as follows (Kuai et al. 2009):

$$J_v = \int_0^{t_p} D(t_p - \tau) \frac{\partial[(K_n * P(\tau)/(t*\sqrt{R})]^2}{\partial \tau} d\tau$$
$$= [K_n/(T * \sqrt{R})]^2 \int_0^{t_p} D(t_p - \tau) \frac{\partial P(\tau)^2}{\partial \tau} d\tau$$
$$= 2 * [K_n/(T * \sqrt{R})]^2 \int_0^{t_p} D(t_p - \tau)\ P(\tau)'P(\tau)d\tau \qquad (4.22)$$

where,
t_p = the time when the load in Figure 4.1(a) reach to the peak point; and
T = thickness of specimen;

By plugging Equation (4.22) into a modified version of Paris law that utilizes the J-integral instead of the stress intensity factor, see Equation (4.1), one may determine the number of cycles required for the crack to propagate from its original position to a final position.

4.4.3 Model Validation

To validate the model presented in Equation (4.22), the strain energy release rate was estimated at various crack lengths from laboratory measurements based on Equation (4.10), (Mull et al. 2006). Figure 4.3 compares model prediction to experimental measurements for the three mixes. As shown in Figure 4.3, there was good agreement between measured and model predicted SCB test results. Based on these results, it is determined that the proposed model provides an acceptable representation of the fatigue SCB test.

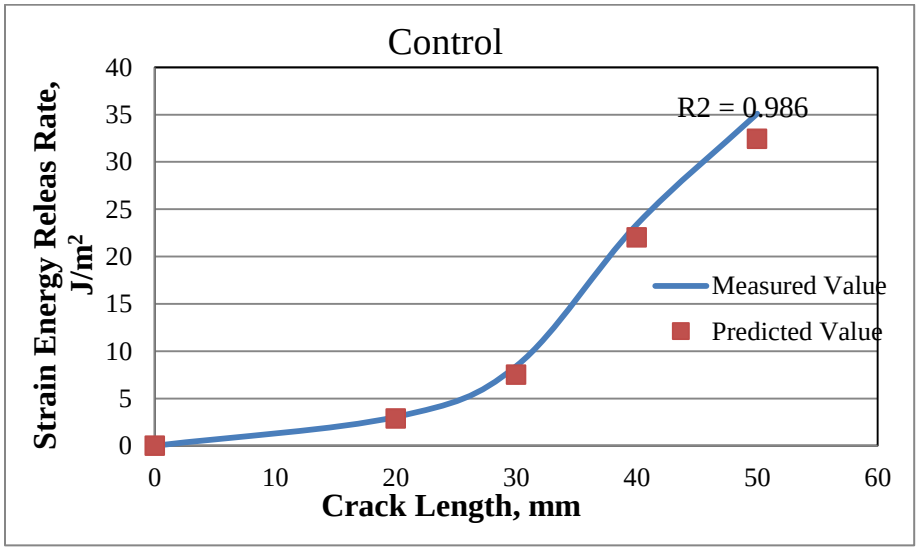

(a)

Figure 4.3 Comparison of Model and Experimental SCB Test Results

(**Figure 4.3** continued)

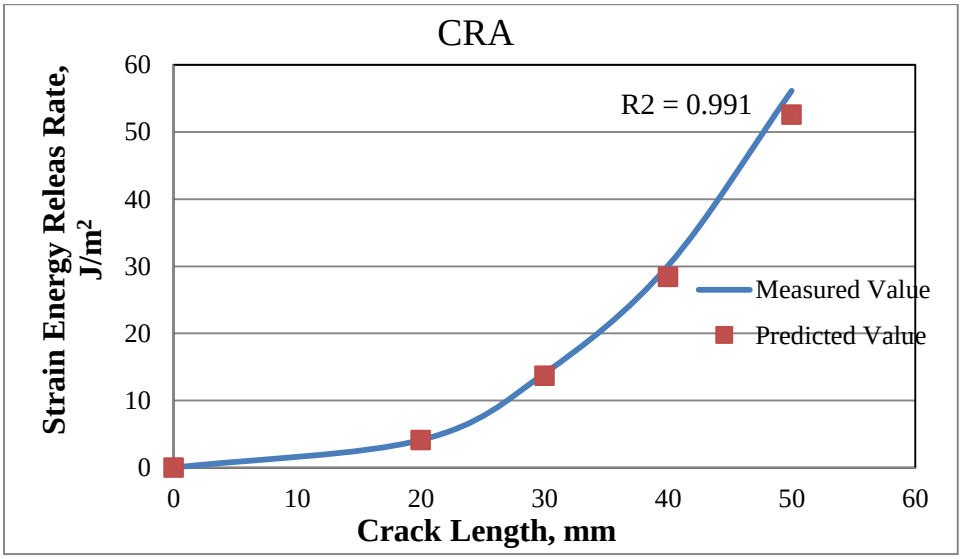

(b)

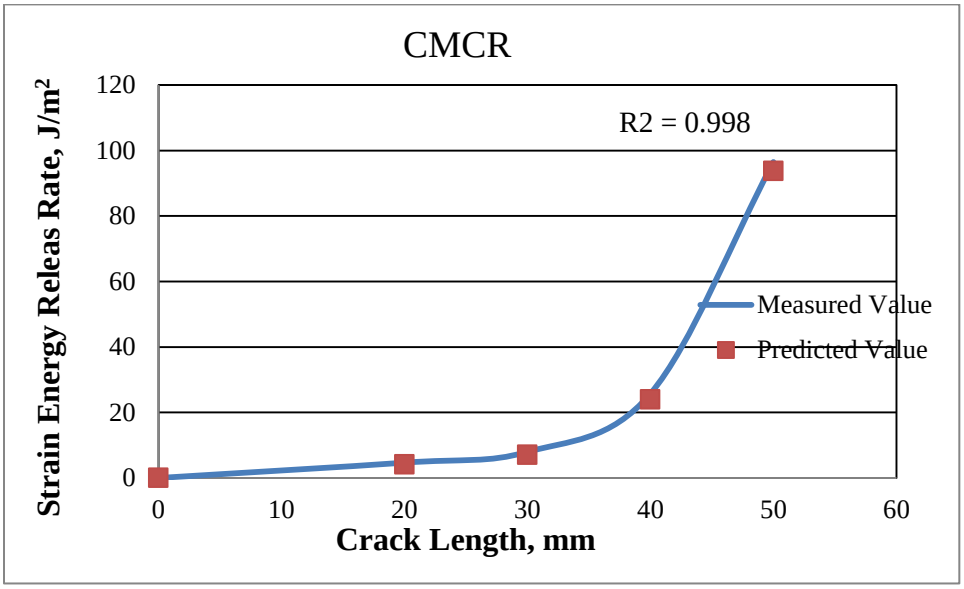

(c)

4.5 Effects of Creep Deformation

Since the SCB test is conducted at intermediate temperature (25°C), concerns were raised that the effects of creep deformation may be significant and that failure in the SCB is due to the combined effects of creep and fracture. To investigate the effects of creep deformation, a finite element (FE) approach was developed. Finite element simulation was performed in this study to analyze the fracture resistance of mixtures in the monotonic SCB test. The commercial FE software ABAQUS version 6.9-1 was selected for the FE modeling of the SCB test procedure

(ABAQUS Theory Manual 2010). 3D FE models were used to investigate the dissipated creep energy during the SCB monotonic testing process. Figure 4.4 presents the general layout of the FE models. With the purpose of simulating the SCB test procedure in the monotonic test, a displacement rate of 0.5 mm/min was applied on the top of the specimen. The modeled specimen was simply supported from the bottom sides as shown in Figure 4.4.

4.5.1 HMA Constitutive Behavior

Dynamic modulus testing was conducted at five temperatures (-10, 4.4, 25, 37.8, and 54.4^{o}C) and six frequencies (0.1, 0.5, 1, 5, 10, and 25Hz) to characterize the viscoelastic behaviors of the prepared mixtures in accordance with AASHTO TP-79. To define the viscoelastic behavior of HMA in the FE model, values of the storage modulus, E', were computed from the dynamic modulus |E*|:

$$E' = |E^*| \cdot \cos\phi \tag{4.26}$$

where,
E^* = dynamic modulus; and
ϕ = phase angle.

In order to describe the linear viscoelastic behavior of asphalt mixes, a sigmoidal model was employed to fit the storage modulus E' and to extend the master curve of E' to frequencies (Figure 4.5), which could not be reached in laboratory (Bonaquist and Christensen 2005):

$$\log_{10}(E') = a_1 + \frac{a_2}{\left\{a_3 + \frac{a_4}{\exp[a_5 + a_6 \log_{10}(\omega)]}\right\}} \tag{4.27}$$

where,
ω = reduced frequency; and
$a_{1....6}$ = fitting parameters.

The relaxation modulus, E(t), is needed to describe viscoelastic behavior in the FE model. In order to convert the frequency domain storage modulus, E', to time domain relaxation modulus E(t), the following Maxwell model was used to fit the extended storage modulus obtained from the sigmoidal model:

$$E'(\omega_n) = E_\infty + \sum_{m=1}^{M} \frac{\omega_n^2 \rho_m^2 E_m}{\omega_n^2 \rho_m^2 + 1} \tag{4.28}$$

where,

E_∞, ω_n ρ_m and E_m = the parameters obtained by fitting the above expression with the extended sigmoidal model.

The time-domain modulus E(t) was then calculated using the following equation based on the fitting parameters obtained from Equation (4.28):

$$E(t) = E_\infty + \sum_{m=1}^{M} E_m \exp\left(\frac{-t}{\rho_m}\right) \quad (4.29)$$

As a required input in the FE model, the shear relaxation modulus was estimated from the relaxation modulus and fitted to a Prony series model as follows:

$$G(t) = 1 - \sum_{i=1}^{N} g_i\left[1 - e^{-t/\tau_i}\right] \quad (4.30)$$

where,
G(t) = shear relaxation modulus at time t (MPa);
g_i = material constants referred to as relaxation strengths; and
τ_i = relaxation times (sec).

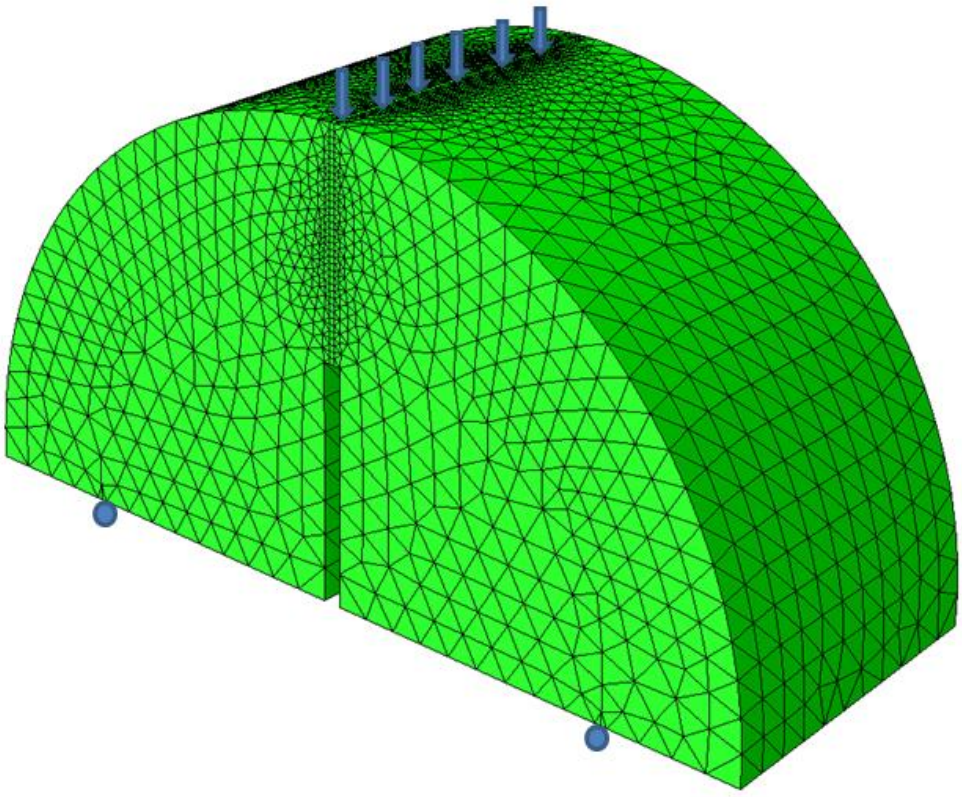

Figure 4.4 General Layout of the FE Model of the SCB Test Setup

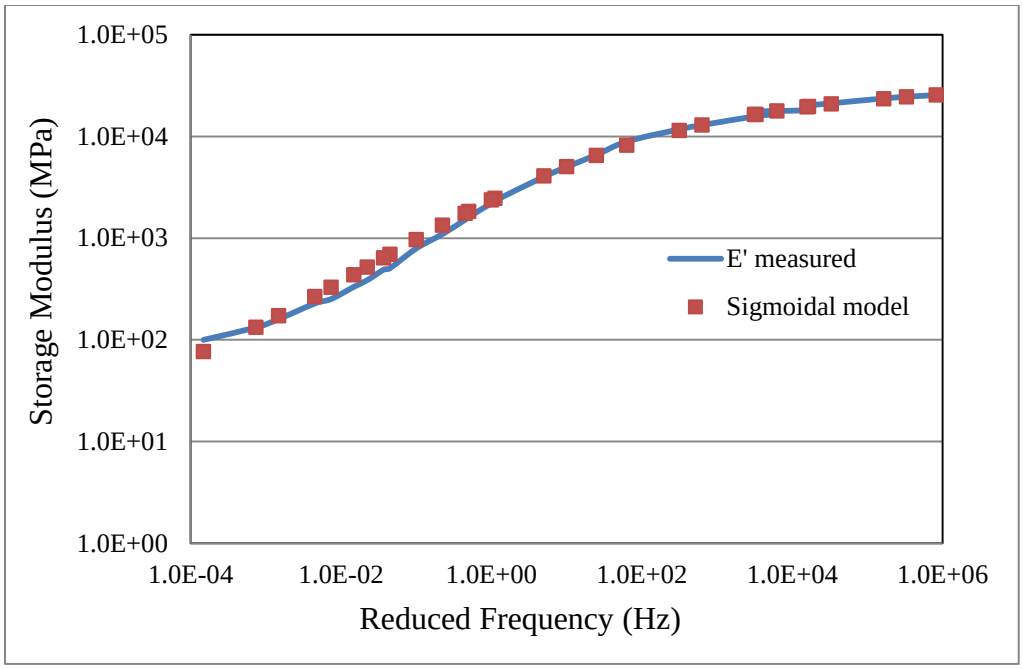

(a) 64CO

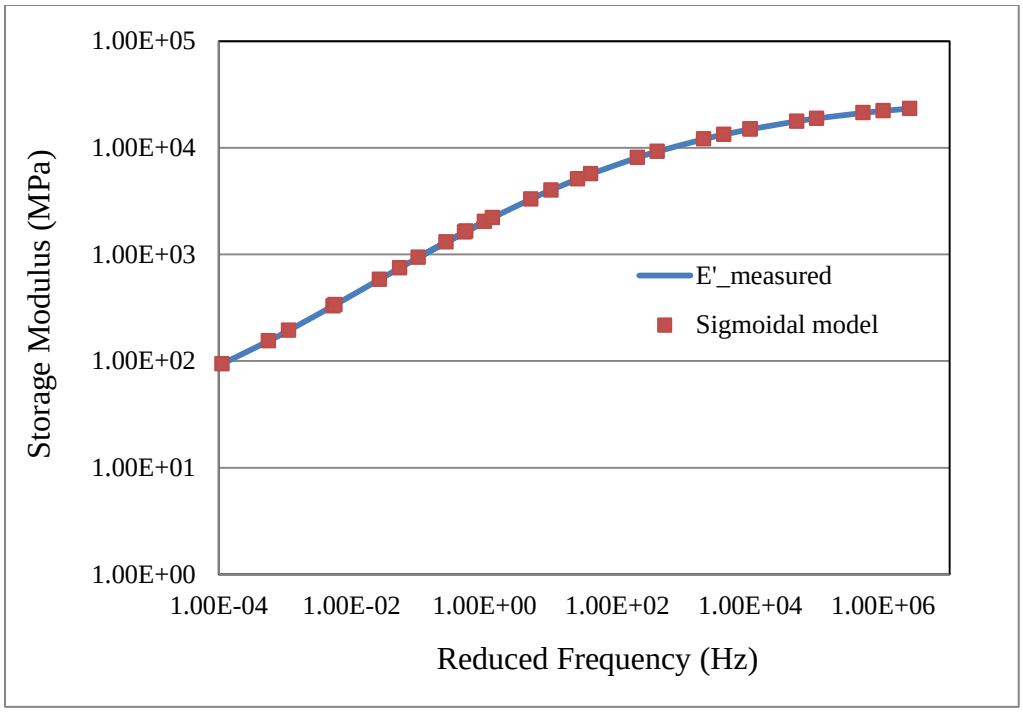

(b) 76CO

Figure 4.5 Fitting storage modulus E' to sigmoidal model for (a) the 64CO mixture and (b) the 76CO mixture

4.5.2 The Dissipated Creep Strain Energy

The dissipated creep strain energy (DCSE) corresponds to the dissipated energy by the time-dependent creep strain until fracture. It was calculated for the entire FE model based on the following equation (4.21):

$$E_c = \int_o^t \left(\int_V \sigma^c : \dot{\varepsilon}^{cr} dV \right) d\tau \quad (4.31)$$

where,
E_c = energy dissipated by creep;
V = output region which equals to the total volume of model in this study
σ^c = effective stress; and
$\dot{\varepsilon}^{cr}$ = creep strain rates.

4.5.3 The Damage Dissipated Strain Energy

The effective stress, σ^c, can be expressed in terms of the decrease in the "undamaged" stress, σ^u (ABAQUS Theory Manual 2010):

$$\sigma^c = (1 - d)\sigma^u \quad (4.32)$$

where,
d = damage parameter which starts at zero (undamaged material) and increases to 1 (fully damaged material).

When damage occurs in the material, the applied elastic strain energy is non-recoverable. The energy dissipated through damage is given as follows (ABAQUS Theory Manual 2010):

$$E_c = \int_o^t \frac{\dot{d}}{2(1-d)} \sigma^u f^c : \varepsilon^{el} dV d\tau \quad (4.33)$$

where,
ε^{el} = elastic strain.

4.5.4 Results and Analysis

Table 4.3 presents the dissipated creep strain energy, the energy dissipated through damage, and the percentage of DCSE with respect to the total dissipated energy for the tested mixes. The total dissipated energy is equal to the sum of the dissipated creep strain energy and the energy dissipated through damage. Figure 4.6 graphically compares the DCSE to the energy dissipated through damage. The critical strain energy rate (J_c) is also presented in this table for the mixtures evaluated in this study based on Equation (4.10) and monotonic SCB test results. As

shown in Table 4.3 and Figure 4.6, the average energy dissipated due to creep deformation in the SCB test was 7.1% of the total dissipated energy in the model. This means that 92.9% of the energy is dissipated due to the propagation of the crack in the SCB test. Results presented in Table 4.3 also show that the 76RAP15 and 76CO mix were the best performers against fracture as indicated by the high J_c. It is noted that the fracture resistance of the mixes was mainly controlled by the binder in the mix with better performance when polymer-modified binders were used (i.e., 70CO, 76CO, and 76RAP15). It is also noted that the 76CO mix had the highest creep energy percentage (8.6%) and the lowest percentage of energy used to propagate the crack. This means that most of the external energy, which originates from the loading, is used to increase the internal energy in the specimen and a smaller percentage of energy is used to propagate the crack.

Table 4.3 Creep Dissipated Strain Energy from FE Models

Mixture Abbreviation	J_c (kJ/m^2)	Diss. Creep Energy (J/mm^3)	Diss. Damage Energy (J/mm^3)	Creep Energy Percentage (%)
70CO	0.92	0.109	2.245	4.6
76CO	0.93	0.225	2.386	8.6
76RAP15	0.50	0.22	2.706	7.5
64CO	0.63	0.082	1.38	5.6
64RAP40	1.09	0.112	1.585	6.6
Average (%)				7.1

Figure 4.7 presents the variation of energy with time for the dissipated energy through damage and the total dissipated energy in the model for the 64CO and 76CO mixes. It is determined from these results that the dissipated energy due to fracture (damage dissipated energy) is the predominant factor controlling failure in the SCB test.

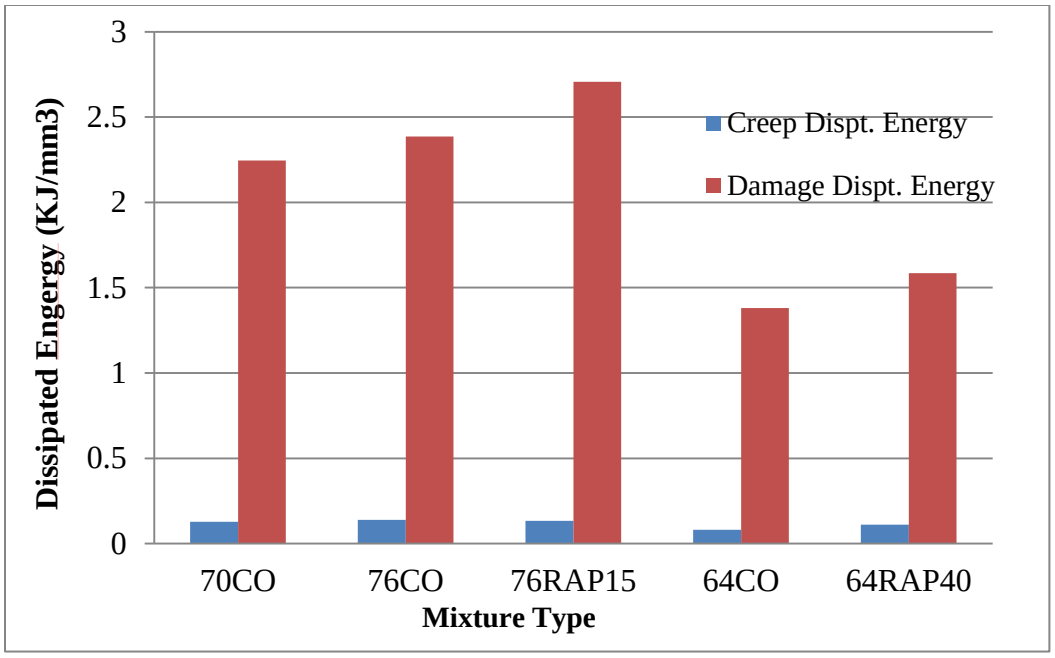

Figure 4.6 Creep dissipated energy and damage dissipated energy for all the mixtures

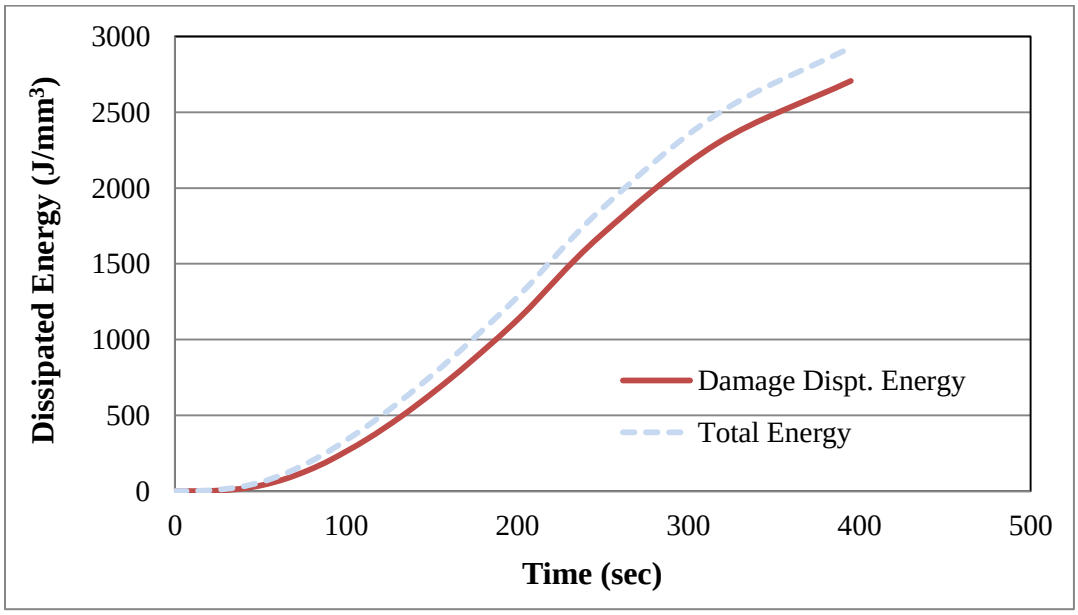

(a)

Figure 4.7 Variation of damage dissipated energy and total energy with time for (a) 76RAP15 and (b) 70CO

(**Figure 4.7** continued)

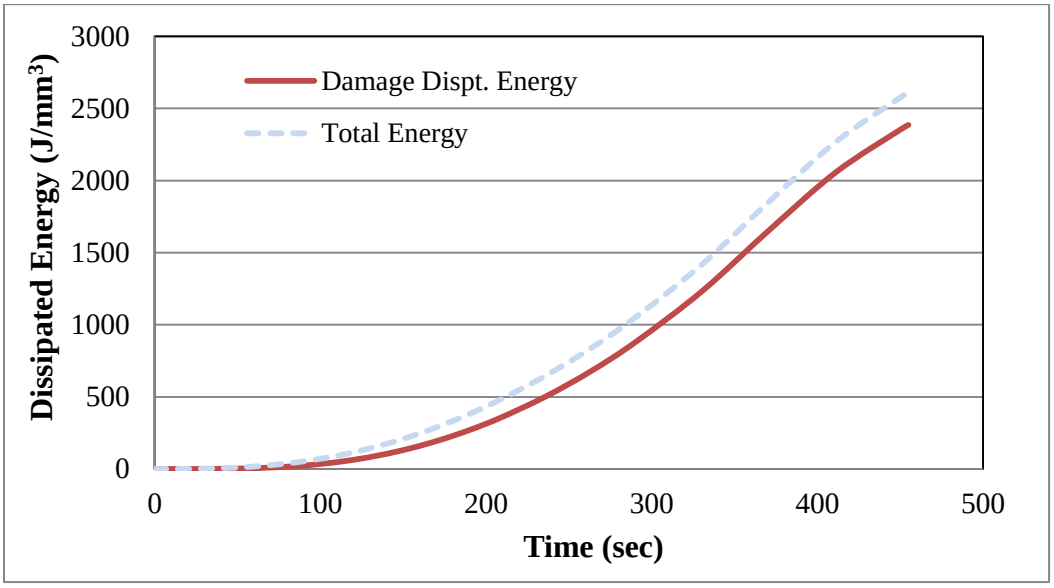

(b)

4.6 Summary and Conclusions

A crack propagation model was developed based on a cyclic SCB test and the generalized J-integral approach. In addition, the effect of creep deformation on the SCB test results obtained at intermediate temperature was investigated. In this study, the necessary theoretical formulation was introduced based on fracture mechanics principles. Results of the model were validated based on laboratory testing of asphalt mixtures using a cyclic SCB test. Based on the results of this study, the following conclusions may be drawn:

- There was good agreement between measured and model predicted SCB test results. Based on these results, it is determined that the proposed model provides an acceptable representation of the fatigue SCB test.
- The average energy dissipated due to creep deformation in the monotonic SCB test conducted at intermediate temperature was 7.1% of the total dissipated energy in the model.
- Dissipated energy due to fracture is the predominant factor controlling failure in the SCB test.

4.7 References

ABAQUS Theory Manual, Version 6.9-1. (2010). Habbit, Karlsson & Sorenson, Inc., Pawtucket, RI.

Adamson, R.M., Dempsey, J.P., and Mulmule, S.V. (1996). Fracture Analysis of Semi-Circular and Semi-Circular-Bend Geometries. International Journal of Fracture, Vol. 77, pp. 213-222.

Anderson, T.L. (2005). Fracture Mechanics - Fundamentals and Applications, 3rd Edition, CRC, Taylor and Francis, Boca Raton, FL.

Arabani, M. and Ferdowsi, B. (2009). Evaluating the Semi-Circluar Bending Test for HMA Mixtures. International Journal of Engineering A: Basics, Vol. 22, No.1, pp. 47-58.

Bayomy, F., A.A. Abdo, M.A. Mull, and M. Santi. (2005). Evaluation of Hot Mix Asphalt (HMA) Fracture Resistance Using the Critical Strain Energy Release Rate, Jc. Paper Presented at the 85th Annual Meeting of the Transportation Research Board, Washington, D.C.

Bonaquist, R., and Christensen, D.W. (2005). A Practical Procedure for Developing Dynamic Modulus Master curves for Pavement Structural Design. Journal of the Transportation Research Board, 1929, Washington, D.C. , pp. 208-217.

Elseifi, M.A., L.N. Mohammad, H. Ying, and S. Cooper. (2012). Modeling and Evaluation of the Semi-Circular Bending Test for Intermediate Temperature Cracking of Asphalt Mixtures. Paper accepted for publication in the Journal of the Association of Asphalt Paving Technologists, Vol. 81, In Press.

Huang, B., Shu, X., and Zuo, G. (2005). Laboratory Evaluation of Semi-Circular Bending Tensile Strength Test for HMA Mixtures. Journal of the Transportation Research Board, 84th Annual Meeting Compendium of Papers CD-ROM.

Hsu, T.W., and K.H. Tseng. (1996). Effect of Rest Periods on Fatigue Response of Asphalt Concrete Mixtures. In Journal of Transportation Engineering, American Society of Civil Engineering, vol. 122, No. 4, 316-322.

Kuruppu, M. (2000). Fracture toughness testing of geomaterials using semi-circular specimen. Proc. Int. Conf. on Geotechnical & Geological Eng(GeoEng), Melbourne, Paper No. Gcc 0806.

Kuai, H.D., H.J. Lee, G.S. Zi and S.H. Mun. (2009). Application of Generalized J Integral to Crack Propagation Modeling of Asphalt Concrete under Repeated Loading. 88th Transportation Research Board Annual Meeting, Washington, D.C, 2009. pp.72-81.

Li, X.J., and Marasteanu, M.O. (2010). Using Semi Circular Bending Test to Evaluate Low Temperature Fracture Resistance for Asphalt Concrete. Journal of Experimental Mechanics, Vol. 50, pp. 867-876.

Molenaar, A., Scarpas, A., Liu, X., Erkens, S. (2002). Semi-Circular Bending Test; Simple But Useful? Journal of Asphalt Paving Technologists, Vol. 71, pp. 794-815.

Mun, S. and Lee, H.J. (2011). Modeling Viscoelastic Crack Growth in Hot-Mix Asphalt Concrete Mixtures Using a Disk-Shaped Compact Tension Test. Journal of Engineering Mechanics, ASCE, Vol. 137, 432.

Mull, M.A., Othman, A., and Mohammad, L. (2006). Fatigue Crack Growth Analysis of HMA Employing the Semi-Circular Notched Bend Specimen. Journal of the Transportation Research Board, 85th Annual Meeting Compendium of Papers CD-ROM.

Paris, P.C. and F.A. Erdogan. (1963). Critical Analysis of Crack Propagation Laws. In Transactions of the ASME, Journal of Basic Engineering, Series D, No. 3,528-533.

Park, S. W., and R. A. Schapery. (1999). Methods of Interconversion between Linear Viscoelastic Material Functions. Part 1 – A Numerical Method Based on Prony Series.Int. J. Solids and Structures, 36(11), pp 1653-1675.

Rice, J.R., (1968). A Path Independent Integral and the Approximate Analysis of Strain Concentration by Notches and Cracks." Journal of Applied Mechanics, Vol. 35, pp.379-386.

Schapery, R.A. (1984). Corresponding Principles and a Generalized J Integral for Large Deformation and Fracture Analysis of Viscoelastic Media. International Journal of Fracture, Vol. 25, pp. 195-223.

Svasdisant, T., M. Schorsch, G.Y. Baladi, and S. Pinyosunun. (2002). Mechanistic Analysis of Top-Down Cracks in Asphalt Pavements. In Transportation Research Record 1809, Transportation Research Board, Washington, D.C., pp. 126-136.

Uzan, J. (1997). Evaluation of Fatigue Cracking. In Transportation Research Record 1570, Transportation Research Board, Washington, D.C., 89-95.

Wu, Z., Mohammad, L.N., Wang, L.B., Mull, M.A. (2005). Fracture Resistance Characterization of Superpave Mixtures Using the Semi-Circular Bending Test. Journal of ASTM International, Vol. 2, No. 3.

CHAPTER 5 –HETEROGENEOUS FINITE ELEMENT MODELING OF THE DYNAMIC COMPLEX MODULUS TEST OF ASPHALT MIXTURE USING X-RAY COMPUTED TOMOGRAPHY

5.1 Introduction

The dynamic modulus test was introduced by NCHRP 9-19 as a simple performance test (SPT), used to characterize the linear viscoelastic properties of asphalt mixtures (Witczak et al. 2002). It is an essential component of the new mechanistic-empirical pavement design guide (MEPDG) to account for the effects of temperature and rate of loading on asphalt mixes in the design phase (Al-Qadi et al. 2010). The standard test method for determining the dynamic modulus of asphalt mixes, AASHTO TP 62-07, assumes that measurements are conducted within the linear viscoelastic region, in which the dynamic modulus is independent of the stress or strain amplitude. Calculation of the dynamic modulus also assumes proportionality of the induced strain to the applied stress on the specimen. Therefore, no damage is assumed to occur during the testing procedure in order to ensure validity of the measurements and the calculations. This assumption was validated as damage analysis of test specimens before and after loading showed that the damage taking place in the dynamic modulus test is minimal and homogeneous (Elseifi et al. 2011).

While the asphalt mixture is a composite material consisting of aggregate, mastic, and air voids, laboratory tests such as the dynamic complex modulus assume that this material can be dealt with as a homogeneous material with no distinction made between its different constituents. In addition, the classical continuum theory is applied in analyzing the measurements obtained in the dynamic modulus test while overlooking the particulate nature of this composite. It is well-established that asphalt mixture is a heterogeneous, composite material that is influenced by the responses of its components to loading (Elseifi et al. 2003; Masad et al. 2007).

Due to the clear limitations of the elastic continuum theory, pavement engineers have recently paid considerable attention to the use of advanced modeling techniques for simulating the accurate behavior of asphalt mixtures. One promising approach consists of adopting an image-based finite element (FE) method, which may be able to predict more accurately the behavior and failure mechanisms in asphalt mixtures. In this approach, the particulate nature of asphalt mixtures is considered as a composite, multiphase material, containing aggregate, mastic,

and air voids (Dai et al. 2005). The mastic can be treated as a viscoelastic/viscoplastic material, and the aggregates can be treated as an elastic material. Each component is described separately, thereby defining load transfer mechanisms between these constituents are essential to ensure accurate description of the composite.

5.2 Research Objectives

The objective of this study is to develop a three-dimensional (3D), heterogeneous model to describe the response of asphalt mixtures in the dynamic complex modulus test using an image-based FE modeling approach and by digitizing X-ray computed tomography (CT) acquired images. The developed heterogeneous models were validated and calibrated against experimental testing results for hot-mix asphalt (HMA) and warm-mix asphalt (WMA) mixtures.

5.3 Background

5.3.1 Digital Image Analysis

Digital image analysis allows one to enhance desired features in acquired digital images and to analyze the image based on the differences in grayscale intensities of the features. Enhanced digital images can also be converted to a numerical FE mesh. In the 1990s, digital image analysis techniques were utilized to analyze HMA (Eriksen and Wegan 1993; Masad et al. 1999). Using digital image analysis, Masad et al. (1999) quantified aggregate orientation, gradation, and aggregate segregation in HMA. This methodology was utilized to investigate the influence of compaction levels in the Superpave Gyratory Compactor and in the field on the internal structure of HMA.

Elseifi and co-workers (2008) employed a high resolution digital camera to investigate the concept of asphalt binder film thickness experimentally. Adhikari and You (2007) used X-ray CT imaging technology to characterize aggregate orientation, aggregate gradation, mastic distribution, and air void distribution in HMA. The locations of aggregate, air voids, and mastic were defined based on the grayscale intensities of X-ray CT images. 3D Distinct Element Model was constructed from 2D X-ray images and used to predict dynamic modulus of the mixture during a range of temperatures and loading frequencies. Kassem et al (2009) successfully employed 3D X-ray CT to evaluate the quality of the compaction of asphalt layers within full-depth pavements. Image analysis technique was used to determine the average percent of air

voids through the depth of the HMA layer. In general, it is widely recognized that X-ray CT is an effective method to evaluate the internal structure of asphalt mixtures.

5.3.2 Heterogeneous Modeling of Asphalt Mixture

The classical approach to predict flexible pavement response to loading is based on the linear elastic continuum theory, in which the material heterogeneity is not considered. Due to the limitations of the elastic continuum theory, micromechanical modeling techniques were introduced to describe the constitutive behavior of asphalt mixtures. You and co-workers (2009) developed an X-ray image-based, three-dimensional, discrete element method (DEM), heterogeneous model to predict the dynamic modulus of asphalt mixture. Results showed that the 3D imaged-based heterogeneous models can successfully predict the asphalt mixture dynamic modulus over a range of temperatures and loading frequencies. Soares et al. (2003) investigated crack propagation in asphalt mixture under monotonic loading. A numerical method of analysis, in which the material heterogeneity was considered, was developed based on the theory of fracture mechanics. Compared to the elastic continuum theory, micromechanical models consider the heterogeneous nature of asphalt mixtures including the effects of aggregate shapes, sizes, and packing geometry (Dai et al. 2005). Dai and You (2006) developed two-dimensional micromechanical finite element (FE) and discrete-element (DE) models to predict the creep stiffness of HMA. Comparison with experimental measurements demonstrated that the developed models successfully predicted the creep stiffness of the mixture. The authors recommended extending the developed models to three dimensions, as it is considered in this study.

5.4 Methodology

5.4.1 Test Materials Preparation

Two types of asphalt mixes, WMA foamed with 15% reclaimed asphalt pavement (RAP) and HMA with 15% RAP, were evaluated in this study, see Table 5.1. The two mixtures utilized the same polymer-modified Superpave Performance Grade (PG) 70–22M binder. Water foaming were used in the preparation of the WMA mix. For the dynamic modulus specimens, loose mixtures were sampled from plant-produced materials for a project in Louisiana, located on US 171, and were compacted in an on-site mobile laboratory using a Superpave pneumatic gyratory compactor with no reheating to a target air voids content of 7.0%. Dynamic modulus specimens

were compacted to a 165-mm height and a 150-mm diameter. Test specimens were then cored and cut from the center of the gyratory specimens to result in 100-mm diameter by 150-mm high specimens.

5.4.2 Dynamic Complex Modulus Test

The dynamic modulus test was conducted in accordance with AASHTO TP 62 by applying a uniaxial haversine compressive stress to an unconfined cylindrical specimen. The haversine compressive stress was applied on each specimen to achieve a target vertical strain level of 100 micro-strains in an unconfined test mode. The dynamic modulus test was conducted at three temperatures (-10, 25, and 54.4°C) and at five loading frequencies (0.5, 1.0, 5.0, 10.0, and 25.0 Hz). Therefore, 15 temperature and frequency combinations were used to characterize the linear viscoelastic properties of the mixture. The testing temperature was increased from the lowest to the highest level. At each temperature, testing began with the highest frequency of loading and proceeded to the lowest one. Figure 5.1 shows the setup for the test procedure.

Table 5.1 Job mix formula for the four mix types

Mixture Designation		**WMA 15% RAP Foamed**	**Conventional 15% RAP**
Aggregate Blend (by mass)	5/8" Stone	11%	10%
	1/2" Stone	46%	52%
	RAP	15%	15%
	Screens	15%	10%
	Coarse Sand	13%	7%
Binder Type		PG 70-22M	PG 70-22M
Binder content, %	Asphalt	4.3	4.2
	from RAP	0.7	0.8
	Total (Design)	5.0	5.0
Anti-Strip		0.6	0.6
Design air void, %		3.3	3.6
VMA, %		14.5	14
VFA, %		78	75
Metric (U. S.) Sieve		Blend Gradation	
37. 5 mm (1½ in)		100	100
25 mm (1 in)		100	100
19 mm (¾ in)		100	100
12.5 mm (½ in)		93	93

(**Table 5.1** continued)

Mixture Designation	WMA 15% RAP Foamed	Conventional 15% RAP
9.5 mm (⅜ in)	82	82
4.75 mm (No. 4)	50	50
2.36 mm (No. 8)	34	34
1.18 mm (No. 16)	27	27
0.6 mm (No. 30)	23	23
0.3 mm (No. 50)	18	18
0.15 mm (No. 100)	8	8
0.075 mm (No. 200)	5	5
G_{sb} Aggregate	2.642	2.642
G_{mb} (N des)	2.386	2.376
G_{se}	2.666	2.65
P_{absorb}	0.35	0.12
Dust/P_{eff}	1.09	1.06

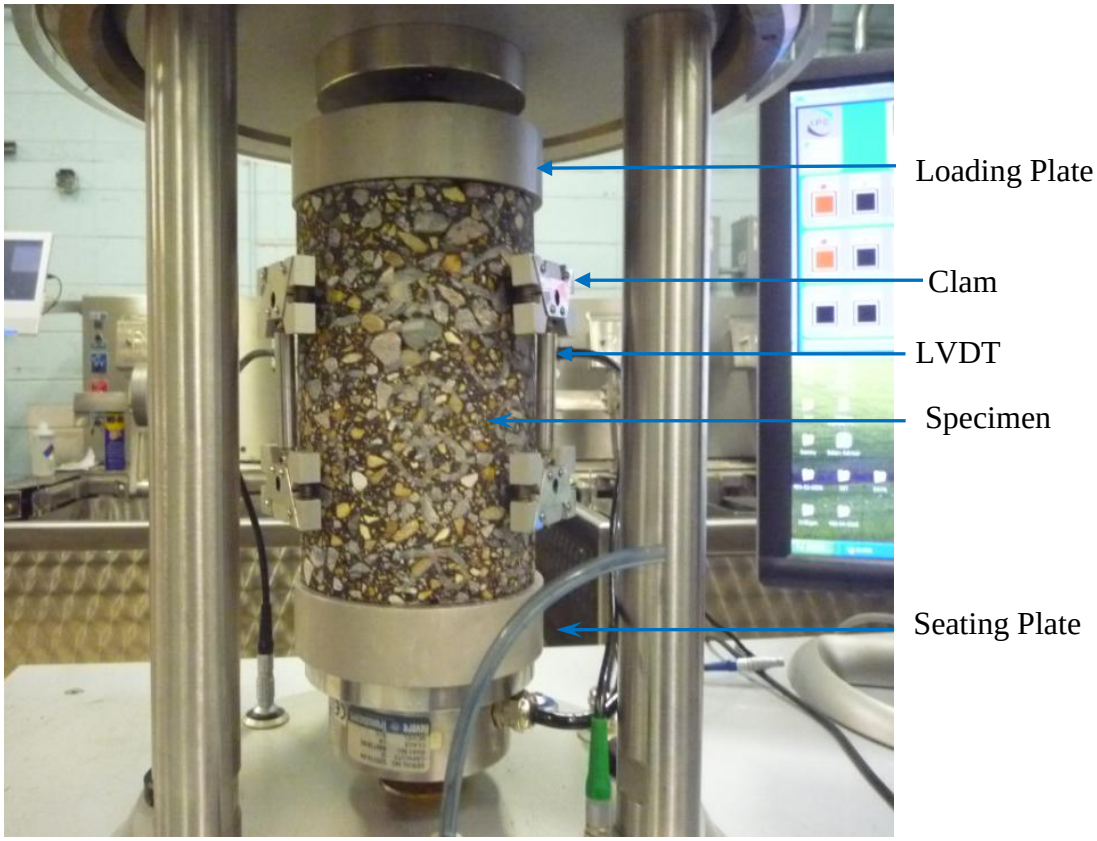

Figure 5.1 Simple performance tester setup for dynamic modules test

5.4.3 Mastic Laboratory Characterization

To characterize the viscoelastic properties of the mastic, its rheological properties were measured by conducting frequency sweeps performed using a dynamic shear rheometer. To prepare the mastic blends, 70 volume percent of PG 70–22M binder was mixed with 30 volume percent of fillers (passing sieve size No. 200) at a temperature of 150°C for 15 minutes (Shenoy et al. 2003). After the calculations, the mass ratio of the fillers to the binder was obtained which is approximately 1 to 1. The frequency sweeps were performed at a uniform set of target strains for all specimens. For the tests conducted at -10, 5, 15, 25, 35, 45°C, the targets strains were chosen to be 0.2, 0.8, 1, 2, 3, and 6.5%. The target strain for the temperature of 55°C was set at 9% (Elseifi et al. 2003).

Dynamical shear testing was performed using an Anton Paar MCR 302 rheometer with parallel plate configuration in a strain-controlled mode (Figure 5.2). The test temperatures ranged from 5 to 75°C in increments of 10°C. Frequency sweeps were performed on all samples over the entire range of temperatures. Twenty frequencies were used at each test temperature ranging from 0.1 to 100 Hz. This wide range of frequencies allowed a strong overlap between the test temperatures in the construction of master curves. The main results of the dynamic shear analysis were the complex shear moduli (G*) and phase angles (δ) over the entire range of applied frequencies at each test temperature.

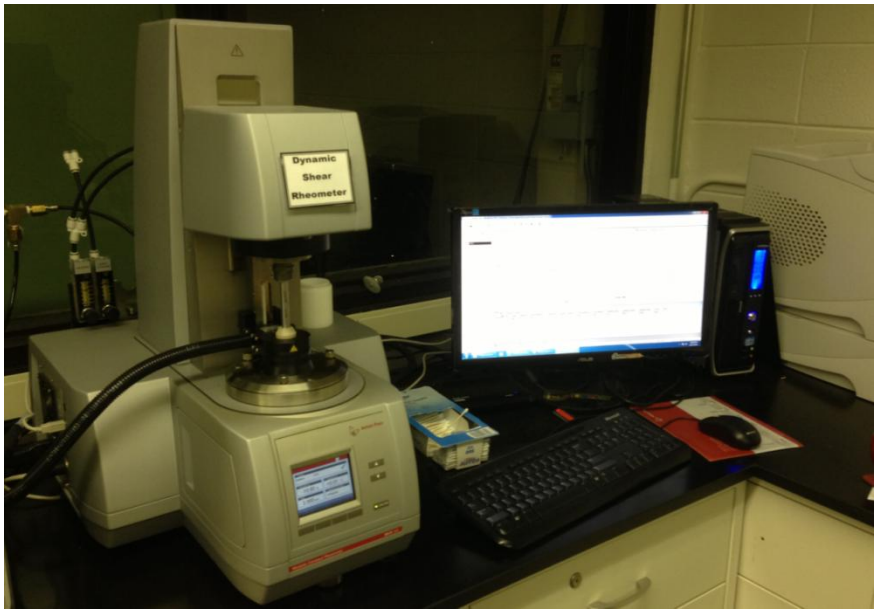

Figure 5.2 Dynamical shear testing system

5.4.4 X-ray CT Imaging Acquisition and Analysis

X-ray CT was used in this study to capture the three-dimensional internal microstructure of the prepared specimens. As illustrated in Figure 5.3, the X-ray CT machine consists of a source, a detector and a stage in which the test specimen is placed. The planar X-ray beams are pointed to the specimen by the high energy source. The specimen stage rotates a full rotation with a constant speed during the scanning, and moves down at a specific speed. The interval between two subsequent X-ray CT images is typically 1 mm and scanning time of each X-ray CT images is 2 minutes. The intensity of the X-ray beams changes after going through the test specimen due to the difference in density of the constituents of the mix (i.e., air voids, aggregate, and mastic). The higher density material will result in a higher attenuation of X-rays. The linear attenuations of a substance in specimen along various directional paths are recorded by the detector. In an X-ray CT image, a low density material is represented by a darker color, while a high density material is represented by a brighter color (on a 256 gray level scale).

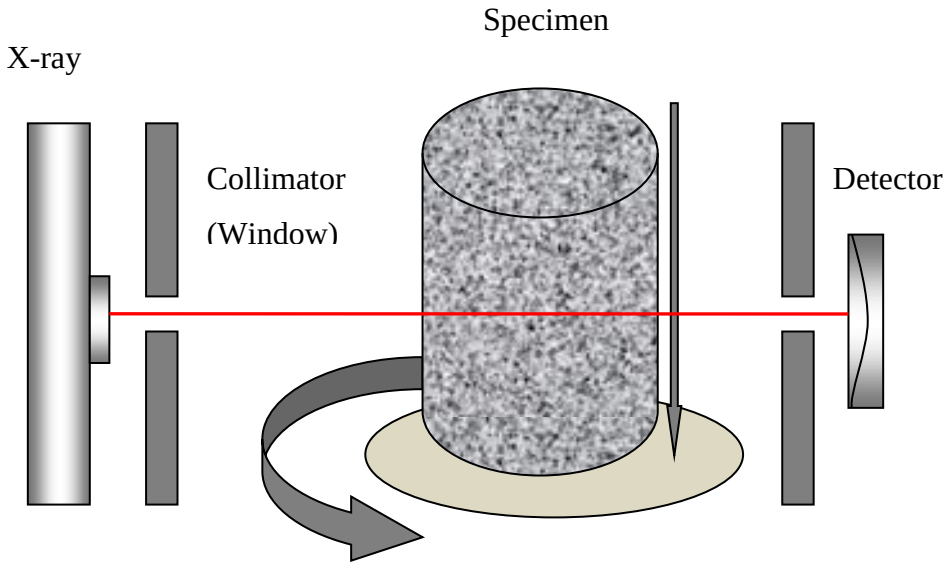

Figure 5.3 Components of X-ray CT system (Masad et al. 2002)

specimens were scanned before conducting the dynamic modulus test. 145 cross-sectional images per specimen were obtained as shown in Figure 5.4. The X-ray CT system in the Advanced Characterization of Infrastructure Materials (ACIM) laboratory at Texas A&M University was used to scan the test specimens. The setup includes two separate X-ray systems; the micro-focus and the mini-focus. The micro-focus system consists of a 225 kV X-ray source

and an image intensifier detector, while the mini-focus has a 350 kV X-ray source and a linear detector. Due to the limited power of the micro-focus system, it is more applicable to scan small asphalt mixture specimens with better resolution. The mini-focus is more applicable to scan large asphalt mixture specimens with an adequate resolution of 0.17 mm/pixel. In this study, the mini-focus was used to scan the test specimens.

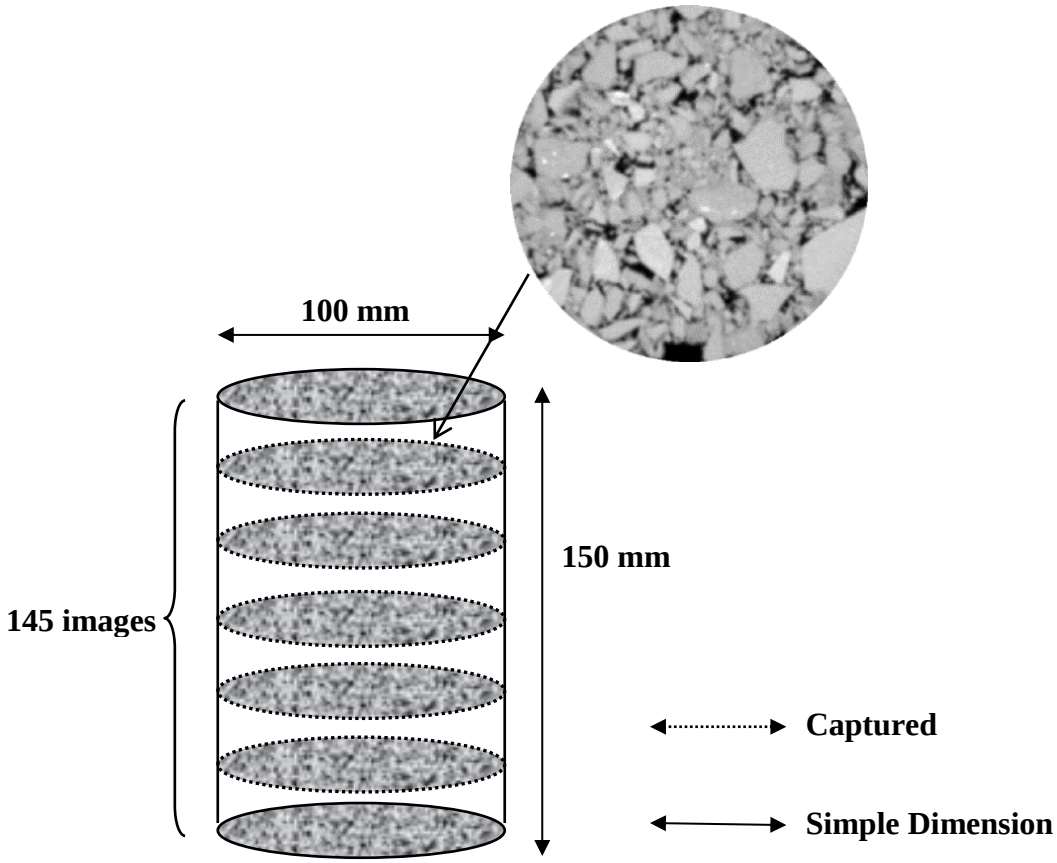

Figure 5.4 X-ray multi-depth testing of HMA specimen

The commercial software SIMPLEWARE scan IP was used in the image analysis and three-dimensional FE meshing in this study. Raw X-ray images were imported into the software and processed in order to obtain an optimum resolution. To separate the three constituents in the images (i.e., asphalt mastic, aggregates, and air voids), the masks option in SIMPLEWARE was used to describe how each phase fills the space. In addition, these masks were processed within the software to optimize the quality of the images and to distinguish between the different constituents in the image. To perform the segmentation of the X-ray images, aggregates, mastic and air voids were assigned to three masks with different colors, based on their grayscale

intensities (threshold index), which ranged from 0 to 255. The aggregate threshold index was set between 176 and 255, the mastic threshold index ranged from 111 to 176, and the air void threshold index ranged from 0 to 111. The threshold segmentation of the three phases is illustrated in Figure 5.5.

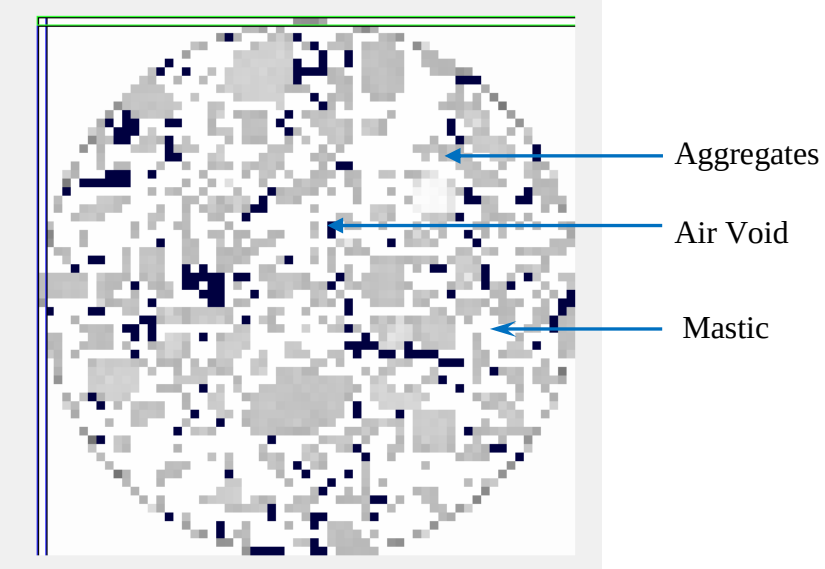

White=Mastic; Grey=Aggregates; Black=Air Voids

Figure 5.5 Threshold segmentation of an X-ray image

5.4.5 Three-dimensional (3D) Heterogeneous Model Construction and FE Meshing

The 3D finite element mesh was created based on the two-dimensional (2D) segmented X-ray images using SIMPLEWARE. In order to develop an image-based 3D FE mesh, the 3D X-ray representation of the specimen was reconstructed first. Each specimen was described by 145 X-ray CT images, which were imported to the software to generate a 3D X-ray representation of the specimen by stacking these 2D image slices. The physical dimension of the 3D image after reconstruction was 50mm x 50mm x 150mm. Figure 5.6 shows an example of the reconstructed 3D image of one of the test specimens. The black and grey portions represent the mastic and aggregates, respectively. The void areas shown in this figure are the air voids. Using this approach, accurate simulation of the heterogeneous nature of asphalt mixture is possible.

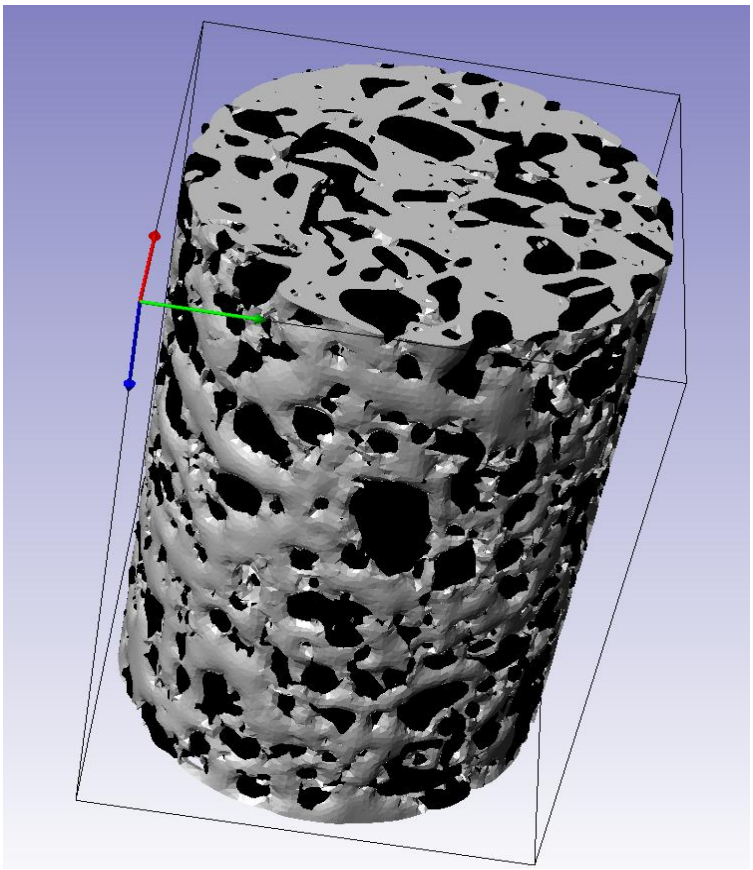

Figure 5.6 Three-dimensional view of reconstructed X-ray CT image after the threshold segmentation

After the construction of the segmented 3D image, FE meshing of the specimens was performed in SIMPLEWARE. The 3D FE mesh was created based on the three segmented masks, which can be processed and modified until satisfactory volume FE meshing was obtained. The processed masks were exported to the commercial FE software, ABAQUS, as "Parts," which are the building blocks in ABAQUS/CAE preprocessing software. Since the mask for air voids does need to be meshed, it was set as non-exportable part. This means that exported part for the air voids will not be meshed. On the other hand, the aggregates and mastic were exported as two separate element sets such that the materials property for each component can be defined separately. As shown in Figure 5.7, the image-based FE mesh accurately represents the asphalt mastic (grey) and aggregates (black) components in the developed 3D FE model. This is not feasible with regular continuum mesh widely used in the literature.

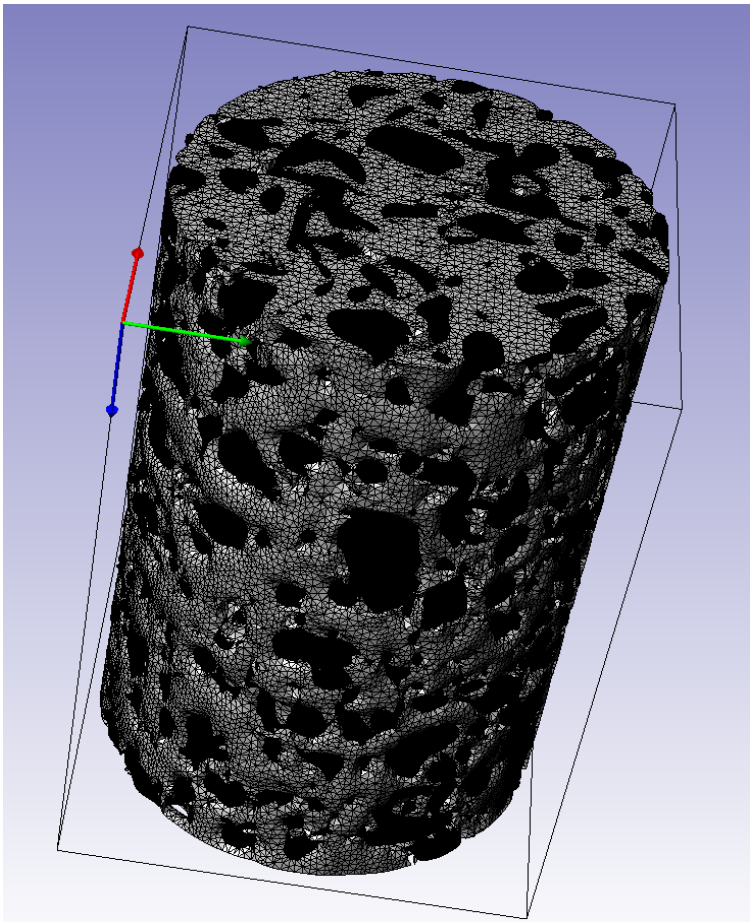

Figure 5.7 Volumetric 3D FE mesh of the test specimen

5.4.6 FEM Simulations of Image-Based 3D Models

The commercial software ABAQUS version 6.9-1 was used for FEM simulation of the dynamic modulus test procedure. The computational procedure for conducting the FE analysis simulation is illustrated in Figure 5.8. The 3D heterogeneous FE model of the asphalt mixture was subjected to a cyclic compressive load. A haversine compressive stress was applied on the top of the cylindrical specimen. The viscoelastic properties of the asphalt mastic were defined based on the results of the DSR test. Since the aggregate modulus is temperature-independent, an estimated elastic aggregate modulus of 95 GPa was defined for the aggregate component as measured in a previous study (Darling et al. 2004). The viscoelastic and elastic material properties were assigned to the mastic and aggregates separately in ABAQUS.

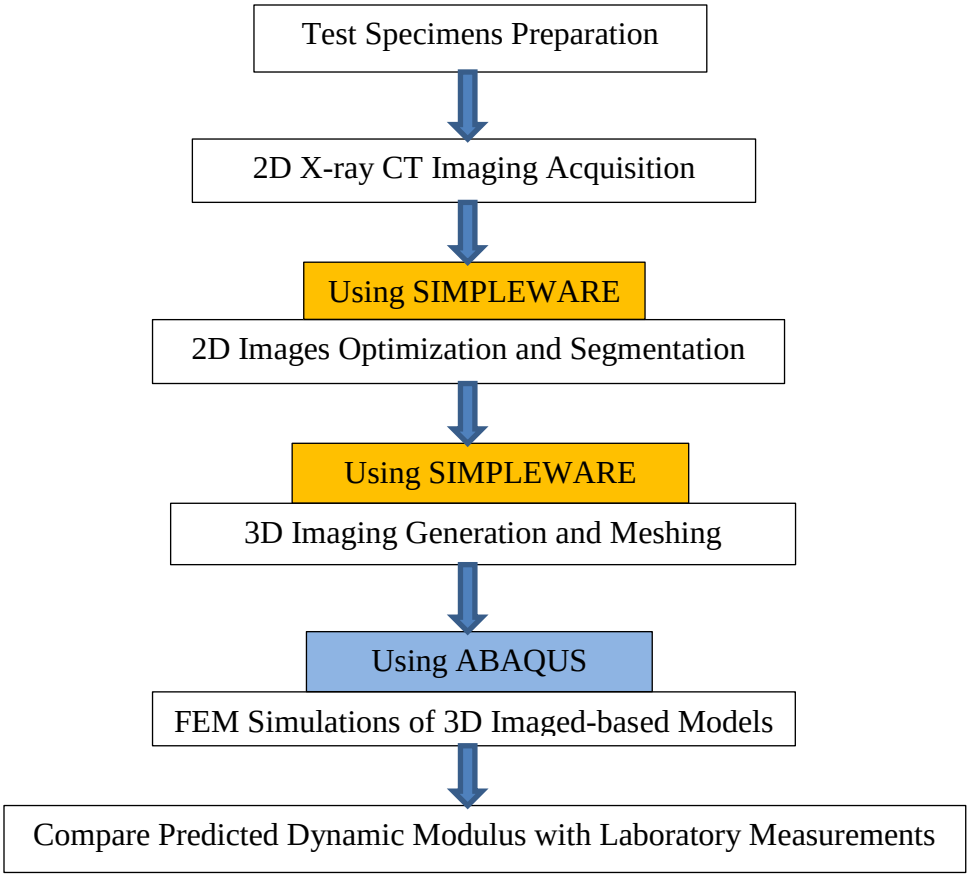

Figure 5.8 Flow chart of 3D FEM development and simulation

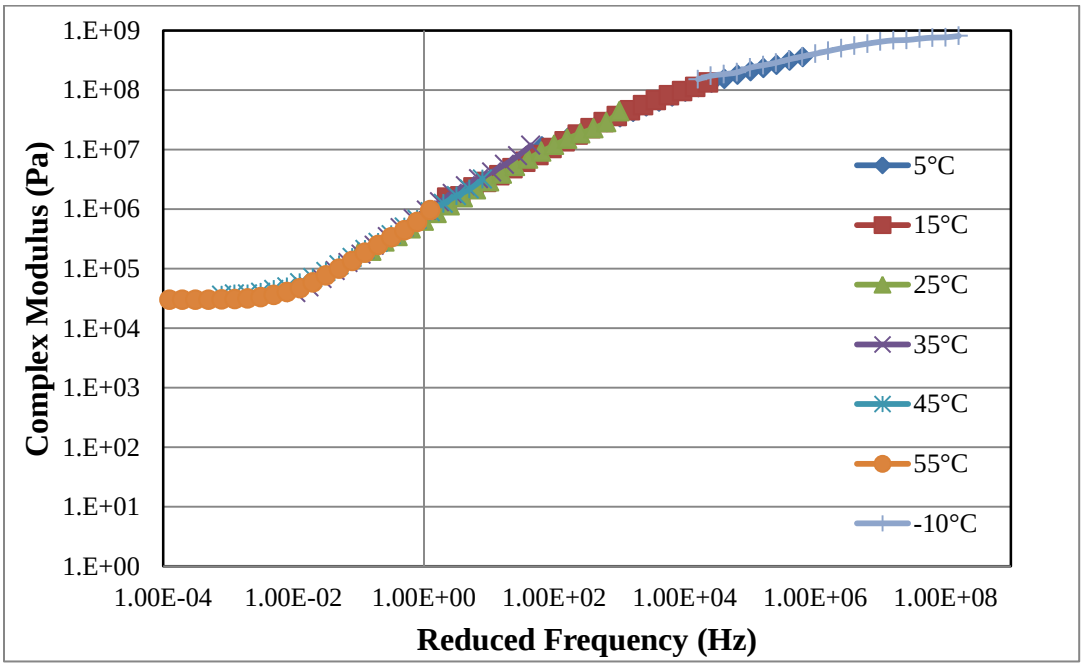

Figure 5.9 Master curve of asphalt mastic at 25^{o}c reference temperature

In order to describe the viscoelastic constitutive behavior of asphalt mastic in the FE model, the experimental data of the asphalt mastic were used to construct master curves at three reference temperatures (-10°C, 25°C and 54°C). Figure 5.9 presents a master curve for the asphalt mastic at a reference temperature of 25°C. The constructed master curve was extended horizontally to very low and high frequencies not attainable experimentally in accordance with the procedure suggested by Bonaquist and Christensen (2005). In this procedure, a sigmoidal model is used to describe the rate dependency of the complex modulus as follows:

$$\log(E^*) = \delta + \frac{(Max - \delta)}{1 + e^{\beta+\gamma\left\{\log(t) - \frac{\Delta E_a}{19.14714}\left[\left(\frac{1}{T}\right) - \left(\frac{1}{295.25}\right)\right]\right\}}} \quad (5.1)$$

where,
E* = complex modulus;
t = loading time;
T = temperature in ° Rankine;
δ, β and γ = fitting parameters; and
Max = limiting maximum modulus.

To define the isotropic, linear viscoelastic behavior of asphalt mastic in the FE model, a generalized Maxwell solid model was used and fitted to the sigmoidal model. The model consists of a spring and n-Maxwell elements connected in parallel (Al-Qadi et al. 2008):

$$G(t) = G_0 - \sum_{i=1}^{N} g_i \left[1 - e^{-t/\tau_i}\right] \quad (5.2)$$

where,
G(t) = shear relaxation modulus at time t;
G_0 = glassy instantaneous shear relaxation modulus;
g_i = material constants referred to as relaxation strengths; and
τ_i = relaxation times.

Using a built-in module in the FE commercial software ABAQUS, variations of the normalized shear modulus with time were fitted to Equation (5.2) through a nonlinear least squares curve fitting process. Eleven to thirteen Prony series terms were used to obtain an accurate fit. Based on this approach, the viscoelastic properties of the asphalt mastic were defined at three reference temperatures (-10°C, 25°C and 54°C) in the FE model. Figures 5.10 shows a comparison between the input data (sigmoidal model) and the Prony series model for the asphalt mastic at 25°C.

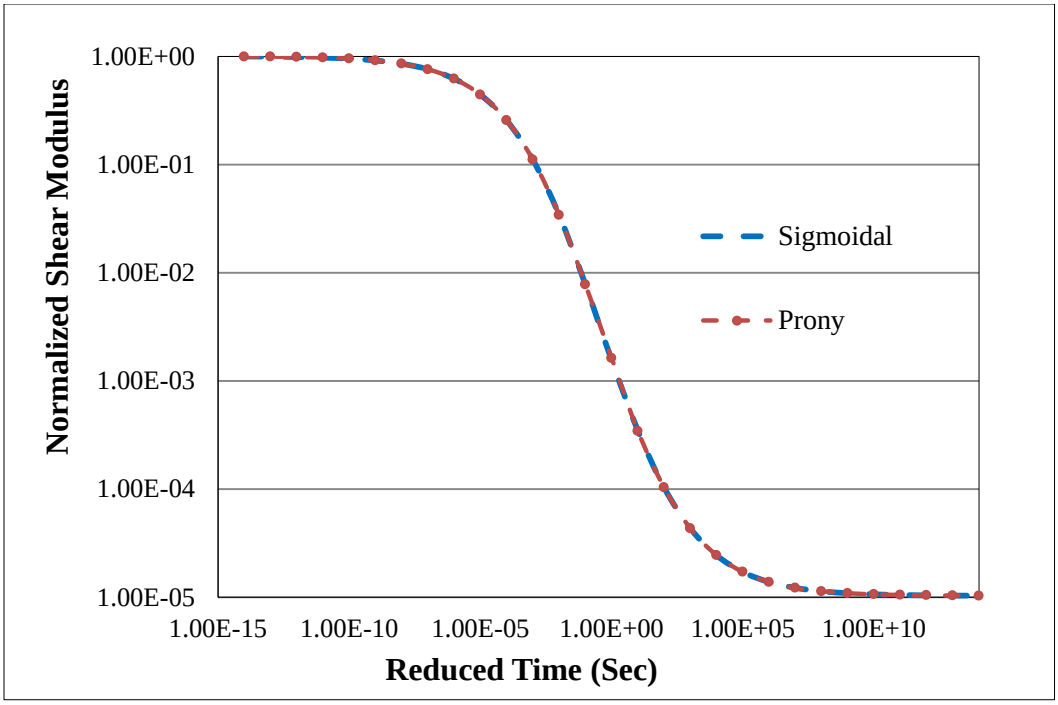

Figure 5.10 Fitting of the master curve to a prony series expansion for the asphalt mastic at 25°C

5.5 Results and Analysis

The dynamic modulus is defined as ratio of the maximum dynamic stress divided to the peak recoverable axial strain. Table 5.2 present the variation of the dynamic modulus with temperatures and frequencies for the two mixtures tested in the laboratory.

Table 5.2 Dynamic modulus test results

WMA 15% RAP (MPa)					
	25	**10**	**5**	**1**	**0.5**
-10°C	17282	17060	15188	13995	14626
25°C	6526	5394	5217	2745	2154
54.4°C	528	284	186	82	64
HMA 15% RAP (MPa)					
	25	**10**	**5**	**1**	**0.5**
-10°C	14986	15649	17082	17577	17899
25°C	2144	2732	4458	5372	6744
54.4°C	76	98	216	313	590

Measurements were repeatable with a coefficient of variation of 15% or less at all test temperatures. As expected, measured E* values decreased with the increase in temperature and the reduction in frequency. These trends demonstrate that asphalt mastic, while a small component by weight of the mix (around 5% asphalt binder is typically used), strongly influences the properties of the whole mix.

The calculated dynamic modulus values were calculated based on the strain outputs from the FE model in the direction of the compressive stress. The comparison between the laboratory measurements and the FE model prediction is shown in Figure 5.11. The strain in the mastic and the aggregates were obtained from the model and are shown in Figure 5.12. As shown in this figure, the strain in the aggregates was much smaller than in the mastic; it was approximately 15 times greater in the mastic than in the aggregates. This may indicate that most of the deformations in the test specimens during the dynamic modulus test are caused by the mastic.

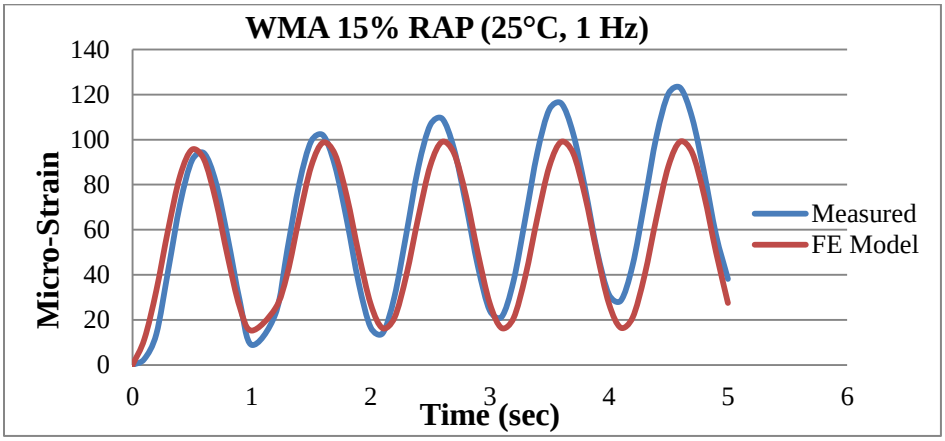

Figure 5.11 Comparison between FE and experimental test results

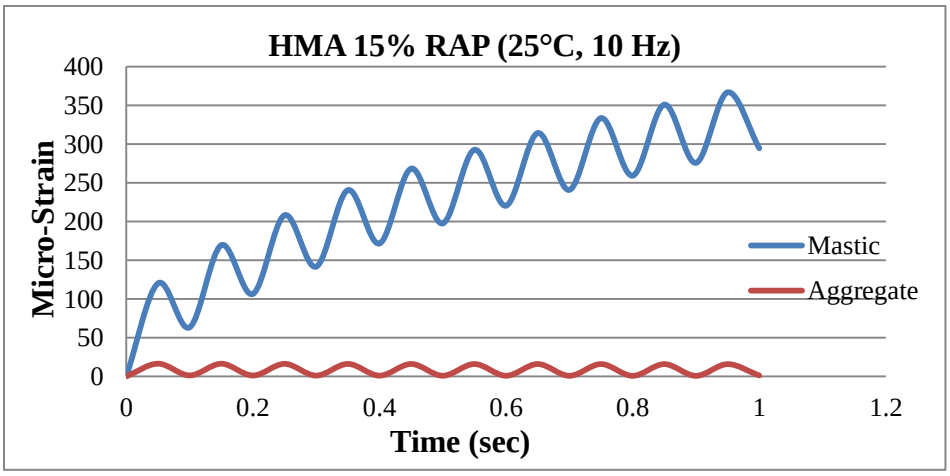

Figure 5.12 Comparison between mastic and aggregates strains

Figure 5.13 presents a comparison between measured and calculated E* values for the WMA and the HMA mixes at the three test temperatures. As illustrated in this figure, an acceptable agreement was obtained between measured and predicted dynamic modulus results.

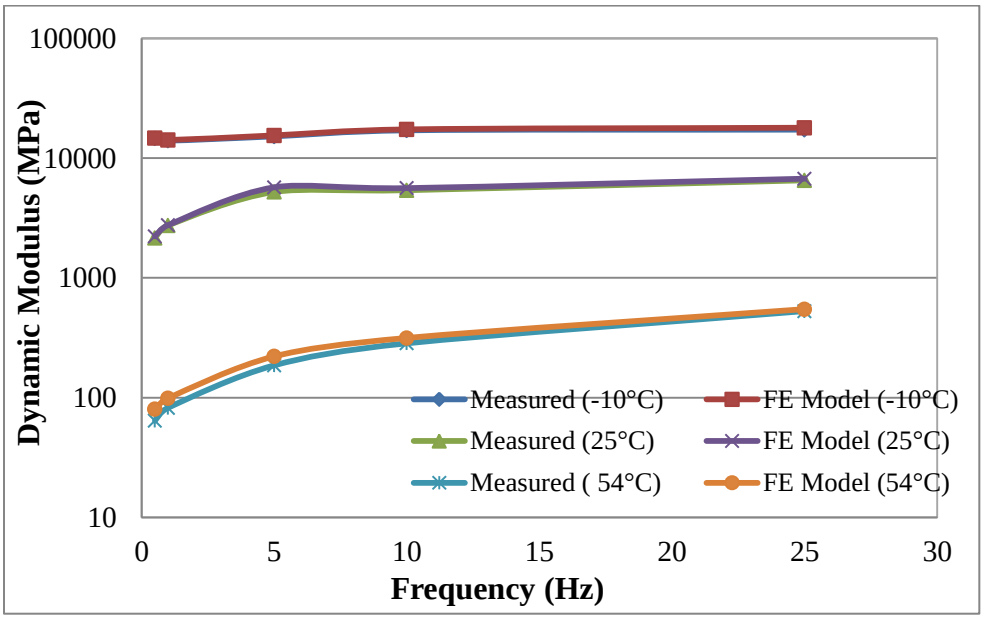

(a)

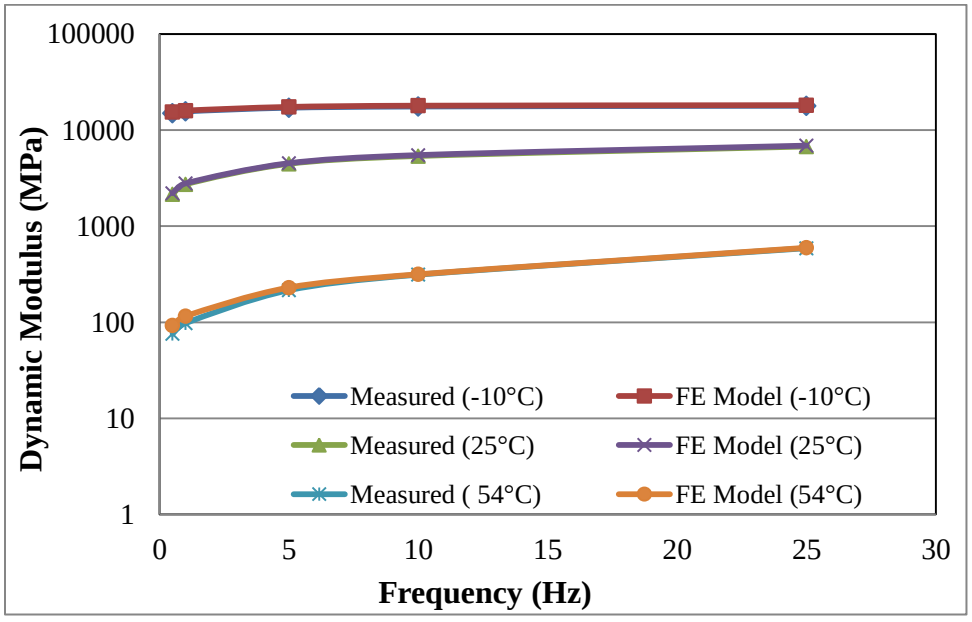

(b)

Figure 5.13 Dynamic modulus (E*) comparison of FE and experimental test results for (a) WMA 15% RAP and (b) HMA 15% RAP

At intermediate (25°C) and high temperatures (54°C), E* isotherms exhibited a curved shape, which is indicative of the viscoelastic behavior of asphalt mixtures at intermediate and high temperatures. In addition, the model-predicted E* values were slightly higher than the measured values, which may indicate softening of the material during the dynamic modulus test at intermediate and high temperatures. Based on these results, one may consider that the proposed FE model provides an acceptable description of the dynamic modulus test across the entire range of test temperatures and loading frequencies considered in this study.

The effects of mastic and aggregates stiffness on the dynamic modulus of the mix were investigated. A parametric analysis was conducted by varying the stiffness of the mastic and the aggregates by 10% and 20% from the mean values. The model predicted E* values for different mastic and aggregates stiffness conditions are shown in Figure 5.14. As shown in this figure, the effect of mastic stiffness on the mix dynamic modulus is more pronounced than the aggregates stiffness. While the mastic only represents a small fraction of the composite mixture, its influence is more pronounced than the aggregates because the majority of the deformation is exhibited in the mastic and the deformation in the aggregates is considered negligible as compared to the mastic. Experimental measurements for different types of binder support these trends observed in the presented model (Elseifi et al. 2011). Similar trends were observed at -10°C and 54°C. The percentage changes on the mix dynamic modulus with the changes in mastic and aggregate stiffness are presented in Table 5.3.

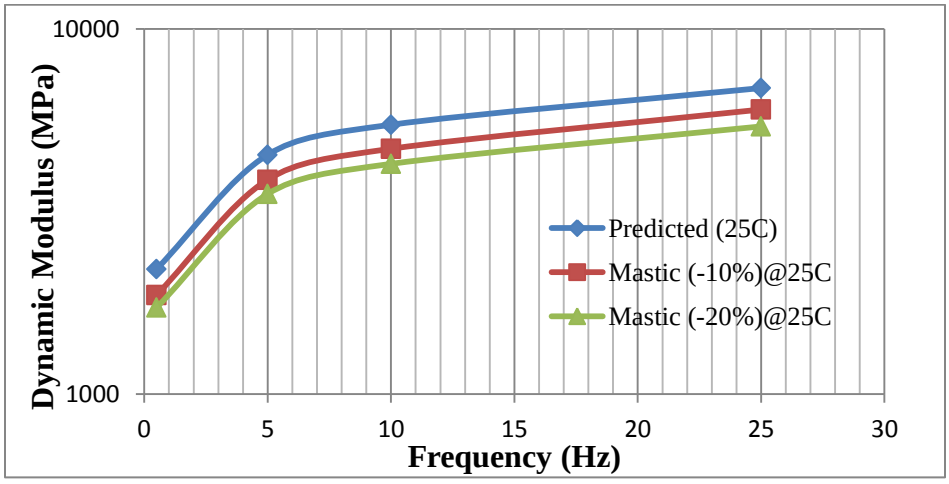

(a)

Figure 5.14 Average percentage change in dynamic modulus with change in mastic and aggregates stiffness

(**Figure 5.14** continued)

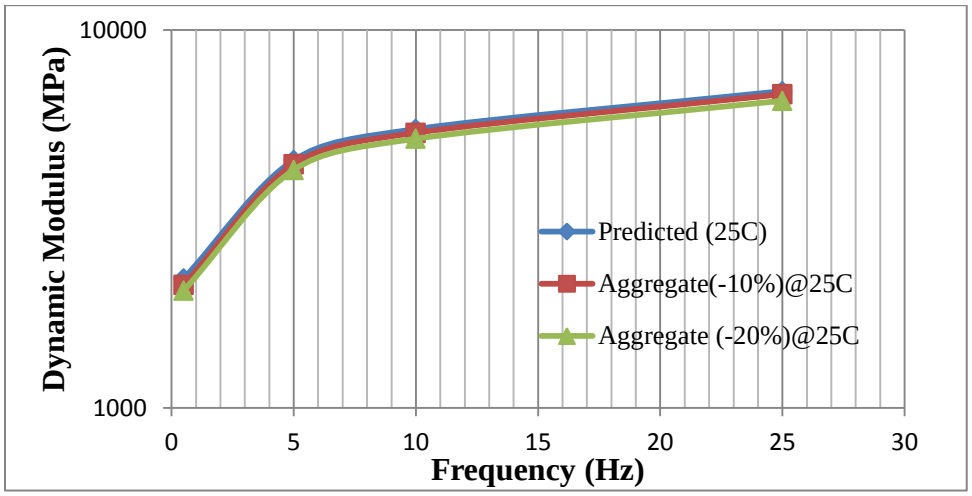

(b)

Table 5.3 Average Percentage Change in Dynamic Modulus with Change in Mastic and Aggregates Stiffness

		Average Percentage Change in Dynamic Modulus (%)		
Component	Change in Stiffness	-10°C	25°C	54°C
Mastic	-10%	12.7	13.8	13.8
	-20%	18.9	21.7	21.9
Aggregates	-10%	2.7	2.3	2.4
	-20%	5.9	5.8	5.8

5.6 Summary and Conclusions

Three-Dimensional heterogeneous finite element models were developed in this study based on X-ray CT images. Internal heterogeneity of the asphalt mixture was considered by using the X-ray CT method, which revealed the microstructure of aggregates, mastic and air. 3D FE models were developed by reconstructing 2D X-ray CT images, which were optimized and processed prior to mesh generation. Based on the results of this study, the following conclusions may be drawn:

- There was good agreement between measured and model predicted dynamic modulus test results. Based on these results, it is determined that the proposed 3D finite element model successfully predicted the dynamic modulus of the composite mixes across a wide range of temperatures and loading frequencies.
- Most of the deformations during the dynamic modulus test are derived from the mastic, which controls the viscoelastic behavior of the composite.
- While the mastic only represents a small fraction of the composite mixture, its influence is more pronounced than the aggregates in the behavior of the mixture in the dynamic modulus test.

5.7 References

ABAQUS Theory Manual, Version 6.9-1. (2010) Habbit, Karlsson & Sorenson, Inc., Pawtucket, RI.

Adhikari ,S., and You, Z., (2007). Distinct Element Modeling of the Asphalt Mixtures: from Two- dimensional to Three-dimensional Models, Transportation Research Board, National Research Council, Washington, D.C.

Al-Qadi, I.L, Elseifi, M.A., Yoo, P.J., Dessouky, S.H., Gibson, N., Harman, T., D' Angelo, J., and Petros, K. (2008) Accuracy of Current Complex Modulus Selection Procedure from Vehicular Load Pulse in NCHRP 1-37A Mechanistic-Empirical Pavement Design Guide. Transportation Research Record: Journal of the Transportation Research Board, No. 2087, Washington, D.C., 81-90.

Bonaquist, R., and Christensen, D.W (2005). A Practical Procedure for Developing Dynamic Modulus Master curves for Pavement Structural Design. Journal of the Transportation Research Board, 1929, Washington, D.C., pp. 208-217.

Dai, Q., Sadd, M.H., Parameswaran, V., and Shukla, A. (2005). "Prediction of Damage Behaviors in Asphalt Materials Using a Micromechanical Finite-Element and Image Analysis." Journal of Engineering Mechanics, ASCE, Vol. 131, No. 7, pp. 668-677.

Dai, Q., and You, Z. (2006). "Prediction of Creep Stiffness of Asphalt Mixture with Micromechanical Finite-Element and Discrete-Element Models." Journal of Engineering Mechanics, ASCE, Vol. 133, No. 2, pp. 163-173.

Elseifi, M.A., Al-Qadi, I.L., and Flinstch, G.W. (2003). "Quantitative Effect of Elastomeric Modification on Binder Performance at Intermediate and High Temperatures." Journal of Materials in Civil Engineering, ASCE, Vol. 15, No. 1, 32-40.

Elseifi, M.A., Al-Qadi, I.L., Yang, S-H., and Carpenter, S. (2008). "Validity of Asphalt Binder Film Thickness Concept in Hot-Mix Asphalt," Journal of the Transportation Research Board, National Research Council, Washington, D.C.

Elseifi, M.A., L.N. Mohammad, E. Kassem, H. Ying, and E. Masad. (2011). Quantification of Damage in the Dynamic Complex Modulus and Flow Number Tests Using X-ray Computed Tomography. Journal of Materials in Civil Engineering, ASCE, Vol. 23, No. 12, 1687-1696.

Elseifi, M.A., L.N. Mohammad, and S.B. Cooper. (2011). Laboratory Evaluation of Asphalt Mixtures Containing Sustainable Technologies. Journal of the Association of Asphalt Paving Technologists, Vol. 80, pp. 227-254.

Eriksen, K., and Wegan, V. (1993). Optical Methods for the Evaluation of Asphalt Concrete and Polymer-Modified Bituminous Binders. Note 244, Danish Road Institute.

Kassem, E., Masad, E., Bulut, R., Lytton, R. (2009). Measurements of the Moisture Diffusion Coefficient of Asphalt Mixtures and its Relationship to Mixture Composition. International Journal of Pavement Engineering, Vol. 10, No. 6, pp. 389-399.

Masad, E., Muhunthan, B., Shashidhar, N., and Harman, T. (1999). "Internal Structure Characterization of Asphalt Concrete Using Image Analysis." Journal of Computing in Civil Engineering, ASCE, Vol. 13, No. 2, pp. 88-94.

Masad, E., Jandhyala, V.K., Dasgupta, N., Somadevan, N., and Shashidhar, N. (2002). Characterization of Air Void Distribution in Asphalt Mixes Using X-ray Computed Tomography. Journal of Materials in Civil Engineering, ASCE, Vol. 14, No. 2, 122-129.

Masad, E., Dessouky, S., and Little, D. (2007). "Development of an Elastoviscoplastic Microstructural-Based Continuum Model to Predict Permanent Deformation in Hot Mix Asphalt." International Journal of Geomechanics, ASCE, Vol. 7, No. 2, pp. 119-130.

Simpleware ScanIP Software Reference Guide V4.2 (2010).

Shenoy, A., Stuart, K., and Mogawer. (2003). Do Asphalt Mixtures Correlate Better With Mastics or Binders in Evaluating Permanent Deformation? Transportation Research Record, pp. 16-25.

Soares, J. B., Colares de Freitas, F. A., and Allen, D. H. (2003). Crack modeling of asphaltic mixtures considering heterogeneity of the material. Proceedings of the 82nd Annual Meeting of the Transportation Research Board (CD-ROM), Transportation Research Board, Washington, D.C.

Witczak, M.W., Kaloush, K., Pellinen, T., El-Basyouny, M., and Von Quintus, H. (2002). Simple Performance Test for Superpave Mix Design, NCHRP Report 465, Transportation Research Board, Washington, D.C.

You, Z., Adhikari ,S., Kutay ,E. (2009). Dynamic modulus simulation of the asphalt concrete using the X-ray computed tomography images. Materials and Structures (2009) 42:617–630.

CHAPTER 6–CONCLUSIONS AND RECOMMENDATIONS

In this study, a comprehensive evaluation of the dynamic modulus and SCB tests was conducted. With respect to the SCB test method, results of the experimental program were used to validate a 3D FE model, which was used to interpret and to analyze the failure mechanisms in the SCB test. The SCB test, as well as the propagation of damage, was successfully simulated using 3D FE and cohesive elements. A fatigue crack propagation model was developed to predict the number of cycles to failure based on a cyclic SCB test and the generalized J-integral approach. The effect of creep deformation on the SCB test results obtained at intermediate temperature was also investigated. With respect to the dynamic modulus test, a 3D heterogeneous FE model was developed to describe the response of asphalt mixtures in the dynamic complex modulus test using an X-ray computed tomography (CT) image-based FE modeling approach. The experimental testing results for two Superpave mixtures including one conventional hot-mix asphalt (HMA) and one warm-mix asphalt (WMA) mix were used to validate and calibrate the developed models. Based on the analysis conducted in this study, the following conclusions may be drawn:

6.1 With Respect to the SCB test

The SCB test process as well as the propagation of damage was successfully simulated using 3D FE and cohesive elements. The presented modeling approach was in good agreement with measured test results for all mixes. Based on the results of the FE model, damage propagates in the vicinity of the notch and is mainly caused by a combination of vertical and horizontal stresses in the specimen. The effect of shear was negligible in progressing damage in the specimen.

A crack propagation model was developed based on a cyclic SCB test and the generalized J-integral approach. Good agreement between measured and model predicted SCB test results was obtained. Based on these results, it is determined that the proposed model provides an acceptable representation of the fatigue SCB test.

The effect of creep deformation on the SCB test results obtained at intermediate temperature was investigated. The average energy dissipated due to creep deformation in the monotonic SCB test conducted at intermediate temperature was 7.1% of the total dissipated energy in the model. It was determined from these results that the dissipated energy due to fracture is the predominant factor controlling failure in the SCB test.

6.2 With Respect to the Dynamic Modulus test

Three-Dimensional heterogeneous finite element models were developed in this study based on X-ray CT images. Based on the results of this study, good agreement between measured and model predicted dynamic modulus test results was found. Therefore, it is concluded that the proposed 3D finite element model successfully predicted the dynamic modulus of the composite mixes across a wide range of temperatures and loading frequencies.

The effects of mastic and aggregate stiffness on the mix dynamic modulus were investigated. Results indicated that most of the deformations during the dynamic modulus test are derived from the mastic, which controls the viscoelastic behavior of the composite. While the mastic only represents a small fraction of the composite mixture, its influence is more pronounced than the aggregates in the behavior of the mixture in the dynamic modulus test.

6.3 Contributions to the Body of Knowledge

The contributions of this study to the body of knowledge include the following:

- This study determined that damage propagates in the SCB test due to a combination of vertical and horizontal stresses in the specimen. In addition, the effect of shear stresses was negligible in progressing damage in the specimen.
- A crack propagation model was developed based on the generalized J-integral approach for the SCB test. It provides an acceptable representation of the fatigue SCB test.
- This study results demonstrated that the dissipated energy due to fracture is the main factor controlling failure in the SCB test.
- 3D heterogeneous FE models were developed in this study based on X-ray CT images. Proposed models can successfully predict the dynamic modulus of the composite mixes across a wide range of temperatures and loading frequencies.
- This study demonstrated that most of the deformations during the dynamic modulus test are derived from the mastic, which controls the viscoelastic behavior of the composite. While the mastic only represents a small fraction of the composite mixture, its influence is more pronounced than the aggregates in the behavior of the mixture in the dynamic modulus test.
- The contribution of the mix components (aggregate, mastic, and air voids) on its performance was investigated using the proposed FE models. Results demonstrated that

the influence of mastic is more pronounced than the aggregates in the behavior of the mixture during the dynamic modulus test.

6.4 Recommendations for Future Research

- In future studies, a numerical model based on the viscoplastic assumption should be developed to predict the crack propagation at low, intermediate, and high temperatures. In addition, a FE model with viscoplastic properties should also be built with the purpose of studying the effect of creep deformation more accurately on the SCB at all the temperatures.
- An advanced mechanistic model based on viscoelastic-viscoplastic theory should be incorporated into a 3D, heterogeneous finite element models to characterize the recoverable and irrecoverable behavior of mastic. The constitutive model should be converted into a numerical formulation, which can capture the relationship between stresses, strains, and temperatures under various load conditions.
- A X-ray CT image-based, 3D, heterogeneous finite element models should be developed for the SCB test in the future. The load transfer mechanisms between the aggregates and mastic should be studied in order to ensure accurate description of the crack propagation during the test. In addition, crack initiations should also be studied by simulating the SCB test with un-notched specimens.

VITA

Hao Ying was born in 1985, in a small town named Changshan, Zhejiang, China. He grew up in Beijing, the capital of China. He earned his bachelor's degree in civil engineering from China University of Geosciences, Beijing, China, in May 2008. He came to Louisiana State University, Baton Rouge, Louisiana, United States, in the Fall of 2008 and received his master's degree in Civil Engineering in August 2011. Hao Ying expects to receive the degree of doctor of philosophy in Civil Engineering in May 2013.